Measurement of Wolfenstein Parameters for the p-p system to determine accurate phase shifts near 500 MeV

GEORGE ARTHUR LUDGATE

BEDFORD COLLEGE

This thesis is submitted for the Degree of Doctor of Philosophy in the University of London.

October, 1976

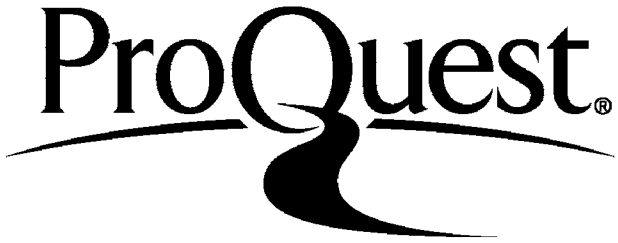

ABSTRACT

The Wolfenstein p-p parameters P, D and R have been measured at the four laboratory scattering angles 6, 9, 15 and 24 degrees together with a single R' measurement at the 15 degree angle. Statistical error on each measurement is typically 0.025. A 518 MeV polarized proton beam was produced at TRIUMF from a Lamb Shift source and free p-p scattering was observed from a liquid hydrogen target. Components of the initial and final polarizations were measured; the former by scintillator telescopes viewing a CH_2 target, the latter by a large solid angle acceptance (carbon) Polarimeter utilizing multiwire proportional chambers. A separate experiment was undertaken to calibrate the Polarimeter at 9 energies and the results from the analysis of this data were used in the final calculation of the Wolfenstein parameters. Time-of-flight and momentum analysis were undertaken to remove inelastic protons and pions above threshold. Straight tracks through the final Polarimeter were rejected by beam defining counters for overall efficiency of the experiments.

A superconducting solenoid was used in the R and R' measurements to precess the vertical primary beam polarization by $\pm$ 90 degrees into the horizontal plane before the hydrogen target. The polarization of the primary beam was reversed at its source for the four parameter's measurements allowing data to be recorded for two polarization orientations. The R' parameter required a precession magnet in the secondary beamline to precess the longitudinal polarization into the horizontal plane.

The measured Wolfenstein parameters have been used in a

single energy phase shift analysis at 515 MeV to improve the precision of the isovector nucleon-nucleon phases.

CONTENTS

"I dedicate this thesis to my loving wife Catherine" - George

ILLUSTRATIONS

TABLES

INTRODUCTION

This report is based on the results of a collaboration experiment between physicists from Bedford College London, AERE Harwell, Surrey University, Queen Mary College London and the Univ ersities of British Columbia & Victoria (Experiments). The acronym BASQUE was therefore used as the group's title. Experiments were carried out at TRIUMF (TRI-University Meson Facility) during 1975-76. This new Canadian research facility is located on the campus of the University of British Columbia (UBC), Canada.

TRIUMF is one of the new medium energy, high intensity Meson Factories (cf SIN, LAMPF) and the first extracted proton beam was obtained in December 1974. Thence followed a year of cyclotron improvements before polarized beam became available in January 1976. Despite severe setbacks over the last year the cyclotron has been operational 51.8% of the time (see TRIUMF Annual Report 1975 for a historical breakdown of the year's operation) and physics has been underway from the outset.

BASQUE experimental equipment was despatched to TRIUMF from the Rutherford Laboratory during the summer of 1974. The author arrived one month later to find the equipment unpacked and arranged on the TRIUMF Proton Hall floor; but little else existed at that time. Within six months the Hall was to fill with shielding and essential services were to be laid on to meet the requirements of our apparatus. Cables were fed from our control caravan, outside the Hall, to scintillators and electronic detectors on the experimental floor: the group was ready to

receive beam before Xmas 1974.

The proton-proton (p-p) elastic scattering amplitude is uniquely determined below 500 MeV, but this cannot be said of the less healthy neutron-proton (n-p) system[I.1,I.2,I.3]. The BASQUE group therefore propose to determine accurately the iso-scalar (T=0) phase shifts over the energy range 200-500 MeV by precise measurements of free n-p Wolfenstein parameters P, D, R, A, D_t, R_t, A_t over 55-125 degrees in the centre of mass (cm) at 10 degree intervals to $\pm$ 0.03 (P to $\pm$ 0.02) together with the differential cross-section over 5-180 degrees in 5 degree steps to 1%. However, although contemporary isovector (T=1) phases are unique they are not quite so well determined as to match the proposed n-p experiments. It appeared that this situation could be remedied by precise measurements of p-p Wolfenstein parameters P, D, R and R' over the laboratory angular range 6-24 degrees, where data are clearly lacking. The problem considered in this thesis was the design and performance of these precise triple scattering experiments. Wolfenstein parameters P, D and R were measured at 6, 9, 15 and 24 degrees lab. together with a single measurement of R' at 15 degrees lab.

Two major runs were undertaken in January and April 1976 though test data and some calibration data had been recorded during 1975. The first run comprised an experiment to calibrate a large solid angle acceptance carbon polarimeter, which was subsequently used in the second run to measure the horizontal and vertical polarization components of a secondary beam scattering from a hydrogen target. A polarized beam was required for the

latter run but unpolarized beam was adequate for the calibration. Data were analysed by the author on the IBM 360/195 of the Rutherford Laboratory in the Spring and Summer of 1976. Final results were produced by Autumn when this report was written.

Chapter 1 of this thesis is devoted to a summary of the theoretical aspects of the nucleon-nucleon (NN) problem. Assuming change independence the p-p system is but one of the three possible combinations of two isospin ½ particles. The general NN system is therefore treated with exceptions for the p-p system being noted in the text. Chapter 2 discusses the purpose and design philosophy for the measurements. Individual items of equipment and their inter-relation form the topic of Chapter 3, with the actual experimental configurations used for the measurements being collected into Chapter 4. Results, including the phase shift analysis are presented in Chapter 5 leaving conclusions to be drawn in Chapter 6.

The author considers himself lucky to have been "in on the ground floor" of this major experiment and to have participated in such widely differing aspects of the project as shielding and cabling to testing our superconducting solenoid, designing and assembling high speed logic and processing data at all levels.

ACKNOWLEDGEMENTS

I would like to thank the many members of TRIUMF, RHEL and the Science Research Council without whom this experiment would have been impossible.

Special thanks go to my supervisor, Dr N M Stewart, for his encouragement and supervision during my three years of study and to my good student friends Mr Christopher Oram and Mr K Shakarchi for much profitable discussion.

I am indebted to Professor D V Bugg, Dr J A Edgington, Professor D Axen, Dr A Clough, Dr J Vavra, Dr R C Brown, Dr S Jaccuard, Dr C Amsler and Mr L Felawka for invaluable help and advice during my stay in Vancouver and to Mr G Waters for outstanding technical assistance.

I would like to acknowledge the support and continuing interest of Professor J R Richardson (Director of TRIUMF until 1976; on leave from the University of California) in the BASQUE group's activities.

Special words of thanks go to Mrs Valerie Goodwin for typing this thesis.

Finally my greatest thanks and appreciation go to my wife Catherine for her unending love and understanding through three long hard irreplaceable years of our youth.

The author was fully supported by the SRC during his three year postgraduate studentship.

CHAPTER 1

The Nucleon-Nucleon System

The importance of the Nucleon-Nucleon (NN) interaction has been recognised since Chadwick announced the discovery of the neutron in February 1932[1.1]. Contemporary accelerators were producing proton beams of up to 1 MeV kinetic energy and Nuclear Physics as we know it today was quietly born.

Within one year of the discovery Heisenberg and Majorana had developed dynamical theories based on space and spin exchange interactions. Heisenberg introduced the concept of isospin in his first paper[1.2]. Later theoretical models concentrated on potential scattering and attempted to fit existing data, but with limited success[1.3]. By 1941 spin-spin forces had been added to the interaction after consideration of n-p and p-p cross-sections[1.4]. Tensor components were predicted by Yukawa[1.5] and deemed necessary after Kellogg found the deuteron quadrupole moment to be non-zero[1.6]. Spin orbit terms were added in a paper by Wigner and Eisenbud[1.7] formulating the most general potential that conserved total angular momentum. Theory was 10 years ahead of experiments and it was not until 1950 that the shell model of the nucleus, proposed by Mayer and Jensen[1.8], gave an indication for the presence of this last force.

Wigner recognised the consequences of charge symmetry and the more important concept of charge independence. In an early paper, which was beyond most physicists of the era, he expounded the theory of super-multiplets as a method for classifying nuclear

states[1.9]. Selection rules, resulting from isospin conservation and charge symmetry, were developed in the early 50's and tested[1.10, 1.11].

Meanwhile theory had developed to the point where proposed N-N interactions were being developed from the exchange of massive particles, but by the end of the 50's it was clear that no firm theoretical explanation of the force would be forthcoming. Experimentalists turned to phenomenological parametrizations[1.12] of the data which theory attempted to reproduce. Many polarization, triple scattering parameters and cross-section data became available during the 60's[1.13] allowing phase shift analyses to be performed up to 750 MeV[1.30, 1.31].

The contemporary experimental and theoretical situation is further classified in section 1.1 of this chapter. Section 1.2 discusses the non-relativistic two-body problem whilst section 1.3 treats polarization formalism as applicable to N-N scattering in this thesis.

1.1 Status of the two nucleon interaction

Worldwide interest in the two nucleon interaction can be measured by the number of review articles devoted to expositions of the experimental and theoretical aspects of this intriguing problem. Historical aspects have been dealt with by Breit[1.14] and Brink[1.15]. Developments up to the early 60's appear in the reviews of Stapp[1.16], MacGregor[1.12], the experimentalists' monograph of Wilson[1.13] and the theoretical discourse by Moravcsik[1.17]. Forward looking papers by McKee[1.18] and

Edgington[1.19] call for further work at all energies (in NN scattering and closely related fields), pinpointing sensitive areas for both theoretical and experimental investigations.

Contemporary models of the NN interaction divide into several classes[1.20]. Phenomenological potentials are more complex descendents of those used so successfully to explain electromagnetism and gravity. Potentials employing spin-spin, spin-orbit, tensor components and a hard or soft core have been fitted to the data and are extensively used in nuclear structure calculations[1.21, 1.20]. Meson theoretical models[1.22] attempt to derive the interaction by considering exchange processes involving pions and the heavier mesons. Its major success has been in the derivation of a one pion exchange contribution[1.20] (OPEC) to the force at large separation ($\gtrsim$ Compton wavelength for the pion:1.4fm) and is now generally confirmed by observations[1.32, 1.23]. The hard core is explained in terms of vector meson exchange (notably ρ, ω, ϕ) and the region $\sim$1 fermi by scalar mesons of mass greater than two pions (equivalently known as $\pi_N, \varepsilon : \sigma_0, \sigma_1 : \sigma, \delta$). Dispersion theory seeks to compute the scattering matrix directly, without recourse to a potential or Hamiltonian[1.24]: the potential energy of two nucleons is not directly measurable and may be an irrelevant concept. Bugg[1.25] has shown how forward NN dispersion relations may be used to extract meson-nucleon coupling constants when other methods are sensitive to theoretical approximations and data fitted.

Data have tended to group around "magic" energies allowing single energy phase shift analyses to be performed. Unitarity

is built in[1.26] and OPEC phases seem a reasonable way to fit the higher partial waves. One disadvantage for phenomenologists is that the number of parameters increase with energy: inelasticity leading to complex phase above threshold. Proposals for parametrizing the data directly in terms of the scalar amplitudes of the elastic scattering matrix[1.27, 1.28] have, however, received little support.

At 515 MeV isovector phases up to and including $\delta(^3H_6)$ are varied[1.32]. Inelasticity in $\delta(^1D_2)$ is allowed, others being set to zero as a reasonable approximation[1.29, 1.30]. Above 450 MeV inelastic processes become very large. Lacking a reasonable way of treating inelasticity no unambiguous isoscalar solutions can be found above 500 MeV (though phase shift analyses have been carried out up to 750 MeV[1.30, 1.31] in this energy region). Isovector phases are certainly judged to be unique below 500 MeV[1.32].

1.2 Two-body scattering theory

The non-relativistic two-body quantum scattering problem as applied to the NN system (in the centre of mass system) can be shown to be equivalent to the scattering of a single particle with reduced mass m (m = M/2, M = Nucleon mass), by a fixed potential V[1.26]. The problem amounts to the solution of Schroedingers equation for $|\psi\rangle$ viz.

$$(E-H^o)|\psi\rangle = V|\psi\rangle \qquad \ldots\ (1.2.1)$$

for all energies E. Defining the Greens operator G(z) and the free Greens operator $G^o(z)$ by

$$G(z) = (z-H)^{-1} \quad G^{o}(z) = (z-H^{o})^{-1} \quad .... \ (1.2.2)$$

for complex energy z, then the relations

$$G = G^{o} + G^{o}VG = G^{o} + GVG^{o} \quad .... \ (1.2.3)$$

hold. These equations are called LIPPMANN-SCHWINGER equations for G(z). The free Greens operator can be explicitly constructed to be

$$G^{o}(z)|\underline{p}> = (z-E)^{-1}|\underline{p}> \quad .... \ (1.2.4)$$

in momentum space, where $E = |\underline{p}|^{2}/2m$. It is possible to further define the T matrix, linearly related to the S matrix, by

$$T(z) = V + VG^{o}(z)\ T(z) \quad .... \ (1.2.5)$$

Matrix elements of this operator are proportional to the amplitude for transitions between basic states. Lippman-Schwinger equations can be iterated to give BORN SERIES, in the limit of "small" potentials. Using the first n terms corresponds to an n^{th} order Born approximation calculation. Explicitly the series is

$$T = V + VG^{o}V + VG^{o}VG^{o}V + ... \quad .... \ (1.2.6)$$

Greens operators are called propagators in modern field theory. The Born series for T can therefore be interpreted as an infinite sum of terms representing interactions with a fixed potential (V) interspersed with free propagation (G^{o}). The usefulness of the T matrix is limited however by the lack of suitable potentials to insert in (1.2.6).

The relationship between symmetry groups and conservation laws is well known[1.33]. It is therefore possible to simplify scattering theory by requiring the T matrix (hence the S matrix) to be invariant under certain physical symmetry operations.

These constraints restrict the possible forms of the T matrix when an attempt is made to explicitly construct the T matrix in the centre of mass (CM), from the available dynamical variables. Moravcsik[1.17] derives the most general form of the M matrix for NN scattering (which up to a normalization constant is the T matrix in the spin space of the two nucleons) if invariance under parity, time reversal, rotations and the extended Pauli principle are assumed. (Tests of the validity of these hypotheses for the NN interaction continually appear in the literature[1.34, 1.35]). If $\underline{k}_i$ and $\underline{k}_f$ are the initial and final CM momenta respectively ($\underline{k}_i = \underline{k}_f$ for elastic scattering) then Moravcsik finds:

$$M(\underline{k}_i,\underline{k}_f) = a+ic[\underline{\sigma}^1.\underline{N}+\underline{\sigma}^2.\underline{N}] + m[\underline{N}.\underline{\sigma}^1\underline{\sigma}^2.\underline{N}]$$
$$+ g[\underline{P}.\underline{\sigma}^1\underline{\sigma}^2.\underline{P} + \underline{K}.\underline{\sigma}^1\underline{\sigma}^2.\underline{K}] +$$
$$+ h[\underline{P}.\underline{\sigma}^1\underline{\sigma}^2.\underline{P} - \underline{K}.\underline{\sigma}^1\underline{\sigma}^2.\underline{K}] \quad .... (1.2.7)$$

where $\underline{N}$, $\underline{P}$ and $\underline{K}$ are unit vectors in the directions $\underline{k}_i \times \underline{k}_f$, $\underline{k}_i + \underline{k}_f$ and $\underline{k}_i - \underline{k}_f$ respectively (figure 1.3.1); a - h are complex scalar amplitudes, having isoscalar and isotriplet components, which depend on E and the CM polar scattering angle (θ_{CM}); $\underline{\sigma}^1$ and $\underline{\sigma}^2$ are the spin operators for the two nucleons.

Unitarity of the S matrix can be incorporated into the formalism by decomposing the S matrix into partial waves. Rotational (isospin) invariance implies the vanishing of matrix elements connecting states of different total angular momentum J (total isospin T). A similar relation holds for all conserved observables. The Extended Pauli Principle requires the wave-function of an NN system to be antisymmetric under interchange of all quantum numbers. Triplet (spin or isospin) states are even

under interchange whilst singlet states are odd. Orbital angular momentum ℓ introduces a factor $(-1)^{\ell}$ and leads to the following classification (of NN states):

a) ISOTRIPLET. SPIN SINGLET. EVEN ANGULAR MOMENTUM ℓ

b) ISOTRIPLET. SPIN TRIPLET. ODD ANGULAR MOMENTUM ℓ

c) ISOSINGLET. SPIN TRIPLET. EVEN ANGULAR MOMENTUM ℓ

d) ISOSINGLET. SPIN SINGLET. ODD ANGULAR MOMENTUM ℓ

Table 1.2.1 illustrates this classification in addition to the decoupling of spin singlet and triplet states due to conservation of parity. Using the spectroscopic notation for a state with total spin S, total orbital angular momentum L and total angular momentum J (designated $^{2S+1}L_J$, where S, P, D ... are used for the values L=0, 1, 2, ...) the only p-p partial waves are seen to be those corresponding to (a) and (b) above, viz.

$$\delta(^1S_0),\ \delta(^3P_{0,1,2}),\ \delta(^1D_2),\ \delta(^3F_{2,3,4}),\ \delta(^1G_4),$$

$$\delta(^3H_{4,5,6}),\ \ldots. \qquad \ldots. \quad (1.2.8)$$

as this system appears only in the isotriplet (T = 1) state. The S matrix becomes block diagonal having submatrices of dimension two (coupling triplet states with the same J but different L) and one. Unitary two dimensional matrices have three degrees of freedom. The most usual parametrization is in terms of the nuclear bar phase shifts and mixing parameters[1.12]; $\bar{\varepsilon}_2$ for $^3P_2 - {}^3F_2$, $\bar{\varepsilon}_4$ for $^3F_4 - {}^3H_4$, etc.

DIVIDING LINE	CONSERVATION LAW WHICH DECOUPLES THE STATES
═══	CONSERVATION OF ISOSPIN & PAULI PRINCIPLE
═══	CONSERVATION OF PARITY
|	CONSERVATION OF TOTAL ANGULAR MOMENTUM

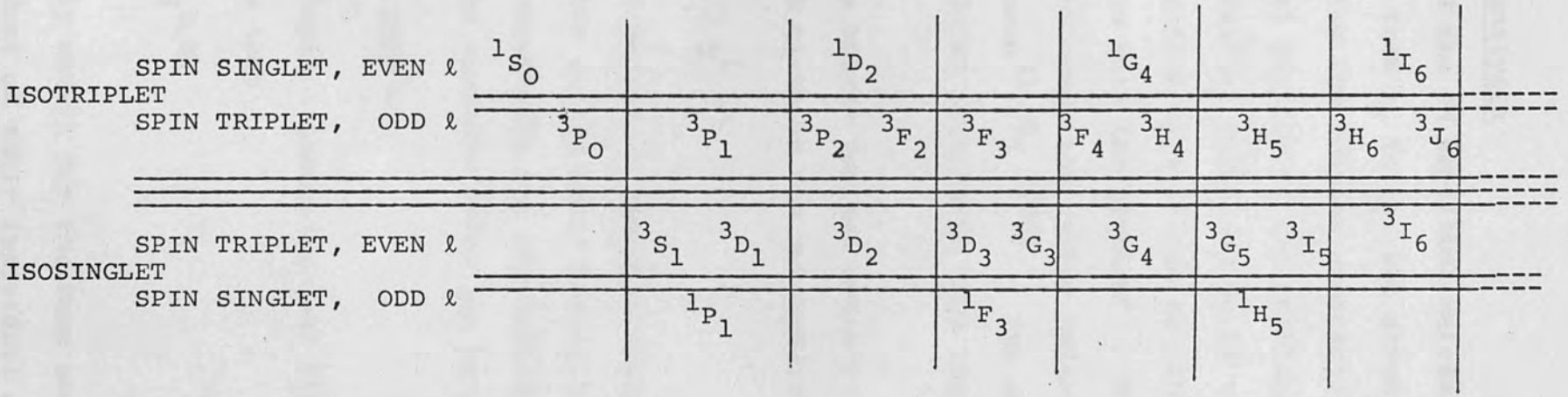

TABLE 1.2.1 Classification of NN states (spectroscopic notation)

1.3 Polarization analysis

In section 1.2 the CM amplitude matrix $M(\underline{k}_i, \underline{k}_f)$ for N-N elastic scattering, from $\underline{k}_i$ to $\underline{k}_f$, was given. We turn now to the problem of determining the complex constants, appearing in M, which contain the essential physics of the problem. To this end a discussion of polarization formalism in NN scattering will follow, finally deriving equation (1.3.18) as an experimentalists' "tool" for "getting to grips with the problem". No proofs of relations used below will be offered, the author believing this material to be fairly well known[1.36, 1.33]. The notation used in this section will be employed throughout this thesis.

A spin density matrix for the primary beam (ρ^b), having spin operator $\underline{\sigma}^b$, is given in the non-relativistic limit by

$$\rho^b = \tfrac{1}{2}(I + \underline{\sigma}^b.\underline{P}^b) \qquad \ldots\ (1.3.1)$$

(where I is the unit matrix in the spin space of the incident proton and $\underline{P}^b$ is known as the axial beam-polarization vector) and leads to a general expression for the expectation value of any observable O over the ensemble described by ρ^b

$$\langle O\rangle^b = Tr(\rho^b O) \qquad \ldots\ (1.3.2)$$

(The notation "Tr" implies summation over the diagonal matrix elements). We note that

$$\underline{P}^b = \langle\underline{\sigma}^b\rangle^b \qquad \ldots\ (1.3.3)$$

A total density matrix for the beam and target may be formed from the direct product of their individual density matrices, viz.

$$\rho^i = \rho^b\rho^t \qquad \ldots\ (1.3.4)$$

The target density matrix reduces to $\frac{1}{2}I$ when the target is unpolarized. The scattered beam density matrix (un-normalized)

$$\rho^s = M\rho^i M^+ \quad \ldots\ldots (1.3.5)$$

can be used in equation (1.3.2) to form expectation values of observables over the scattered beam viz.

$$\langle O \rangle^s = Tr(\rho^s O)/Tr(\rho^s) \quad \ldots\ldots (1.3.6)$$

The normalization factor in the denominator can be shown[1.13] to be the differential cross-section for scattering of polarized beam with CM energy E off an unpolarized target, when no selection occurs on the final spin. Denoting this by $d\sigma^s/d\Omega$ we see that at CM scattering angle θ_{CM} (figure 1.3.1)

$$\frac{d\sigma^s}{d\Omega}(E,\theta_{CM}) = Tr(\rho^s) \quad \ldots\ldots (1.3.7)$$

For unpolarized targets this reduces to

$$\frac{d\sigma^s}{d\Omega} = \tfrac{1}{2}Tr(M\rho^b M^+) \quad \ldots\ldots (1.3.8)$$

Explicitly inserting the form of ρ^b we find

$$\frac{d\sigma^s}{d\Omega} = \tfrac{1}{4}\{Tr(M^+M) + Tr(M\underline{\sigma}^b M^+).\underline{P}^b\} \quad \ldots\ldots (1.3.9)$$

The polarization vector ($\underline{P}^s$) of the scattered beam follows from (1.3.6) to be

$$\underline{P}^s(E,\theta_{CM}) = \frac{Tr(M^+\underline{\sigma}^b M) + Tr(\underline{\sigma}^b M\underline{\sigma}^b.\underline{P}^b M^+)}{Tr(M^+M) + Tr(M\underline{\sigma}^b M^+).\underline{P}^b} \quad \ldots\ldots (1.3.10)$$

If the original beam was unpolarised ($\underline{P}^b = 0$) then

$$\frac{d\sigma^s}{d\Omega}_{unpol.} = I_o = \tfrac{1}{4}\,Tr(M^+M) \quad \ldots\ldots (1.3.11)$$

$$\underline{P}^{s}_{unpol.} = P(E,\theta_{CM})\underline{\eta}^{s} = \frac{Tr(M^{+}\underline{\sigma}^{b}M)}{Tr(M^{+}M)} \quad .... (1.3.12)$$

Conservation of parity restricts $\underline{P}^{s}_{unpol}$ to lie in the direction $\underline{\eta}^{s}$ (figure 1.3.2).

Wolfenstein[1.38] showed how the assumption of time reversal invariance, for N-N scattering, implied

$$Tr(M\underline{\sigma}^{b}M^{+}) = Tr(M^{+}\underline{\sigma}^{b}M) \quad .... (1.3.13)$$

using this in (1.3.12) we find that the differential cross-section can be expressed very concisely as

$$\frac{d\sigma^{s}}{d\Omega} = I(\underline{P}^{b}) = I_{o}(1 + PP^{b}\cos(\phi_{s})) \quad .... (1.3.14)$$

where ϕ_s is the azimuthal angle between $\underline{\eta}^{s}$ and $\underline{P}^{b}$. The quantity $\varepsilon^{s} = PP^{b}\cos(\phi_{s})$ is called the asymmetry of the scatter. Its magnitude varies with both P (the magnitude of the polarization induced by the scatter) and P^{b} (the magnitude of the incident polarization). If, in an initial experiment with known P^{b}, the asymmetry amplitude (henceforth used synonemously with asymmetry)

$$\varepsilon^{s} = PP^{b} \quad .... (1.3.15)$$

is determined then the analysing power (A^{s}) of the scatter is defined to be

$$A^{s}(E,\theta_{CM}) = \frac{\varepsilon^{s}}{P^{b}} \quad .... (1.3.16)$$

For elastic scattering in the NN system this reduces to

$$A^{s}(E,\theta_{CM}) = P(E,\theta_{CM})$$

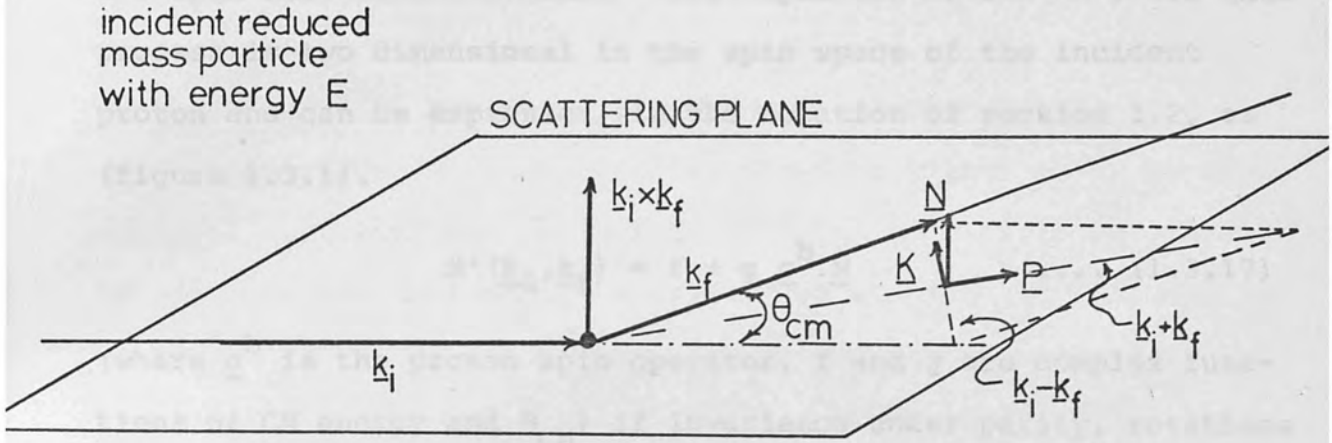

FIGURE 1.3.1 "K,N,P" COORDINATE SYSTEM FOR SCATTERING IN THE CENTRE OF MASS FRAME

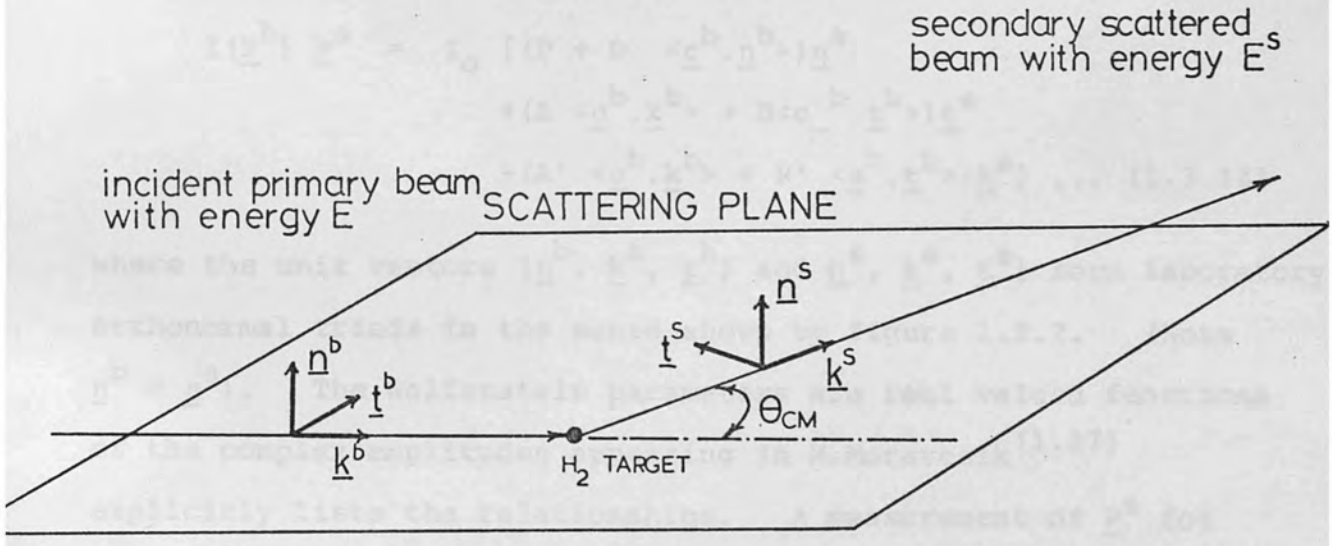

FIGURE 1.3.2 "t,n,k" COORDINATE SYSTEM FOR SCATTERING IN THE LABORATORY FRAME

Formula (1.3.13) is easily verified for protons scattering off spin-zero carbon nuclei. The amplitude matrix (M') for this process is two dimensional in the spin space of the incident proton and can be expressed, in the notation of section 1.2, as (figure 1.3.1).

$$M'(\underline{k}_i,\underline{k}_f) = f + g\ \underline{\sigma}^b.\underline{N} \qquad \ldots. (1.3.17)$$

(where $\underline{\sigma}^b$ is the proton spin operator, f and g are complex functions of CM energy and θ_{CM}) if invariance under parity, rotations and time reversal are required. The treatment following equation (1.3.13) again holds, with the analysing power of carbon being denoted by Ac.

As a final result the expression for the polarization of the scattered beam in terms of the Wolfenstein parameters P, D, A, R, A', R' will be presented. A little algebra turns (1.3.10) into:

$$\begin{aligned} I(\underline{P}^b)\ \underline{P}^s = I_o\ [&(P + D\ \langle\underline{\sigma}^b.\underline{n}^b\rangle)\underline{n}^s \\ &+(A\ \langle\underline{\sigma}^b.\underline{k}^b\rangle + R\langle\sigma\_^b.\underline{t}^b\rangle)\underline{t}^s \\ &+(A'\ \langle\underline{\sigma}^b.\underline{k}^b\rangle + R'\ \langle\underline{\sigma}^b.\underline{t}^b\rangle)\underline{k}^s] \quad \ldots (1.3.18) \end{aligned}$$

where the unit vectors ($\underline{n}^b$, $\underline{k}^b$, $\underline{t}^b$) and ($\underline{n}^s$, $\underline{k}^s$, $\underline{t}^s$) form laboratory orthonormal triads in the sense shown by figure 1.3.2. (Note $\underline{n}^b = \underline{n}^s$). The Wolfenstein parameters are real valued functions of the complex amplitudes appearing in M.Moravcsik[1.17] explicitly lists the relationships. A measurement of $\underline{P}^s$ for known $\underline{P}^b$ therefore constitutes a determination of a linear combination of the parameters P, D, A, R, A' and R'. These parameters satisfy simple relationships if the primary beam spin-average coefficients $\langle\underline{\sigma}^b.\underline{n}^b\rangle$, $\langle\underline{\sigma}^b.\underline{k}^b\rangle$ or $\langle\underline{\sigma}^b.\underline{t}^b\rangle$ are chosen to be 0 or ± 1. Figure 1.3.3 illustrates the measurements necessary to evaluate

individual Wolfenstein parameters when the primary beam polarization has been arranged to give simple values for the coefficients

Hanna[1.37] has dealt simply with the methodology of polarization measurements. For a given detector system error on the measured asymmetry can be minimized if it is possible to reverse the sign of the incident polarization in addition to reducing it to zero. These conditions are easily met in practise, during individual A, R, A' or R' measurements, by aptly arranging the orientation of the primary beam polarization. The D parameter, however, relies on the precise measurement of two linear combinations of the P and D parameters. Values for the parameters lie in the range -1 to +1 and they are therefore seen to be a measure of the change in polarization brought about by scattering a polarized primary beam from an unpolarized target.

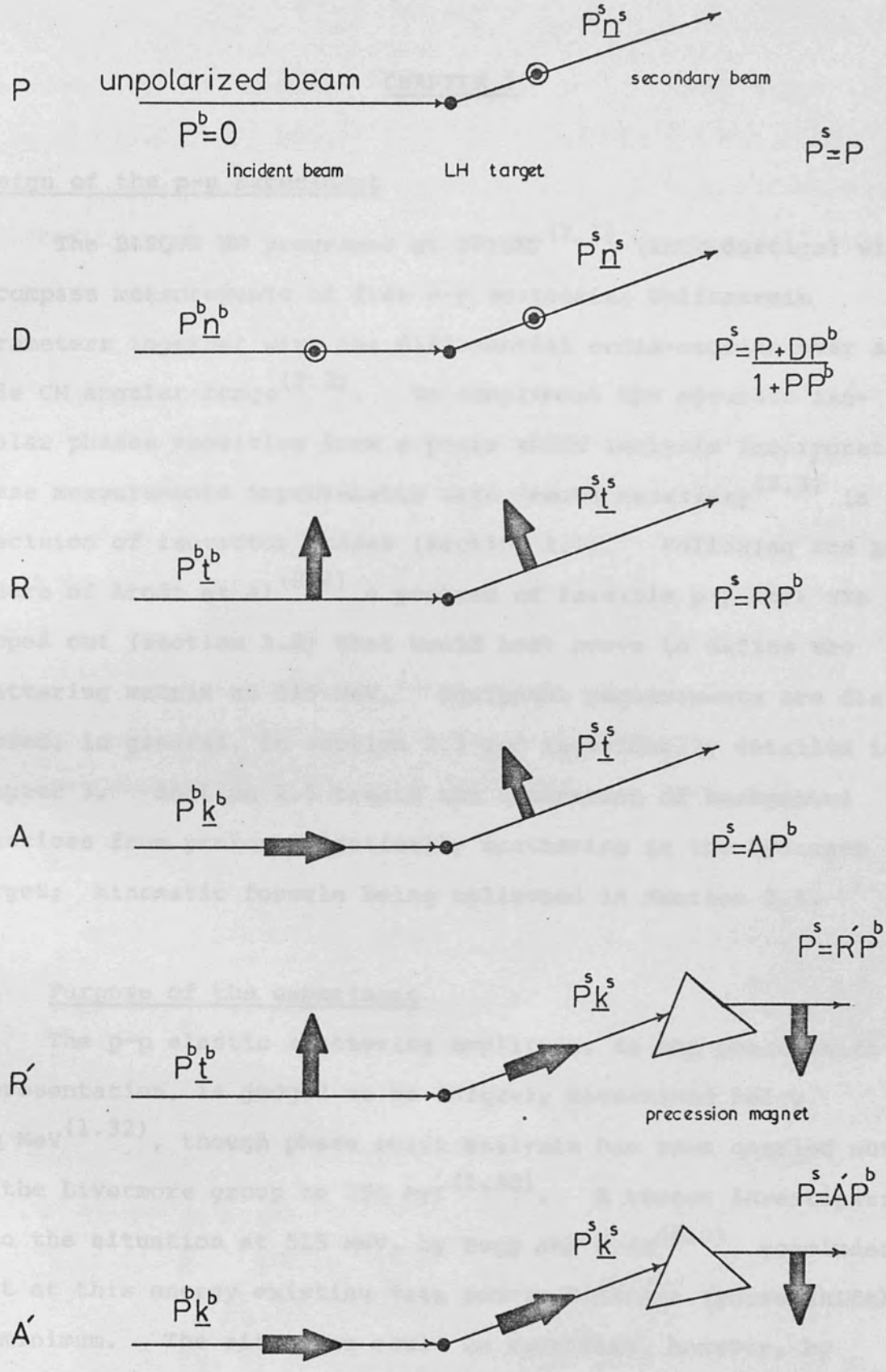

FIGURE 1.3.3 POLARIZATION MEASUREMENTS THAT DETERMINE WOLFENSTEIN PARAMETERS

CHAPTER 2

Design of the p-p Experiment

The BASQUE NN programme at TRIUMF[2.1] (introduction) will encompass measurements of free n-p scattering Wolfenstein parameters together with the differential cross-section over a wide CM angular range[2.2]. To compliment the accurate isoscalar phases resulting from a phase shift analysis incorporating these measurements improvements were deemed necessary[2.3] in the precision of isovector phases (section 2.1). Following the procedure of Arndt et al[2.4] a program of feasible p-p work was mapped out (section 2.2) that would best serve to define the scattering matrix at 515 MeV. Equipment requirements are discussed, in general, in section 2.3 and individually detailed in Chapter 3. Section 2.5 treats the separation of background reactions from protons elastically scattering in the hydrogen target; kinematic formula being collected in section 2.4.

2.1 Purpose of the experiment

The p-p elastic scattering amplitude, in the phase shift representation, is judged to be uniquely determined below 500 MeV[1.32], though phase shift analysis has been carried out by the Livermore group to 750 MeV[1.30]. A recent investigation into the situation at 515 MeV, by Bugg and Oram[2.5], concludes that at this energy existing data poorly define a (phase shift) χ^2 minimum. The situation could be rectified, however, by precision measurements of Wolfenstein parameters P, D, R at 6, 15 and 24 degrees lab. (table 2.1) where little or no data exists[2.6,2.7]. Further reduction of the phase shift errors could be obtained by measurements of R' at 15 degrees and PDR over

the centre of mass range 65-115 degrees in 10 degree steps. An accuracy of 0.017 was assumed for P; 0.025 for all other Wolfenstein parameters, with a common normalization having an uncertainty of 0.025: only experiments in the range 0-27 degrees lab. were feasible (section 3.2.3).

This series of pp measurements were designed (section 2.2) to compliment the np work now being carried out at TRIUMF. It was intended that the error associated with each pp partial wave be reduced to an equivalent level as is planned to be obtained from a phase shift analysis of the np data[2.2]. Figures 2.1.1-2.1.4 show the predicted values of P, D, R, R' over the centre of mass region 0-120 degrees together with their error from phase shift analysis. Plotted on these graphs are some of the only existing measurements:

1. P at 498 $\pm$ 11 MeV by CHENG[2.8] over 33-82 degrees CM (not plotted).
2. P at 498 $\pm$ 11 MeV by CHENG[2.8] over 33-82 degrees CM (not plotted).
3. P at 500 $\pm$ 8.3 MeV by ALBROW[2.9] over 36-90 degrees CM (not plotted).
4. P at 500 $\pm$ 4.2 MeV by COZZIKA[2.10] over 34-93 degrees CM (not plotted).
5. P at 520 $\pm$ 20 MeV by SURKO[2.11] over 35-118 degrees CM.
6. D at 520 $\pm$ 20 MeV by SURKO[2.11] over 35-118 degrees CM.
7. R at 520 $\pm$ 20 MeV by LEUNG[2.12] over 35-118 degrees CM.
8. R' at 520 $\pm$ 20 MeV by LEUNG[2.12] over 35-118 degrees CM.
9. P at 530 MeV by AEBISCHER[1.27] over 0-24 degrees CM (not plotted).

The D, R and R' experiments described in this thesis extend the measurements of SURKO and LEUNG to move forward angles where

no data presently exist whilst those of P fall midway between and overlap the small angle measurements of AEBISCHER and the large angle measurements, which (arbitrarily) start at ∿35 degrees CM. Measurements in this region serve to constrain the large errors on the low partial waves[2.5].

2.2 Selection of observables

Following the procedure suggested by Arndt[2.4] single energy phase shift analyses were carried out at 200, 320, 380, 425 and 515 MeV. The data base was similar to that of Arndt et al[1.32] but incorporated the recent Maryland cross-section data[2.13] and Geneva small angle polarization measurements[1.27]. Phases were found that minimised a χ^2 goodness of fit function: initial conditions being the use of phases from Arndt (reference 1.32) as reasonable starting values for the search. Phases up to and including $^3H_6$ were varied, higher waves being fixed at OPEC values. Inelasticity was allowed in $^3P_1$ at 320 MeV and $^1D_2$ in all higher energies (see section 1.1 for further details).

The full ERROR MATRIX was available for assessing the uncertainty on each phase (diagonal elements) and correlations between phases (off diagonal elements). An augmented error matrix (modified as described by Arndt[2.4]) was determined after the addition of proposed experiments to the data base. It was then possible to list the predicted values of any observable over the CM angular range 10-170 degrees (calculated from the phases that minimised χ^2) and its error (calculated from the augmented ERROR MATRIX). Predicted error on any one observable was found to oscillate with CM angle. Choosing to measure an observable at an angle where predictions were softest (had largest predicted

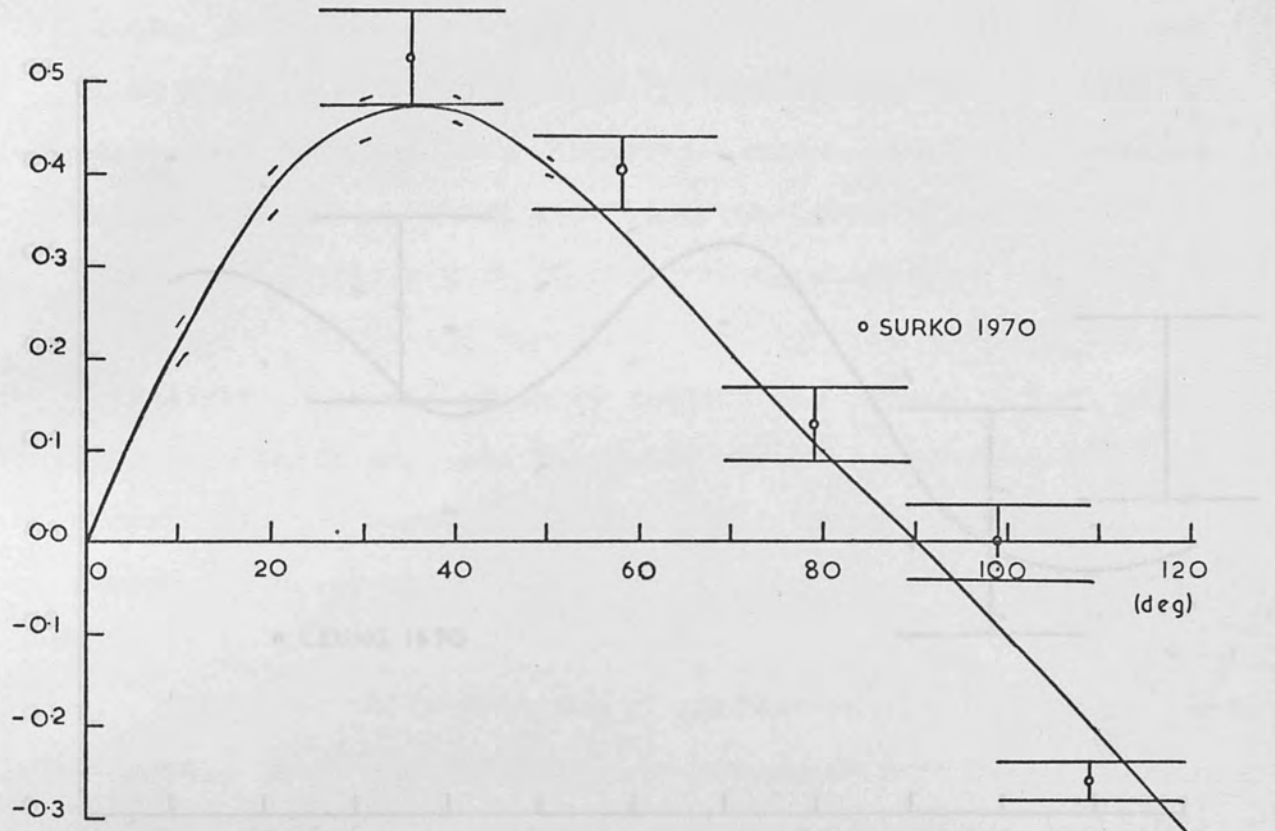

FIGURE 2·1·1 PHASE SHIFT PREDICTION OF P IN P-P SCATTERING AT 515MeV.

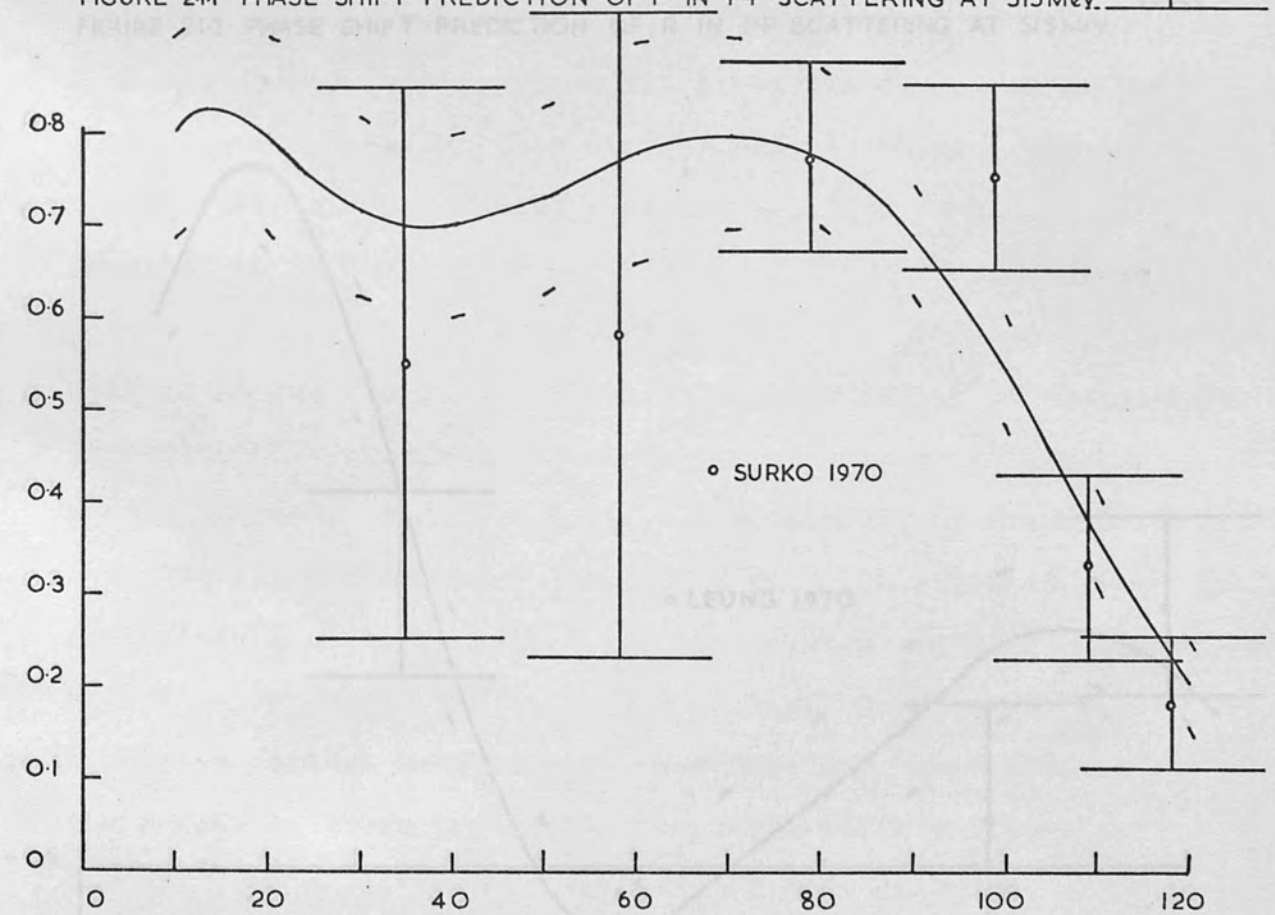

FIGURE 2·1·2 PHASE SHIFT PREDICTION OF D IN P-P SCATTERING AT 515 MeV
(& predicted error)

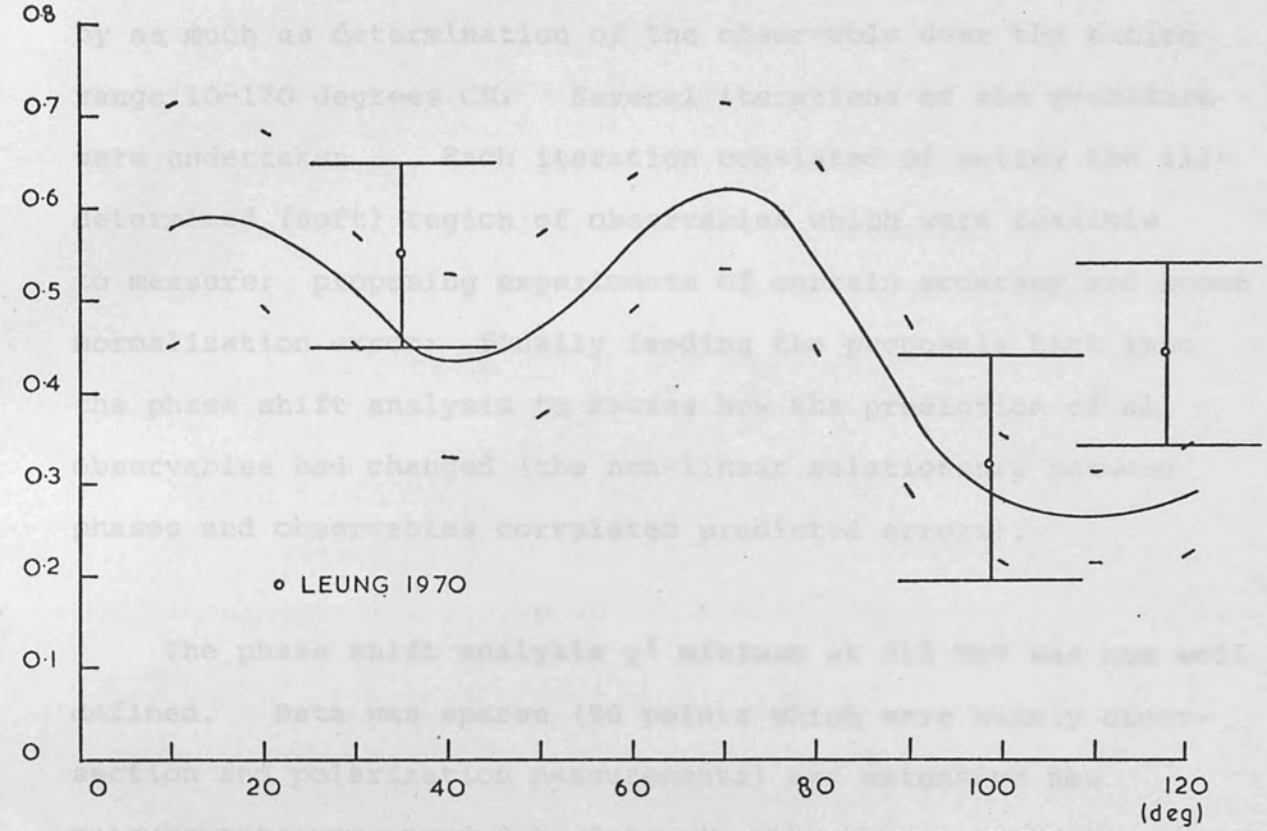

FIGURE 2·1·3 PHASE SHIFT PREDICTION OF R IN P-P SCATTERING AT 515 MeV

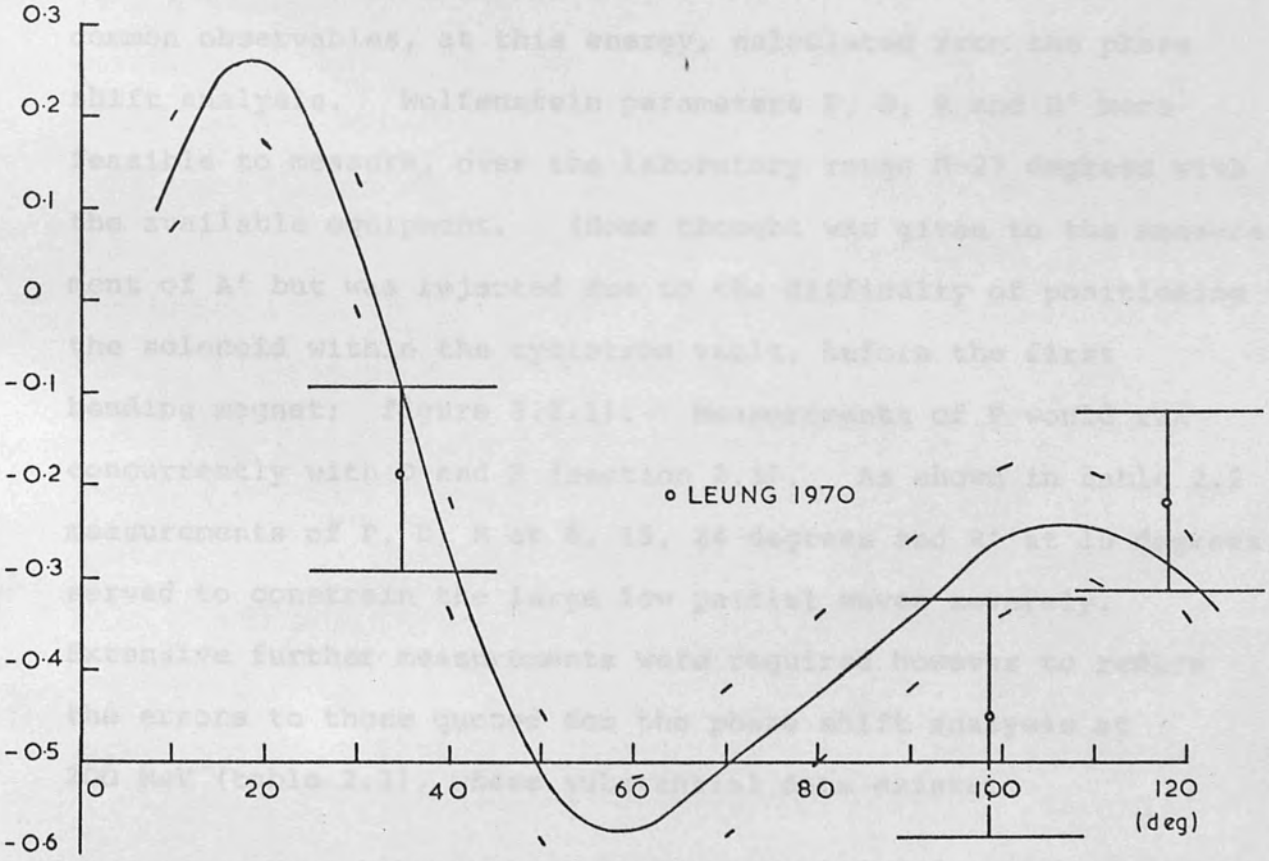

FIGURE 2·1·4 PHASE SHIFT PREDICTION OF R' IN P-P SCATTERING AT 515 MeV

errors) served to constrain phase shift errors: in some cases by as much as determination of the observable over the entire range 10-170 degrees CM. Several iterations of the procedure were undertaken. Each iteration consisted of noting the ill-determined (soft) region of observables which were feasible to measure; proposing experiments of certain accuracy and known normalization error; finally feeding the proposals back into the phase shift analysis to assess how the prediction of all observables had changed (the non-linear relationship between phases and observables correlated predicted errors).

The phase shift analysis χ^2 minimum at 515 MeV was not well defined. Data was sparse (96 points which were mainly cross-section and polarization measurements) and extensive new measurements were needed to determine the phases to better than 1 degree (table 2.2). Table 2.1 lists the errors on some common observables, at this energy, calculated from the phase shift analysis. Wolfenstein parameters P, D, R and R' were feasible to measure, over the laboratory range 0-27 degrees with the available equipment. (Some thought was given to the measurement of A' but was rejected due to the difficulty of positioning the solenoid within the cyclotron vault, before the first bending magnet; figure 3.2.1). Measurements of P would run concurrently with D and R (section 2.3). As shown in table 2.2 measurements of P, D, R at 6, 15, 24 degrees and R' at 15 degrees, served to constrain the large low partial waves severely. Extensive further measurements were required however to reduce the errors to those quoted for the phase shift analysis at 200 MeV (table 2.3), where substantial data exists.

In keeping then with the philosophy of Arndt et al a set of feasible experiments had been determined which best served to define the p-p scattering matrix at 515 MeV. These were:

a) D, R at 6, 15, 24 degrees lab. to an accuracy of $\pm$ 0.025.

b) P at 6, 15, 24 degrees lab. to an accuracy of $\pm$ 0.017.

c) R' at 15 degrees lab. to an accuracy of $\pm$ 0.025.

having a common normalization with uncertainty $\pm$ 0.025.

2.3 Equipment requirements

This section briefly describes the more important items (and conditions) necessary to perform the measurements proposed in section 2.2.

A proton target can be formed by filling a thin walled flask with liquid hydrogen. Primary beam protons will scatter in the target and emerge through suitable concrete shielding surrounding the target, into an experimental area where measurements are to be made. A polarimeter is required to measure the polarization produced in the scattered beam. This is accomplished by observing the asymmetry generated by scattering the secondary beam from a target which has a known analysing power. Carbon is a suitable element in the proton energy range (200-500 MeV) available from TRIUMF, being easy to handle, having a measurable analysing power and a large amount of calibration data exist in the literature (for reference purposes only as our polarimeter was to be calibrated in a separate experiment).

Hanna[1.37] has shown how systematic errors in the determination of an asymmetry can be minimised by reversing the sign

Angle (c.m. deg)	$\delta\sigma/\sigma$	δP	δD	δR	δA	$\delta R'$	$\delta A'$	δC_{KP}	δC_{NN}	δC_{KK}	δC_{PP}	δA_{XX}	δA_{ZZ}	δA_{ZX}
10	0.101	0.019	0.068	0.121	0.077	0.073	0.165	0.143	0.193	0.267	0.209	0.290	0.200	0.123
20	0.052	0.031	0.069	0.066	0.097	0.105	0.046	0.179	0.066	0.078	0.226	0.117	0.182	0.189
30	0.036	0.027	0.098	0.060	0.084	0.091	0.037	0.131	0.094	0.083	0.141	0.070	0.125	0.142
40	0.015	0.013	0.103	0.094	0.103	0.095	0.046	0.107	0.098	0.100	0.089	0.085	0.125	0.098
50	0.012	0.009	0.116	0.096	0.099	0.101	0.057	0.118	0.127	0.104	0.091	0.082	0.163	0.090
60	0.011	0.006	0.117	0.088	0.073	0.083	0.050	0.121	0.124	0.072	0.095	0.083	0.184	0.055
70	0.011	0.004	0.106	0.087	0.078	0.078	0.070	0.140	0.111	0.046	0.091	0.117	0.192	0.027
80	0.011	0.003	0.092	0.100	0.086	0.079	0.096	0.196	0.130	0.039	0.100	0.162	0.258	0.017
90	0.019	0.000	0.069	0.096	0.097	0.085	0.109	0.231	0.149	0.074	0.074	0.185	0.301	0.000
100			0.058	0.071	0.104	0.082	0.099							
110			0.055	0.049	0.101	0.061	0.083							
120			0.048	0.073	0.104	0.043	0.100							
130			0.052	0.109	0.094	0.035	0.122							
140			0.084	0.117	0.093	0.050	0.120							
150			0.109	0.163	0.123	0.053	0.141							
160			0.095	0.219	0.192	0.111	0.172							
170			0.089	0.152	0.174	0.197	0.128							

TABLE 2.1 Predicted error on some common observables at 515 MeV

Data	$^3P_0$	$^1S_0$	$^3P_1$	$^3P_2$	$\bar{\varepsilon}_2$	$^3F_2$	$^1D_2$	$^3F_3$	$^3F_4$	$\bar{\varepsilon}_4$	$^3H_4$	$^1G_4$	$^3H_5$	$^3H_6$
W	19.2	35.8	8.77	1.53	9.09	2.12	23.6	3.55	0.54	2.00	1.10	4.49	1.36	0.40
W + PDR(13,33,53 deg)	6.33	5.50	2.88	0.62	1.32	0.42	4.60	0.47	0.37	0.56	0.35	1.21	0.31	0.17
Ditto + R'(33 deg)	5.87	5.33	1.94	0.52	1.32	0.40	3.10	0.45	0.16	0.45	0.25	0.99	0.31	0.16
Ditto + PDR(65-115 deg, 10 deg steps) = X	0.87	1.04	0.50	0.33	0.65	0.16	2.29	0.31	0.12	0.095	0.15	0.23	0.15	0.11
X + A'(13,33,53 deg)	0.71	0.98	0.39	0.19	0.51	0.12	1.56	0.24	0.086	0.089	0.097	0.20	0.10	0.072
X + $d\sigma/d\Omega$(10-90 deg, 5 deg steps) = Y	0.62	0.78	0.28	0.17	0.47	0.072	1.31	0.21	0.035	0.075	0.059	0.17	0.066	0.028
Ditto + C_{NN}(30-90 deg, 10 deg steps) = Z	0.52	0.46	0.27	0.11	0.17	0.069	0.44	0.19	0.025	0.045	0.041	0.087	0.059	0.027
Y + A(65-115 deg, 10 deg steps)	0.58	0.75	0.25	0.10	0.22	0.053	0.58	0.16	0.028	0.058	0.045	0.14	0.051	0.024
Z + C_{KP}(90 deg)	0.51	0.46	0.26	0.10	0.13	0.063	0.39	0.19	0.025	0.040	0.041	0.087	0.058	0.027
Ditto + R(160 deg)	0.48	0.44	0.24	0.096	0.068	0.060	0.17	0.14	0.022	0.024	0.041	0.042	0.013	0.025

TABLE 2.2 Diagonal elements of the error matrix (degrees^2) at 520 MeV as a function of adding proposed experiments to the data base $\delta P = \pm 0.017$, all others ± 0.025)

Data	$^3P_0$	$^1S_0$	$^3P_1$	$^3P_2$	$\bar{\varepsilon}_2$	$^3F_2$	$^1D_2$	$^3F_3$	$^3F_4$	$\bar{\varepsilon}_4$	$^3H_4$	$^1G_4$	$^3H_5$	$^3H_6$
W	0.264	0.272	0.042	0.028	0.016	0.059	0.078	0.031	0.027	0.007	0.050	0.010	0.035	0.022

TABLE 2.3 Diagonal elements of the error matrix (degree^2) at 200 MeV

of the incident polarization. Wolfenstein parameter measurements therefore require the use of a high quality polarized beam and the ability to reverse its polarization. Formula (1.3.18) shows that secondary beam polarization components reverse in sign when the primary beam lies in the scattering plane and itself reverses in sign. This is suitable for R and R' (A and A' also) measurements but for D and P measurements, when the primary beam polarization is normal to the scattering plane, reversing the polarization allows two linear combinations of P and D to be measured; hence each can be determined.

Reversing the primary beam polarization could be carried out by our superconducting solenoid, but this solution is both too costly (in terms of liquid helium consumption) and time-consuming (a large inductance must be reversed slowly). A solenoid is required however to precess the primary beam polarization about the beam-line to desired angles (usually $\pm$ 90 degrees from the vertical at TRIUMF): reversal of the polarization at source exactly reverses the beam polarization incident on the hydrogen target leaving only a possibly systematic error in the precession angle to be determined. The line integral of the magnetic field through the solenoid has to be known therefore to better than 1% to keep the systematic error from this uncertainty below the statistical error level.

Measurements of P & R or P & D can be undertaken simultaneously (P & R' also if a precession magnet is available in the secondary beam-line) if the vertical and horizontal components of the secondary beam are determined together. Viewing the

carbon analyser with multiwire proportional chambers allows both the polar angle (θ_s) and azimuthal angle (ϕ_s) of protons scattering in the carbon, to be determined. The expected azimuthal distribution of these protons is determined by equation (1.3.14) and the method for deducing the required asymmetries is discussed in section 5.2. A factor appearing in this equation is the primary beam polarization. This quantity must be reliably determined as it feeds directly into the calculations of P, D, R and R' as a common normalization factor and leads to a systematic error in the determination of these parameters. Scintillator telescopes viewing primary beam scattering from hydrogen in a thin CH_2 target are simply constructed to accept high rates of elastic events, though corrections to the observed asymmetry are necessary before the true beam polarization is deduced (section 5.3.1).

2.4 Two-body kinematics

In section 1.3 it was noted that the analysing power of a reaction was a function of the incident beam energy and polar angle of scatter in the analyser. Proton-proton Wolfenstein measurements at a particular laboratory scattering angle in the hydrogen target therefore had to use the analysing power of carbon corresponding to the scattered protons' energy in the polarimeter. Allowances were made for proton energy loss, whilst traversing the secondary beam-line, to the centre of the carbon analyser. This included degradation of the proton's energy in the hydrogen target, air, scintillators, multiwire proportional chambers and 30 mm of carbon analyser.

The kinematics of relativistic two-body scattering are well

known[2.14] (Appendix E). Laboratory scattering angle in the target (θ_s) was related to the beam kinetic energy (T_b), the scattered beam's initial kinetic energy T_s) and the mass of the proton (M_p) by:

$$\cos(\theta_s) = \sqrt{\frac{T_b + 2M_p}{T_b}} \sqrt{\frac{T_s}{T_s + 2M_p}} \quad \ldots\ (2.4.1)$$

(illustrating the one to one correspondence between θ_s and T_s for given T_b, which characterises two-body scattering). This simple formula allowed initial values for the kinetic energy of the scattered beam to be computed at each laboratory angle.

The time-of-flight (τ) of scattered protons over a path length L was given by:

$$\tau = 3.333L \frac{(T_s + M_p)}{\sqrt{T_s(T_s+2M_p)}} \text{ nanoseconds} \quad \ldots\ (2.4.2)$$

Small changes ($\Delta\tau$) in τ were related to small changes (ΔT_s) by:

$$\Delta\tau = \frac{-\tau}{\alpha\ (1+\alpha)(2+\alpha)}\ \Delta\alpha \quad \ldots\ (2.4.3)$$

where the dimensionless parameter α was given by $\alpha = T_s/M_p$. The "energy resolving power" ($\Delta\alpha$) of a time-of-flight system is thus seen to be linearly related to the time-of-flight acceptance "bite" ($\Delta\tau$) for fixed τ. Evidently long time-of-flights give better energy resolution. This formula has been used when deriving conclusions about the separation of inelastic reactions from elastic p-p scattering in section 2.5.

2.5 Background separation

Above the pion production threshold (290 MeV kinetic energy for protons on hydrogen) the following inelastic reactions were considered as background for the Wolfenstein experiments and polarimeter calibration.

$$pp \rightarrow np\pi^+ \quad - (1)$$
$$\rightarrow d\pi^+ \quad - (2)$$
$$\rightarrow pp\pi^o \quad - (3)$$

Inelastic protons from (1) and (3) have a polarization differing from that of pp elastic scattering; whilst pions from (1) and (2), being spin zero particles, decrease the observed asymmetry in the polarimeter by scattering uniformly in ϕ_s (equation 1.3.14). Attempts had to be made therefore to separate this background else systematic errors in the asymmetry determination would have arisen.

An N-Body Phase Space program was used to produce distributions of phase space as a function of the laboratory scattering angle and time-of-flight (TOF) of a given particle. Figure 2.5.1 shows this distribution for inelastic protons from (1) and (3); well separated from elastic events at large angles. At all angles inelastic protons would have an energy difference of at least 70 MeV (half the pion mass). Formulae 2.4.1 and 2.4.3 show that a resolution of 3 nanoseconds was adequate to separate these protons down to 6 degrees, for all TRIUMF beam energies, over a path length of 7.5m.

Pions from the two body reaction (2) have a shorter TOF than

elastically scattered protons (for the same beam energy). As the deuteron breaks up and carries off more of the available momentum the pions "smear" themselves across the elastic peak, forming the characteristic three body TOF spectrum. Those pions falling within the 3 nanosecond "resolution bite" about the elastic peak had a very much lower momentum (due to their mass). They were separable from the protons by applying a small magnetic field from a beam-line steering magnet to the scattering beam. The field was chosen to allow the polarimeter to resolve deflected pions and essentially undeflected protons (section 5.1.2) whose bend angles, for the same TOF, were in the ratio 7 (their mass ratio).

Although it is possible to evaluate three body phase space analytically, a short digression will be undertaken on the evaluation of the general N-body phase space integral to show the complexity of its evaluation and its usefulness in planning experiments. Lorentz invariant phase space for N bodies is given by[2.14]

$$R_N(P;\ m_1,\ldots,m_N) = \int_{-\infty}^{\infty}\cdots\int_{-\infty}^{\infty} \prod_{i=1}^{N} \delta(p_i^2-m_i^2)\,d^4p_i\ \ \delta^4\Big(\sum_{j=1}^{N} p_j - P\Big) \qquad \ldots\ (2.5.1)$$

where p_i and m_i are the four momentum and mass of the i^{th} particle respectively and P is the total 4 momentum available for the reaction. This formula describes the phase space availabe to the reaction

$$(A) + (B) \rightarrow (1) + (2) + (3) + \ldots + (N) \qquad \ldots\ (2.5.2)$$

(quantities in brackets refer to particle labels, A and B are destroyed in the reaction). Particles are constrained to the mass shell ($p_i^2 = m_i^2$) and conserve four momentum ($P = \sum_j p_j$).

Separating out the N^{th} integration and performing the integral over the energy, we find the recurrence relation

$$R_N(P;m_1,\ldots m_N) = \int_{-\infty}^{\infty} \frac{d^3p_N}{2\,E_N} R_{N-1}(P-p_N;\, m_1,\, \ldots,\, m_{N-1}) \quad .. \quad (2.5.3)$$

Using Lorentz invariance to evaluate R_N in the CM frame (centre of mass) $P = (E,\underline{O})$ and R_{N-1} in the frame where

$$P-p_N = (\varepsilon,\underline{O})$$

i.e. $$\varepsilon^2 = (E-E_N)^2 - |\underline{p}_N|^2 \quad .... \quad (2.5.4)$$

then

$$R_N(E;m_1,\ldots,m_N) = \int_{-\infty}^{\infty} \frac{d^3p_N}{2\sqrt{\underline{p}_N^2 + m_N^2}} R_{N-1}(\sqrt{E^2+m_N^2-2E\sqrt{\underline{p}_N^2+m_N^2}};m_1,\ldots m_{N-1})$$

This integral can be numerically integrated starting from the phase space for one particle:

$$R_i(E;m_1) = \delta(E-m_1)/2m_1 \quad .... \quad (2.5.5)$$

or (2.5.1) can be estimated directly by Monte Carlo methods.

The probability distribution for particle r making an angle β with particle s is given by

$$w(\beta)d\beta = \frac{1}{R_N} \int_{-\infty}^{\infty} \prod_{i=1}^{N} \delta(p_i^2-m_i^2)d^4p_i\ \delta^4\left(\sum_{j=1}^{N} p_j - P\right) \quad .... \quad (2.5.6)$$

$$\times\ \delta\left(\cos(\beta) - \frac{E_rE_s - p_rp_s}{|\underline{p}_r|\,|\underline{p}_s|}\right) \sin(\beta)d\beta$$

as can be seen by integrating the right hand side over all β. Similar relationships can be written down for invariant mass distributions of groups of particles, TOF versus laboratory scattering angle, etc. Deriving these distributions from phase space integrals give results which would occur only if kinematics completely determined all properties of reaction (2.5.2). (This is equivalent to saying that the T matrix elements for reaction 2.5.2 were unity). Dynamic effects show up above the "kinematic background" (e.g. in the discovery of the ρ meson) and can be immediately identified.

Re-iterating then, the use of phase space in this experiment was to provide TOF vs. laboratory scattering angle distributions for those particles coming from background reactions. Knowledge of the dynamics was unimportant as the results were only to aid in deriving suitable methods for separating the background reactions from elastic p-p scattering.

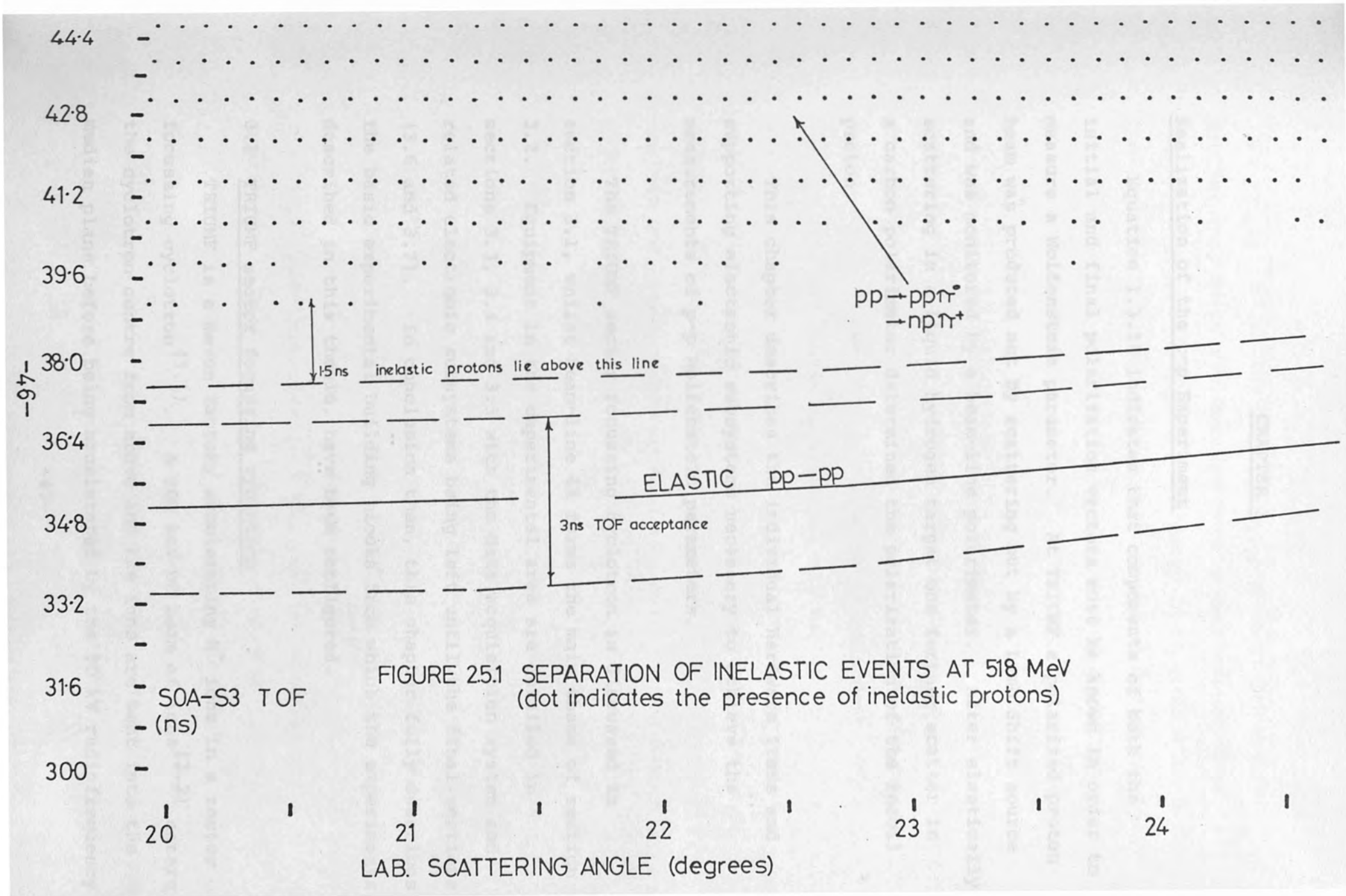

FIGURE 2.5.1 SEPARATION OF INELASTIC EVENTS AT 518 MeV
(dot indicates the presence of inelastic protons)

CHAPTER 3

Realization of the p-p Experiment

Equation 1.3.18 indicates that components of both the initial and final polarization vectors must be known in order to measure a Wolfenstein parameter. At TRIUMF a polarized proton beam was produced not by scattering but by a Lamb Shift source and was monitored by a beam-line polarimeter. After elastically scattering in a liquid hydrogen target one further scatter in a carbon polarimeter determined the polarization of the recoil proton.

This chapter describes the individual hardware items and supporting electronic subsystems necessary to achieve the measurements of p-p Wolfenstein parameters.

The TRIUMF sector focussing cyclotron is discussed in section 3.1, whilst beam-line 4A forms the main theme of section 3.2. Equipment in the experimental area are detailed in sections 3.3, 3.4 and 3.5 with the data acquisition system and related electronic subsystems being left until the final sections (3.6 and 3.7). In conclusion then, this chapter fully describes the basic experimental building blocks from which the experiments, described in this thesis, have been configured.

3.1 TRIUMF sector focussing cyclotron

TRIUMF is a meson factory accelerating H^- ions in a sector focussing cyclotron[3.1]. A 300 keV DC beam of ions[3.2] enters the cyclotron centre from above and the ions are bent into the median plane before being accelerated by the 90 kV radiofrequency

(RF) supply[3.3]. The phase acceptance is 40 degrees and implies that 9% of the injected beam is accelerated after injection, with 7% reaching full energy if no extraction occurs. The 2% loss in the cyclotron can be accounted for by residual-gas stripping the H^- ions at low energies and Lorentz stripping at the highest energy.

The magnetic field[3.4] has been sculpted to give isochronous orbits for a fixed RF frequency and main magnet current. Hence an "almost continuous" beam can be extracted over the entire energy range of the machine. The macroscopic duty factor is usually 100% whilst the microscopic duty factor is 12%: a 5ns pulse every 43ns. One of the most useful features of TRIUMF is the ability to simultaneously extract two beams of differing intensity and energy. This property allows users to operate completely independent of each other in the Proton and Meson Halls.

Figure 3.2.1 illustrates the present experimental areas. The Proton Hall and Meson Hall have been build on opposite sides of the cyclotron. At present two beams are extracted (one for each area) by lowering 25μm aluminium foils into the median plane of the cyclotron. The foil strips off two electrons from each H^- ion and the H^+ ion leaves the machine automatically, entering the first beam-line element if the foil has been correctly positioned. From early 1976 TRIUMF was able to provide both polarized and unpolarized beam over the energy range 180-520 MeV. The polarized beam is provided by a Lamb Shift[3.9] source and polarizations of 80% have been measured in the experimental areas.

The energy resolution (ΔE) of TRIUMF has been determined as follows[3.1]:

1. Measurements within the tank (at the 70 MeV beam radius) indicate the beam is centred to 3.8 ± 2.5mm and the radial betatron amplitude is approximately 17.9mm. Further measurements at the 500 MeV radius confirm this centring accuracy and assuming no change in the betatron amplitude a ΔE of 3.5 MeV should be observed.

2. Beam-line 4B in a dispersive mode (at 500 MeV) gave ΔE = 3 MeV full width.

3. An extracted 400 MeV beam was scattered from a polyethylene target and the recoil protons' total energy measured. A ΔE of 3 MeV full width at half maximum (FWHM) was observed.

Assuming the precise centring of the beam in the machine, nominal extraction energies are determined from the stripping foil position.

The cyclotron main magnet consists of six identical sectors each weighing 610 metric tonnes, driven by a common coil of 30 turns. The regions between the sectors are known as valleys. Its complete upper half can be raised to allow access to the vacuum tank. Wound on the top and bottom of the horizontal vacuum tank are 54 concentric trim coils and 13 sets of harmonic coils per sector. These can be excited to raise or lower the beam in the machine, modify the phase acceptance or correct the

main magnet field to achieve isochronous orbits. The gap between the upper and lower sections is 530mm and the vacuum tank radius is 8.13 metres. The main magnet excitation of 18,500 A is regulated to 5 parts in 10^8 over 8 hours.

Mounted along a vacuum tank diameter are 80 resonators that act as quarter wavelength cavities at 23.05 MH_z. To minimise gas stripping, a vacuum of 2-3 x 10^{-7} torr is maintained. Hydrogen gas forms the principle constituent of this residual pressure. This vacuum allows a nominal RF voltage of 90 kv regulated to 2.5 parts in 10^5 with a frequency held to 7.5 parts in 10^8. The total RF power dissipation is 1.2 MW.

3.2 Beam-line 4A

Figure 3.2.1 shows the general layout of beam-lines at TRIUMF in both the Proton and Meson Halls. Quadrupoles are shaded whilst other beam-line elements are clear.

Research in the Proton Hall will be mainly in the fields of Nucleon Nucleon and Nucleon Nucleus physics. Beam-line 4A was designed therefore to transport up to 10μA of unpolarized or 0.1μA of polarized beam to this experimental area, over the entire energy range of TRIUMF (180-520 MeV). A liquid H_2/D_2 target (section 3.2.3) installed in the beam-line widens the scope of possible experiments by providing a source of polarized protons or neutrons from polarized beam. The beam polarization vector may be rotated about the beam-line axis by a super-conducting solenoid positioned upstream of the target (section 3.2.2). Heavy shielding surrounds the target assembly in anticipation of

neutron experiments. A 25 ton lead-steel collimator (section 3.2.4) rests on 30cm cubic steel blocks and is itself overlain by steel and concrete shielding. Scattered particles from the target enter the main experimental area through the collimator over the laboratory angular range -3 to +27 degrees, in 3 degree steps. Unscattered protons are taken to the 10μA beam dump situated in the north-west corner of the Proton Hall.

The beam-line was installed during summer and autumn of 1974 in preparation for the first extraction of beam, from the cyclotron, at Christmas. Shielding was specifically designed to allow access to the target assembly (figure 3.2.3.1) and for the solenoid to be removed.

3.2.1 Beam transport

A proton beam was extracted from valley 4 of the cyclotron and steered into the first arm of beam-line 4A by the combination magnet. This magnet corrected for the energy dependent exit angles of the beam as it curved out of the machine from the stripping foil. Higher excitation currents were required at lower energies.

A singlet and doublet of quadrupoles focussed the beam before a 35 degree bending magnet deflected the beam into the second arm. Two doublets were used to achieve double waists at 16m downstream (the Simon Frazer University Scattering Chamber) and 22m, for a liquid hydrogen target. At all energies the target waists were better than 8x8mm FWHM to ensure minimal beam halo interactions with the target's steel walls. The remaining beam line elements transported the beam to the beam-dump.

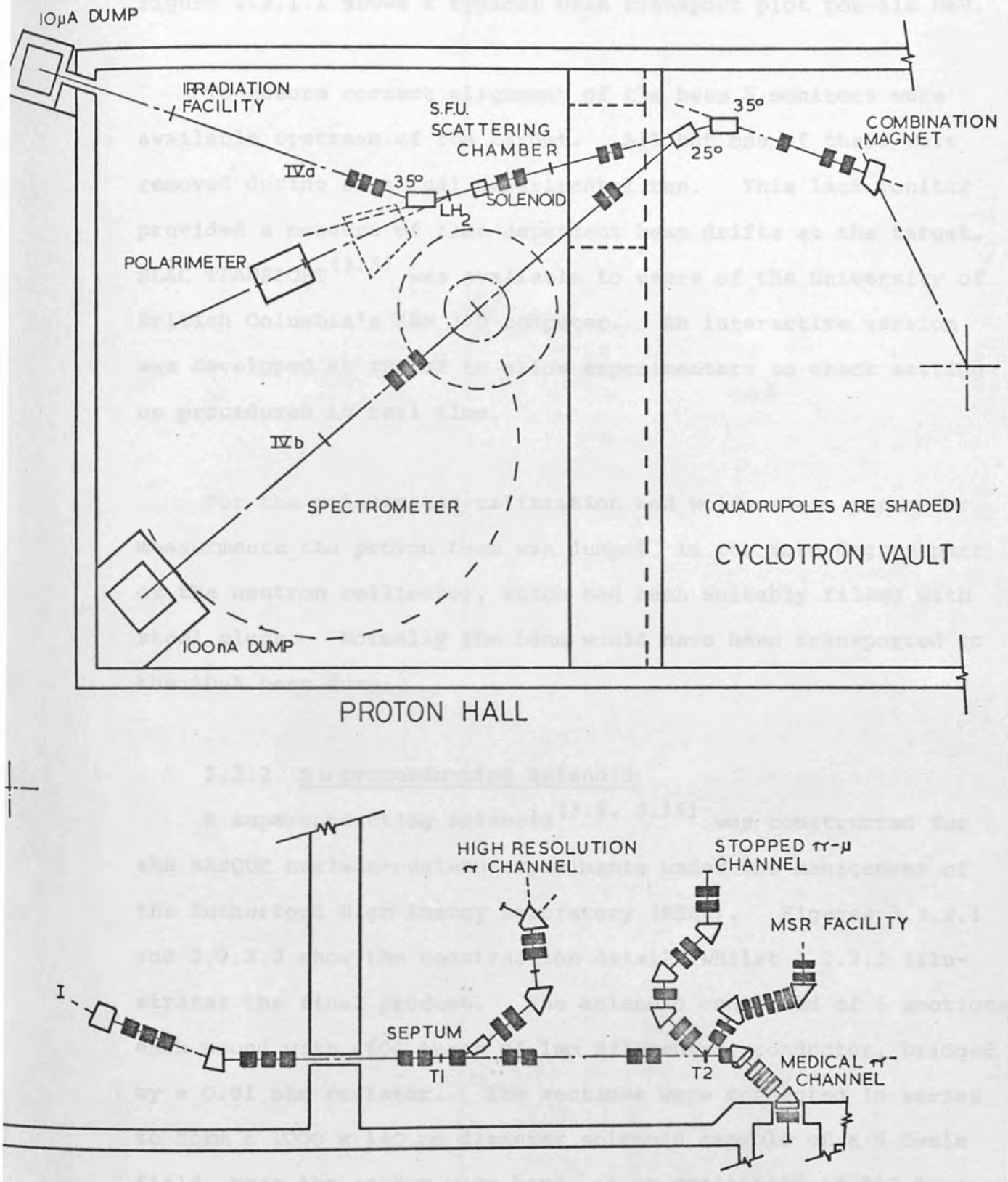

FIGURE 3·21 TRIUMF BEAMLINES

Figure 3.2.1.1 shows a typical beam transport plot for 518 MeV.

To ensure correct alignment of the beam 5 monitors were available upstream of the target. All but one of these were removed during an actual experimental run. This last monitor provided a measure of time dependent beam drifts at the target. SLAC TRANSPORT[3.5] was available to users of the University of British Columbia's IBM 370 computer. An interactive version was developed at TRIUMF to allow experimenters to check setting up procedures in real time.

For the polarimeter calibration and Wolfenstein parameter measurments the proton beam was dumped in the zero degree port of the neutron collimator, which had been suitably filled with steel plugs. Normally the beam would have been transported to the 10μA beam dump.

3.2.2 Superconducting solenoid

A superconducting solenoid[3.6, 3.16] was constructed for the BASQUE nucleon-nucleon experiments under the management of the Rutherford High Energy Laboratory (RHEL). Figures 3.2.2.1 and 3.2.2.2 show the construction details whilst 3.2.2.3 illustrates the final product. The solenoid consisted of 5 sections each wound with 4600 turns of 1mm filamentary conductor, bridged by a 0.91 ohm resistor. The sections were connected in series to form a 1000 x 140 mm diameter solenoid capable of a 6 Tesla field, over the entire warm bore, at an excitation of 212 Amperes. The solenoid was supported inside a helium cryostat, which in turn was surrounded by a liquid nitrogen radiation shield and vacuum vessel. All instrumentation, power leads and plumbing

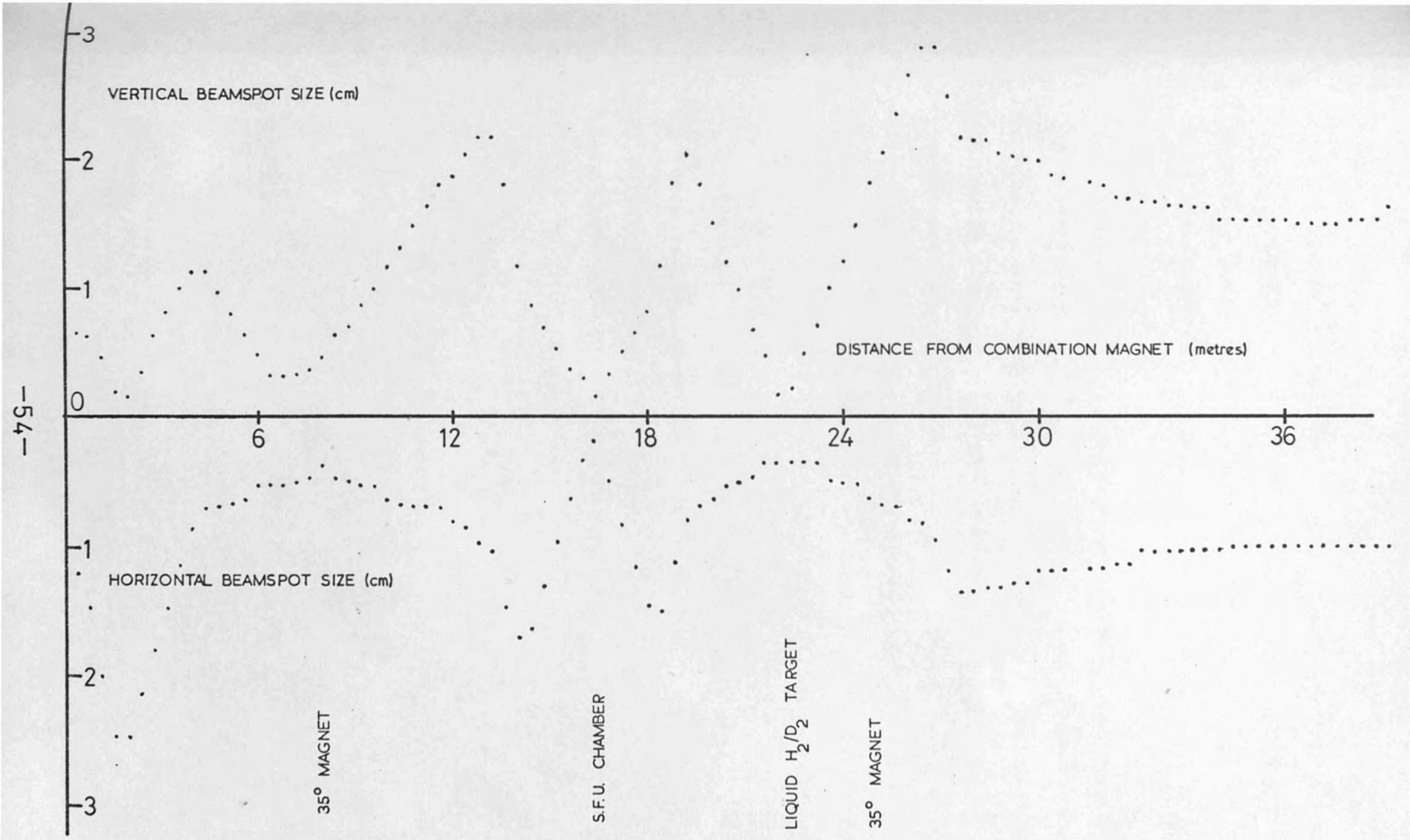

FIGURE 3.2.1.1 VERTICAL & HORIZONTAL BEAM-SPOT SIZES ALONG BEAMLINE 4A AT 518 MeV

were brought out of the containing vacuum vessel via a turret superstructure. Power was delivered to the inner solenoid by two hollow vapour cooled current leads 12mm in diameter and 0.1mm thick that connected to 6mm diameter busbars within the cryostat.

The five resistors were located above the solenoid windings and dissipated energy into the cryostat whenever the solenoid current changed. During a normal charge 2% of the total energy was dumped into the cryostat whilst in the unlikely event of a quench (the magnet going normal) they dumped 60-70% of the field energy, limiting the voltage and temperature rise in the windings to safe levels. The 60 litre capacity cryostat was sufficient to allow up to 40 hours of continuous operation at 5 Tesla's.

Protons having mass M_p(kg), charge e (Coulombs), magnetic moment μ (nuclear magnetrons) passing through a magnetic field of B (Tesla) with their spins perpendicular to the field precess about their direction of motion with angular velocity ω given by:

$$\omega = eB\mu/M_p \qquad \ldots\ (3.2.2.1)$$

This leads to a simple expression for the total precession angle (α) along a path (ℓ)

$$\alpha = \frac{e\mu}{P} \int_{\text{along proton path } \ell} \underline{B}.\underline{dl} \qquad \ldots\ (3.2.2.2)$$

The integral has been evaluated for our solenoid to be 5.919298T at 210 A (i.e. 0.0281871Tm A^{-1}) when integrated from -294cm to 294cm along the beam axis.

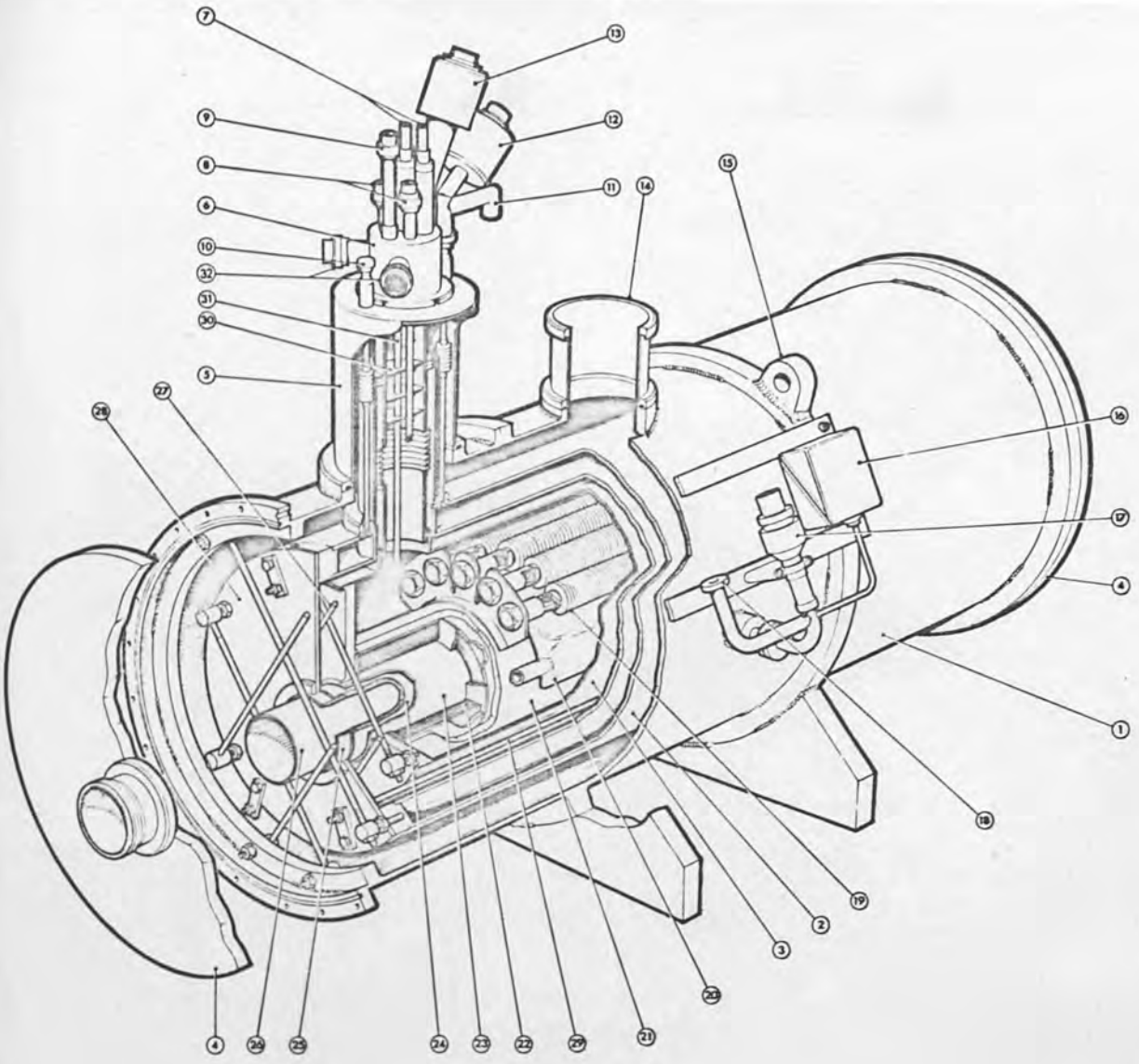

FIGURE 3.2.2.1

THE BASQUE 6TM SUPERCONDUCTOR SOLENOID AND CRYOSTAT

1. CRYOSTAT VACUUM VESSEL
2. LN_2 COOLED RADIATION SHIELD
3. HELIUM VESSEL
4. VACUUM VESSEL END PLATES
5. SERVICES TURRET
6. SERVICE TURRET TOP HAT
7. CURRENT LEADS
8. NITROGEN PRE-COOLER INLET/OUTLET
9. LIQUID HELIUM TRANSFER ENTRY
10. LIQUID NITROGEN TRANSFER ENTRY
11. NITROGEN VENT-RADIATION SHIELD
12. INSTRUMENTATION CONNECTOR-LN_2 COOLED RADIATION SHIELD
13. INSTRUMENTATION CONNECTOR-He VESSEL
14. VACUUM VESSEL PUMPING PORT
15. LIFTING EYES ON CRYOSTAT REINFORCING HOOP
16. PRESSURE SWITCH
17. PRESSURE BURSTING DISC
18. PRESSURE RELIEF VALVE (NOT SHOWN)
19. PROTECTION RESISTORS
20. PRE-COOLING HEAT EXCHANGER
21. SOLENOID (AL. ALLOY) SUPPORT CYLINDER
22. SOLENOID WINDING (FIRST OF 5 SECTIONS)
23. HELIUM VESSEL INNER CYLINDER
24. SUPER INSULATION IN VACUUM SPACE
25. LN_2 COOLED RADIATION SHIELD INNER CYLINDER
26. VACUUM VESSEL INNER CYLINDER
27. HELIUM VESSEL SUPPORT STRUTS
28. LN_2 COOLED SHIELD END PLATE SHOWING SUPPORT STRUTS
29. LN_2 COOLED RADIATION SHIELD OUTER CYLINDER
30. RADIATION SHIELDS
31. CURRENT LEADS-VAPOUR COOLED-OTHER SERVICES NOT SHOWN
32. HELIUM VENTS

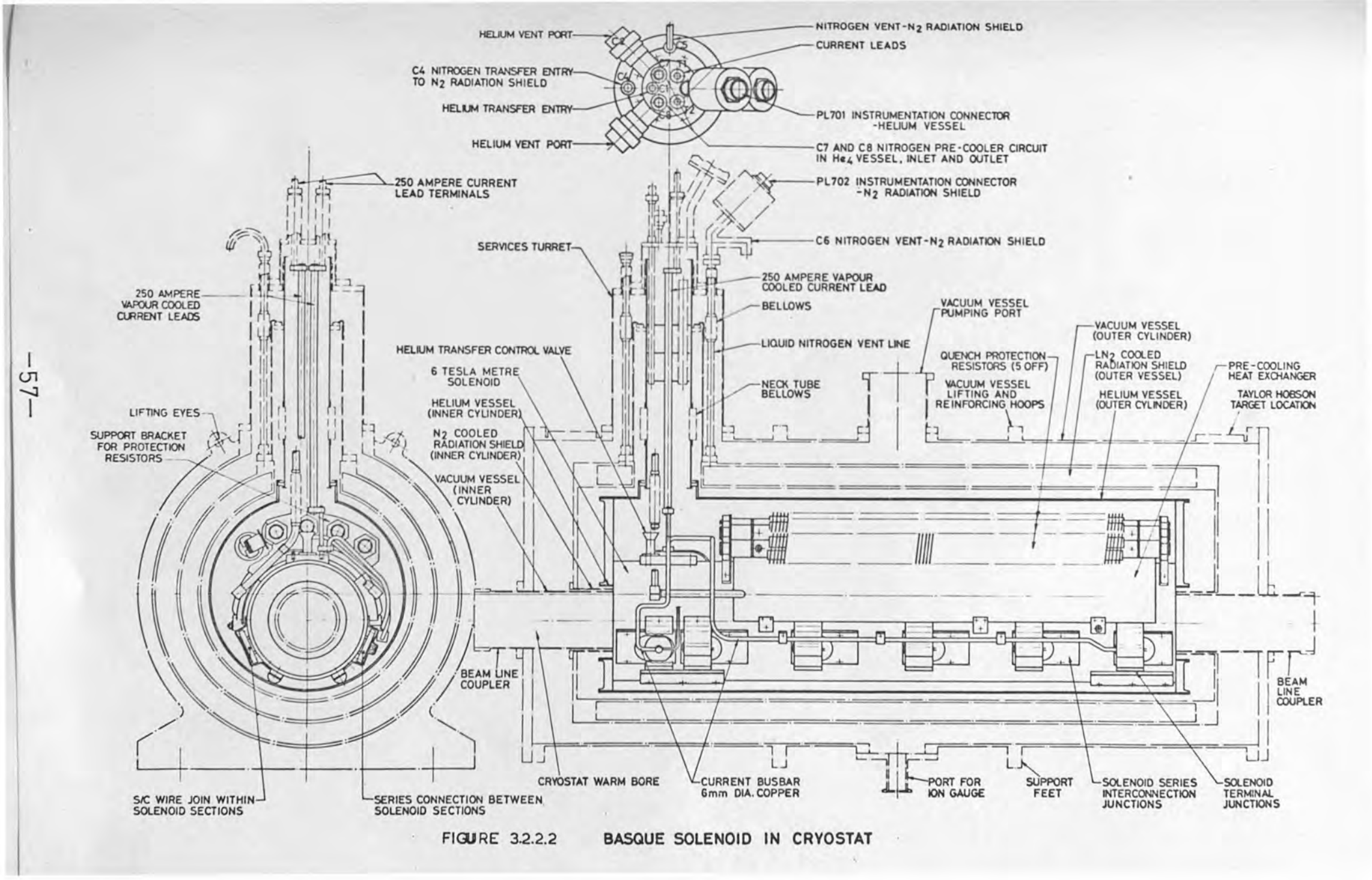

FIGURE 3.2.2.2 BASQUE SOLENOID IN CRYOSTAT

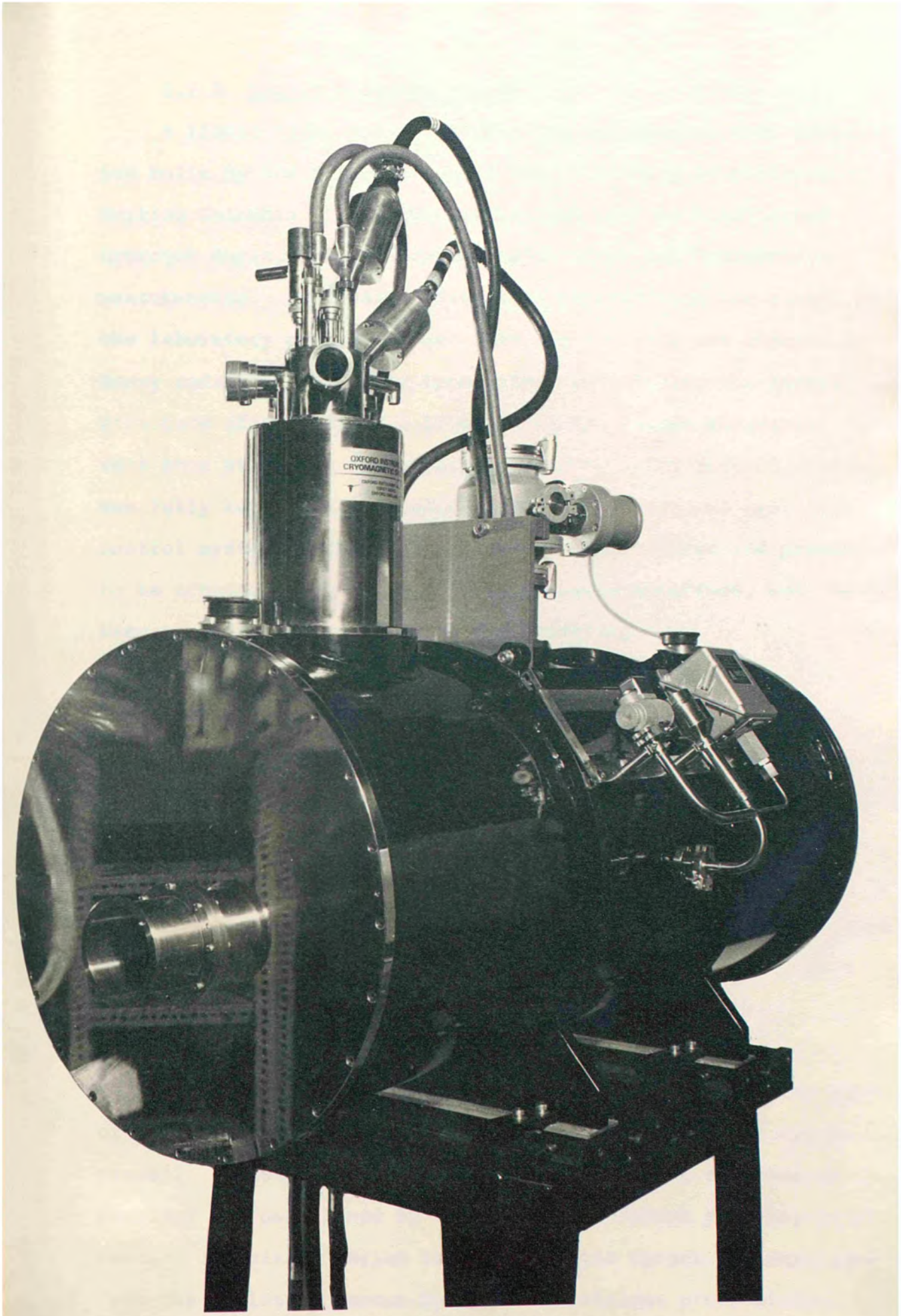

FIGURE 3.2.2.3 BASQUE SOLENOID

3.2.3 Liquid hydrogen target

A liquid H_2/D_2 target and its control systems were designed and built by the TRIUMF group of the University of Victoria, British Columbia[3.7]. The target was used to hold liquid hydrogen during the polarimeter calibration and Wolfenstein measurements. Particles scattering forward from the target over the laboratory angular range -3-30 degrees were not impeded by heavy radiation shielding immediately surrounding the target structure (figure 3.2.3.1 illustrates the target structure) and were thus available for physics research. Its control system was fully automatic and interfaced with the general cyclotron control system. This allowed target temperatures and pressures to be accessed from any cyclotron computer interface, and for beam shut-off in the event of a malfunction.

A cryogenerator provided two stages of cooling for the target. Its 80K line cooled a chromium plated copper (thermal) radiation shield surrounding the target assembly, whilst the 20K line connected directly to the target flask's heat exchanger. Temperature control was achieved by running the cryogenerator at maximum cooling load and adding heat to the liquid hydrogen under the feedback control of a Hydrogen Bulb Thermometer. Carbon resistors indicated when the target was full or empty.

Movement of the target vertically was accomplished by means of a jack and drive motor mounted above the containing vacuum vessel. Thus "dummy" or "target full" could be selected as required and positioned by a cam and microswitch assembly in the control circuit. Whilst in operation the target was separated from the cyclotron vacuum by a 120μm stainless steel window.

When not in use this window was removed and the target raised to leave the beam line unobstructed. Pressure in the target vacuum vessel was better than 10^{-6} Torr. Selecting "dummy target" moved a "chinese copy" of the main target flask into the beam. This allowed rapid changes between target "full" and "empty" during experiments.

The target flask was modified from its original conception[3.7]. A flask 203mm long by 51mm diameter was provided during the polarimeter calibration, whilst for the Wolfenstein parameter measurements the length was reduced to 101mm. Target walls were 250μm stainless steel foils and end windows 50μm. This latter modification was necessary to allow the target to be fully raised out of the beam when not in use, the original target being too long for this to be feasible.

3.2.4 Neutron collimator

In preparation for future neutron experiments at TRIUMF a collimator was installed in the concrete shielding. Particles scattering in the liquid H_2/D_2 target emerged through the collimator every three degrees of laboratory angle, over the range -3 to 27 degrees.

Each collimator port was constructed from two sections of pipe having equal lengths. The upstream entrance was 100mm in diamter whilst the downstream exit was 125mm, the length of the 24 degree port being 3.53m. The pipes were sandwiched between two load bearing steel plates of 50mm thickness and the whole assembly was filled with lead. The final 25 ton collimator was installed in the shielding during the Autumn of 1974.

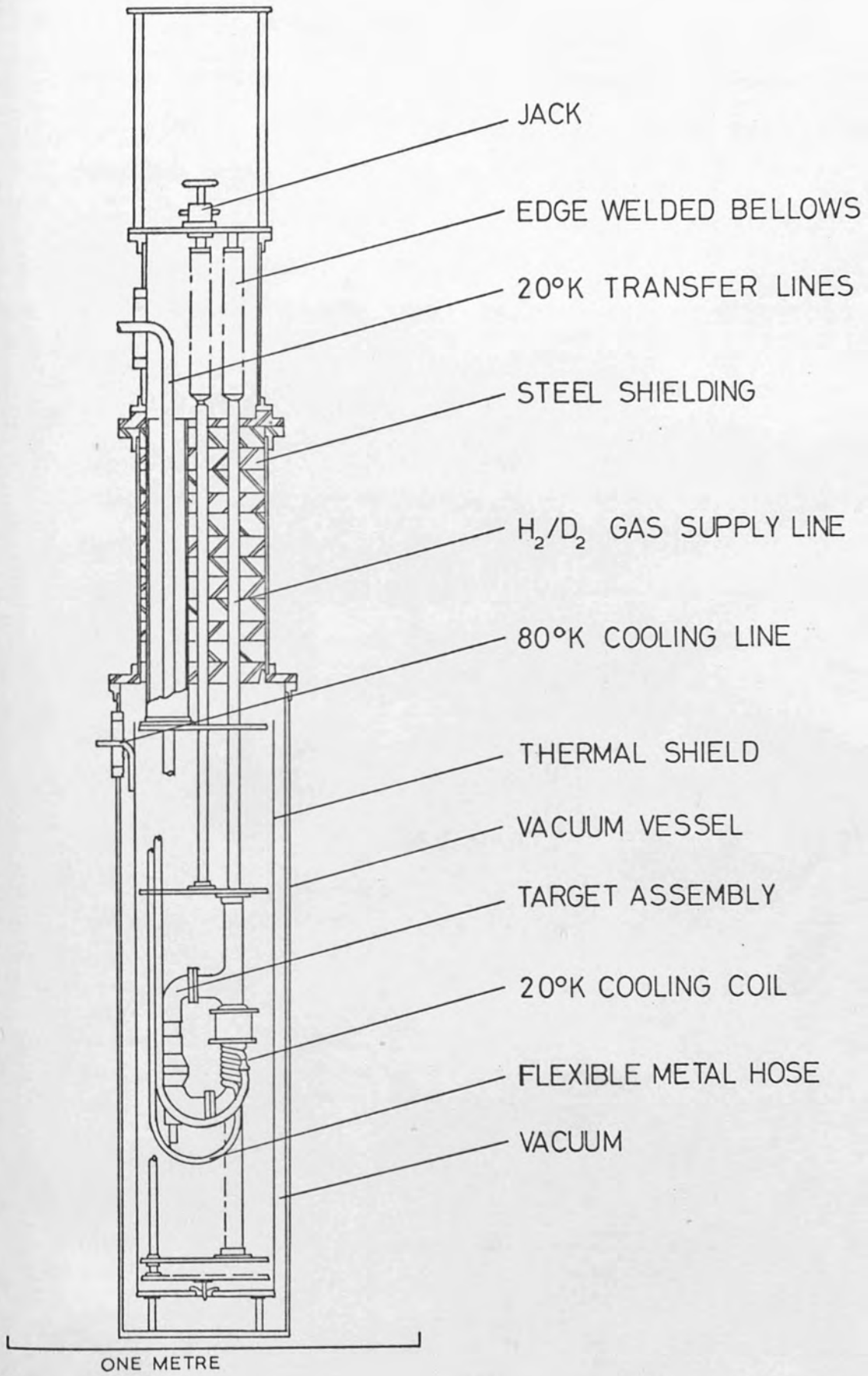

FIGURE 3·2·3·1 LIQUID H_2/D_2 TARGET

For the pp experiments a collimator was superfluous and scattered beam was defined by a scintillator telescope (section 3.3) viewing the target through the collimator port. The hydrogen target centre was 6m upstream of the 24 degree port exit. Figure 3.2.1 shows the location of the collimator with respect to the beam-line. Unused ports were filled with specially made steel plugs to reduce radiation levels in the experimental area.

3.2.5 Beam monitor

A polarimeter was constructed to monitor the intensity and polarization of the extracted proton beam (EPB). Figure 3.2.5.1 shows the polarimeter schematically. Polarized protons freely scattering from hydrogen in a polyethylene target had the intensity distribution given by formula 1.3.14. Measurements of this intensity distribution at ϕ = 0 degrees (rate in left arm $\equiv$ L) therefore gave

$$L = I_o (1 + \varepsilon^s) \qquad \ldots. (3.2.5.1)$$

and at ϕ = 180 degrees (rate in right arm $\equiv$ R)

$$R = I_o (1 - \varepsilon^s) \qquad \ldots. (3.2.5.2)$$

solving these for ε^s we find the asymmetry (in the lab. figure 1.3.2) given by

$$\varepsilon^s = (L - R)/(L + R) \equiv P(\theta^s, E^b) P^b \qquad \ldots. (3.2.5.3)$$

and assuming normally distributed intensities L and R, the error squared ($\delta^2 \varepsilon^s$) in ε^s by

$$\delta^2\varepsilon^s = \frac{(1 - (\varepsilon^s)^2)}{L+R} \quad \ldots\ (3.2.5.4)$$

where P^b was the required beam polarization and $P(\theta^s, E^b)$ was the polarization produced by scattering an unpolarized beam of energy E^b, from hydrogen, at angle θ^s in the lab.

To ensure the elastic scattering intensity, from hydrogen, was being monitored both the forward scattering (left or right) and recoil protons were detected in separate scintillator telescopes. Each telescope was dubbed FORWARD or RECOIL, accordingly as it detected the forward or recoil proton, and comprised two detectors termed FRONT and REAR. Thus an event in either the left or right arm of the polarimeter was a four-fold coincidence. Signals from the left and right were summed to form a beam monitor, whilst individually they were used to calculate the asymmetry ε^s. Table 3.2.5.1 lists all signals derived from the polarimeter scintillators.

Forward arms used 32 x 30mm scintillators in the FRONT and 51 x 20mm in the REAR, separated by 250mm. RECOIL arms used 41 x 49mm and 99 x 70mm in FRONT and REAR respectively, with the same separation. All scintillators were 1.5mm thick. Solid angle acceptance was determined by the FORWARD telescope of each arm; whose centre-line made an angle of 26 degrees with respect to the beam-line axis. Recoil protons were detected at the conjugate angle of 60 degrees.

Corrections to ε^s were necessary before the true value of the beam polarization (P^b) could be extracted from measurements

of L and R; these are dealt with in section 5.3.1.

Signal nomenclature	Origin (see fig.3.2.5.1)	Monitors rate of
LF	$LF_F.LF_R$	Left forward telescope
LR	$LR_F.LR_R$	Left recoil telescope
RF	$RF_F.RF_R$	Right forward telescope
RR	$RR_F.RR_R$	Right recoil telescope
L	LF . LR	Left forward elastic scatters
R	RF . RR	Right forward elastic scatters
L+R	L . R	Beam monitor

TABLE 3.2.5.1 Signal nomenclature for primary beam monitor. (dot implies logical product of signals)

3.3 Proton telescope

In section 3.2.4 the physical collimation of the beam was discussed. The scattered proton beam from the target was defined by a three counter scintillator telescope whose axis was through one of the neutron collimator ports. This section details the construction of the proton telescope.

Figure 3.6.1.1 shows the general arrangement of the three counters SOA, SOA' and SOB comprising the 24 degree telescope. Counter SOA' was not installed for the polarimeter calibration, performed at the 24 degree part. Wolfenstein parameter measure-

1st LETTER	2nd LETTER	SUBSCRIPT
R RIGHT	R RECOIL	F FRONT
L LEFT	F FORWARD	R REAR

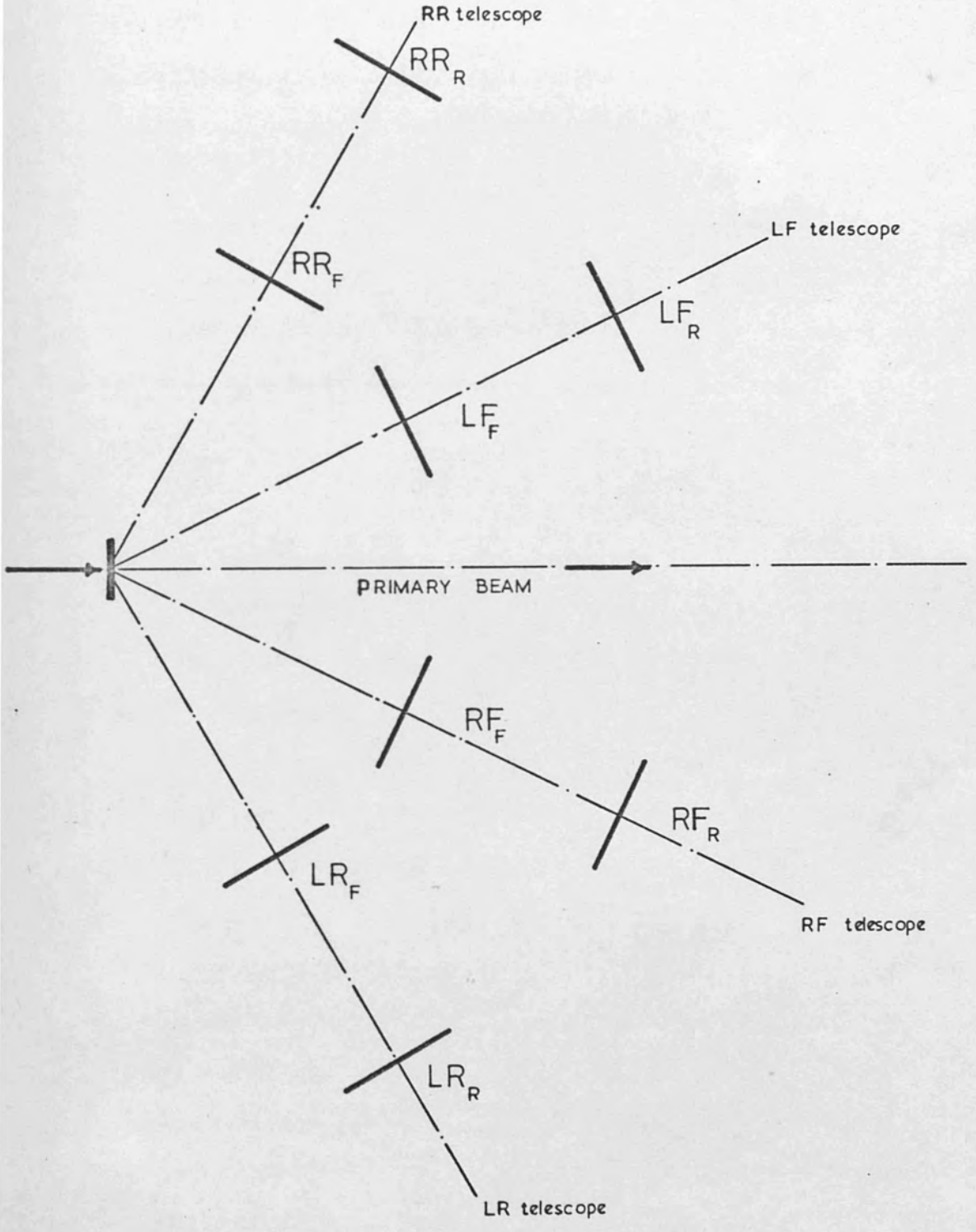

FIGURE 3.2.5.1 BEAMLINE POLARIMETER

ments required identical telescopes at the 6, 9, 15 and 24 degree ports. For these latter experiments a coincidence

$$SOAA' \equiv SOA.SOA'$$

was formed from two 25mm diameter by 1.5mm thick scintillators positioned upstream of the collimator entrance. The high radiation field of the liquid hydrogen target produced rates $\sim 10^5\ s^{-1}$ in these counters for 1nA of EPB. Counter SOB (51mm diameter) gave typically $\sim 10^4\ s^{-1}$ under these conditions, whilst the MASTER TRIGGER (event) rate was $\sim 400\ s^{-1}$ (see section 3.6.1 for details of the MASTER TRIGGER). SOAA' reduced the random rate in the proton telescope coincidence

$$SO \equiv SOAA'.SOB$$

to the level of 1%.

Counter signals were fed through NIM discriminators forming 20ns wide pulses. A time-of-flight measurement was made over the 3.5m length of each telescope. The SOB signal formed the START pulse for a time to digital converter (TDC) and SOAA' the STOP (see section 3.6.3 for details of TOF measurements).

3.4 Carbon polarimeter

Central to the experimental philosophy was a large solid angle acceptance carbon polarimeter. The large solid angle acceptance was achieved by positioning multiwire proportional chambers (MWPC's)[3.11, 3.12] (described in section 3.4.1) both before and after a 60mm carbon analyser. Figure 3.4.1 shows the polarimeter as set up for a n-p experiment. For the p-p

experiments counter S1 was removed to minimise multiple scattering effects.

Six 0.5 x 0.5 metre MWPC's spaced 358mm apart were used before the carbon to determine alternately the X (to the right facing the polarimeter) and Y (downward) co-ordinates of an incident proton. The outgoing proton's track was determined (after scattering in the carbon) by 6 1x1 metre MWPC's spaced 287mm apart. .The positive Z axis was defined to be parallel to incident proton tracks (see figure 3.4.1). MWPC sense wires were aligned with respect to the rails on which the chambers were mounted. With the carbon removed, unscattered proton tracks fitted to straight lines were used to remove small misalignments of the chambers (see section 5.1.1 for further details). Front MWPC's were positioned to give the maximum possible resolution of the incident protons track; rear chambers and S4 were positioned to allow protons to scatter usefully through 30 degrees.

Counters S2 and S3 were constructed from four scintillators, 250 x 285 x 3mm edge butted together; S4 consisted of six fingers 365 x 744 x 6mm edge butted together in threes but overlapping by 350mm at their extremities. This gave an active area of 1095 x 1140mm. The carbon analyser block was 530 x 530 x 60mm. Counters S2, S3 and S4 provided a threefold coincidence trigger for events in the polarimeter.

Following the polarimeter calibration experiment, the polarimeter was mounted on four castors. This simplified the process of moving the polarimeter between collimator ports, an essential part of the Wolfenstein parameter measurements.

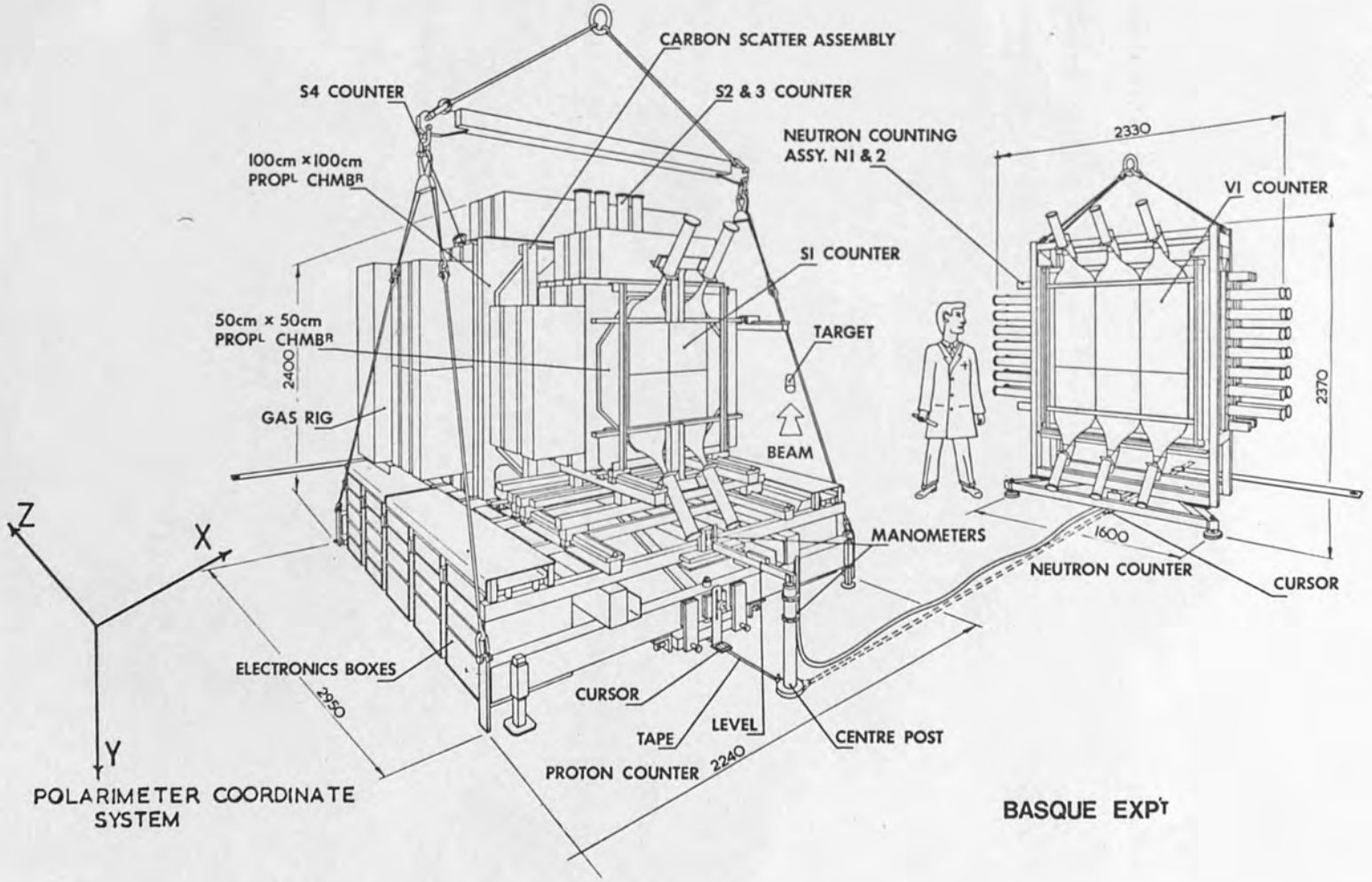

FIGURE 3.4.1 CARBON POLARIMETER AND NEUTRON COUNTER
(DIMMENSIONS IN MM.)

3.4.1 Multiwire proportional chambers

Multiwire proportional chambers with 0.5 x 0.5 metre and 1 x 1 metre active areas were used in the carbon polarimeter. Both sizes were constructed similarly hence only general features will be described below. Figure 3.4.1.1 illustrates a typical chamber[3.13, 3.14].

Three wire planes were assembled within a gas tight container Polyester glass fibre frames were used to support the planes and keep them mutually parallel. The central plane, termed the sense plane was constructed from 20μm diameter gold plated tungsten wires tensioned to 0.1N and pitched by 2mm. Two high voltage planes used 122μm beryllium copper wires. These planes were assembled orthogonal to the sense plane but separated by an 8mm gap. Positioning of the sense wires was established to better than 120μm with respect to the MWPC's external mountings. Windows of 120μm melinex were provided in the gas enclosure, over the MWPC's active area, to minimise extraneous material in the polarimeter.

Typical operating voltages were -5.6kV, with efficiencies of better than 99% in a gas mixture of 56% argon, 46% isobutane, 4% methylal and 0.4% freon. Table 3.4.1.1 classifies (as described in section 3.7) the type of "hits" seen in the MWPC's under normal experimental conditions. Adjacent sense wires were electronically connected giving an effective pitch of 4mm to each chamber. The data readout system for the polarimeter MWPC's is described in section 3.6.4, in order to logically present the fast electronics system.

MWPC No.	Event Type in MWPC							
	Type 0	Type 1	Type 2	Type 3	Type 4	Type 5	Type 6	Type 7
1	9.75	80.30	3.42	8.14	1.64	0.80	0.06	2.90
2	1.62	66.43	16.58	1.32	2.50	1.16	0.00	10.39
3	3.16	83.44	5.97	1.02	1.98	0.90	0.02	3.52
4	7.17	73.95	9.23	1.38	2.62	0.92	0.02	4.72
5	1.64	84.40	6.45	1.22	1.48	1.12	0.04	3.66
6	4.16	77.82	8.19	1.36	2.62	0.92	0.08	4.86
7	0.80	65.47	23.16	2.12	1.62	2.40	0.06	4.38
8	4.02	72.94	9.15	7.85	1.10	2.02	0.20	2.72
9	0.54	71.51	19.18	1.72	2.12	1.58	0.04	3.32
10	0.34	69.37	20.20	1.64	2.72	1.46	0.04	4.24
11	0.44	70.55	19.08	2.02	2.48	1.52	0.06	3.86
12	0.96	71.25	18.34	1.46	1.96	1.36	0.00	4.68

KEY

Type	Description
0	No activated wires
1	1 activated wire
2	2 adjacent activated wires
3	2 non-adjacent activated wires
4	3 adjacent activated wires
5	Type 1 + Type 2
6	3 non-adjacent activated wires
7	More than three activated wires

TABLE 3.4.1.1 Typical MWPC efficiency figures (%)

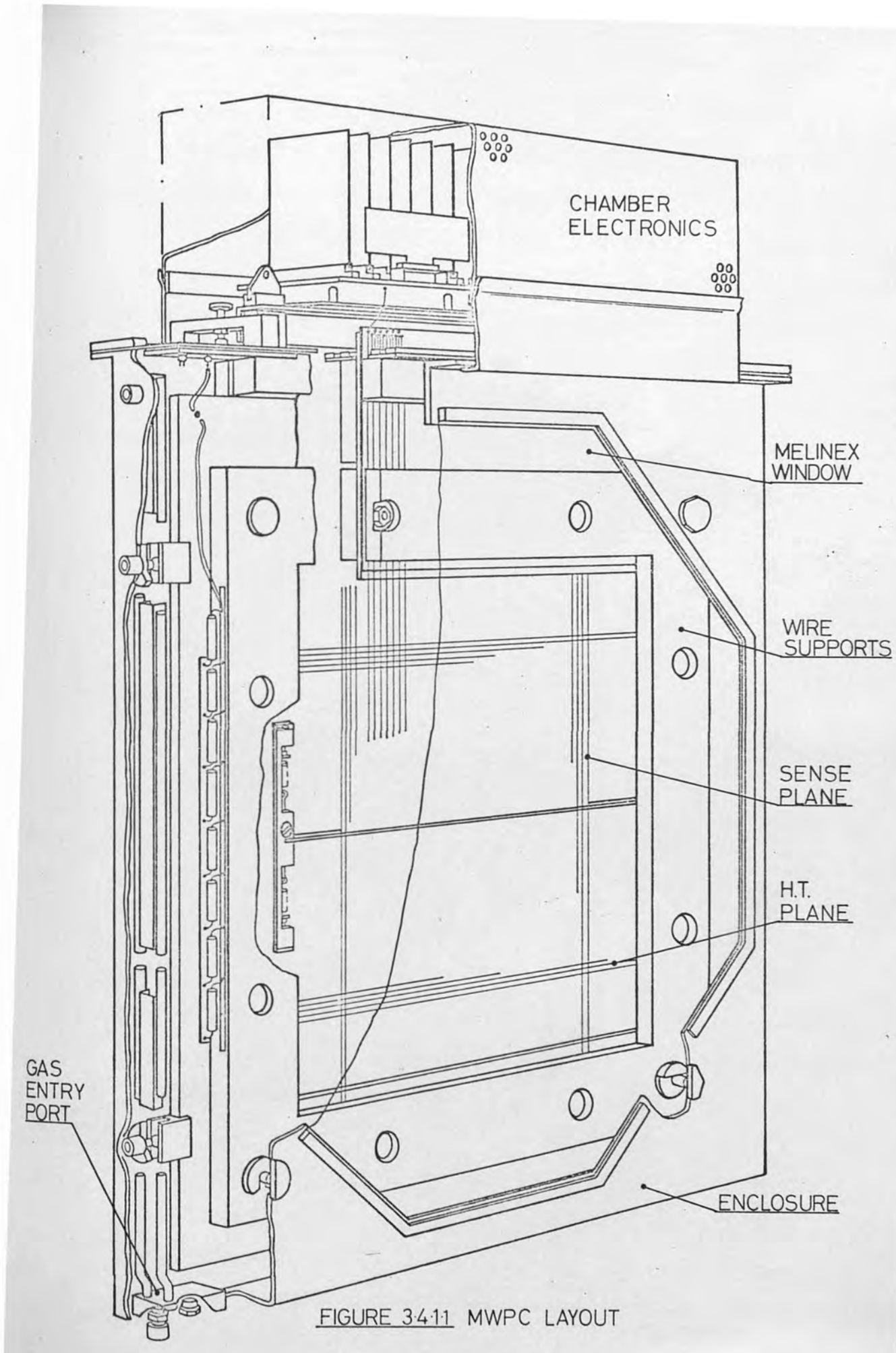

FIGURE 3·4·1·1 MWPC LAYOUT

3.4.2 Momentum analysing magnet

To aid in the removal of pion contamination from the scattered beam, above threshold, a magnet was placed downstream of the proton telescope (see figure 3.6.1.1). The magnet was a standard TRIUMF 100mm pole-separation beam-line steering magnet. The line integral of its magnetic field along the beam axis was 0.0272 T.m. at 5A. Its excitation was varied to deflect the scattered proton beam by 7 milliradians in the horizontal plane. In general particles with charge e and momentum p passing through a magnetic field $\underline{B}$ will experience an angular deflection θ_B given by

$$\theta_B = \frac{e}{p} \int_{path} \underline{B}.\underline{dl} \quad \ldots\ldots (3.4.2.1)$$

Where the line integral is evaluated over the particles path through the field $\underline{B}$. For equal velocity two particles of mass m^a and m^b will be deflected on the ratio

$$\frac{\theta_B^a}{\theta_B^b} = \frac{m^b}{m^a} \quad \ldots\ldots (3.4.2.2)$$

assuming the line integral for the two paths are equal (which is usually met in practice). Applying this formula to the case where the two particles considered are protons and pions we see that the ratio of bend angles for equal velocities is ~ 7.

Although the magnet was not an original part of the polarimeter its usefulness in the polarimeter calibration measurements necessitated its inclusion in later experiments. Mounted on the front of the polarimeter, the magnet's centre had co-ordinates

(0,0,-1528) with respect to the polarimeter co-ordinate system shown in figure 3.4.1. This solution allowed the magnet to be moved with the polarimeter during the Wolfenstein measurements, when rapid changes in laboratory angle were undertaken. The magnet was removed for the R' measurements.

3.5 R' spin precession magnet

For R' measurements the momentum analysing magnet was removed from its mounting and a large magnet placed upstream of the polarimeter (figure 4.3.2 shows the actual experimental configuration). The magnet used had deep historical connections with TRIUMF and in particular the director Professor J R Richardson (UCLA). Originally designed at the University of California, Los Angeles (UCLA) as a component of a frequency modulated cyclotron it was decided in Spring 1958 to use the magnet in constructing a sector focussed cyclotron[3.10]. At that time the benefits of having a lower maximum (50 MeV) but widely varying energy outweighed the alternative of a fixed higher maximum energy machine. Preliminary operation of this machine began in November 1960, just 14 years before TRIUMF first extracted beam. It is somehow ironic that this forerunner of TRIUMF (H^- ions were first accelerated in the old machine) should have come to be a mere experimentalists' tool in the shadow of the larger machine and illustrates vividly the pace of modern physics.

The magnet is 106" long, 63" wide and 54" high. The top, bottom and side yokes are detachable and made from special low carbon steel. Having a pole diameter of 49" the magnet weighs 40 tons and consumes 112kW at 2700A when producing a 2T magnetic field. A concrete plinth was constructed to bring the centre

line of the magnet up to the beam height in the experimental area.

The purpose of the UCLA magnet was to precess the longitudinal polarization component of the scattered beam into the transverse direction. It is well known[3.8] that the anomalous magnetic moment of the proton allows the polarization vector of a (proton) beam to be rotated into arbitrary directions using only bending magnets. For the R' geometry (section 4.3) the laboratory bend angle of the beam Θ_B was related to the polarization precession angle Θ_p by

$$\Theta_p = (\mu_p - 1)\gamma\, \Theta_B \qquad \ldots\ (3.5.1)$$

where γ was the proton energy (in units of $M_p c^2$), μ_p is the protons magnetic moment in nuclear magnetons and M_p is the rest mass of the proton.

3.6 Electronic subsystems

Three major electronic subsystems formed the data acquisition system. This section describes the operation of each subsystem individually whilst section 3.7 relates to their dynamic interaction as a complete system, in conjunction with a PDP 11/20 mini computer.

All signals were brought to the BASQUE experimental trailer, situated outside the Proton Hall, for processing. A MASTER TRIGGER (section 3.6.1) was generated and fanned out by the CO-ORDINATING CIRCUIT (section 3.6.2). One signal triggered the

polarimeter readout system (section 3.6.4) whilst others provided gating and inhibit signals to CAMAC electronic units. Three TOFs were recorded (section 3.6.3) to aid in the selection of "good" events (section 5.1.2).

A PDP 11/20 computer was interfaced to the CAMAC system[3.18] Digitized data were transferred from CAMAC modules (TDCs, scalars, etc.) into the computer memory under the autonomous control of a program running in the computer. Histograms of these data were stored in contiguous areas of the computer memory and were available to experimenters on local display devices. The computer buffered events onto 2400ft magnetic tapes, recorded at 800 characters per inch: 200K events were stored on each tape. These tapes formed the input to off-line data analysis programs.

3.6.1 Master trigger generation

Figure 3.6.1.1 shows a typical arrangement for the polarimeter calibration experiment and illustrates the scintillator nomenclature to be used in this thesis.

A fast electronics subsystem (figure 3.6.1.2) was designed to generate a MASTER TRIGGER for the CAMAC system upon receipt of appropriately timed signals from the scintillator counters. The events of interest were those that scattered in the hydrogen target, passed through the collimator (triggering the proton telescope S0), scattered in the carbon polarimeter (triggering S2, S3 and S4) and finally missed the veto counter (V). Thus the MASTER TRIGGER (T) was given by (dot implies logical product):

$$T = SOA.SOA'.SOB.S2.S3.S4.\overline{V} \equiv SO234\overline{V}$$

The coincidence SOAA' was used to reduce "random" MASTER TRIGGERS resulting from:

1. protons scattering in the target, missing SOA and/or SOA' but passing through the collimator (triggering SOB.S2.S3.S4.$\overline{V}$),
2. background particles from the high radiation field of the target providing correctly timed signals (SOA and/or SOA') for the coincidence SOAA'.

Thus the (entire) proton telescope signal (SO) normally ensured that particles traversed the collimator either in straight lines, within the angular acceptance of SO ($\sim$ 10 milliradians), or by scattering from the collimator walls. The two cases were distinguished by off-line track reconstruction using polarimeter data and the TOF difference of scattered particles due to energy loss in the collimator walls (see section 5.1.2 for further details of event selection).

Straight tracks through the polarimeter were vetoed by the counter V, whose size and location had been determined by simple geometry and multiple scattering coisiderations (Appendix A). Events with scatter angles in the carbon of less than 3.5 degrees were vetoed. These events have a poor analysing power (see section 5.3 for values of the analysing power) and the polarimeter was less able to determine their azimuthal scattering angle $\emptyset$, which is necessary for asymmetry measurements (Appendix C contains further details pertaining to the geometrical resolving power of the polarimeter).

All scintillator signals were taken outside the experimental area to the BASQUE counting trailer. The anode signals from counters SOA, SOA' and SOB were discriminated by NIM logic modules, whilst S2, S3, S4 and V were handled by the Miniature Logic System (MLS)[3.19] of the Rutherford Laboratory. Figure 3.6.1.2 illustrates the method by which these signals were brought together to form the MASTER TRIGGER. In order to fully monitor the experiment a selection of signals were provided for scaling. These divided naturally into three classes.

a) singles rates in all counters; these were monitored to ensure the MASTER TRIGGER subsystem and scintillator counters were functioning correctly and that SOAA', being closest to the target, did not suffer rate effects;

b) coincidences; these were monitored to check counter consistencies;

c) delayed coincidences; these monitored the random rates in pairs of counters. The delayed coincidence $\widetilde{\text{SOAA'}}$.SOB.S2.S3.S4 monitored the random MASTER TRIGGER rate and was typically 1% for the pp experiments. (The tilde indicates that the signal was delayed by 43ns with respect to the normal coincidence timing. This delay equals the time between beam bursts at TRIUMF for all energies).

Signals for scaling were fed to CAMAC "blind" scalars and displayed for experimenters by the on-line program of the computer.

Timing of the MASTER TRIGGER was determined by the S3 counter.

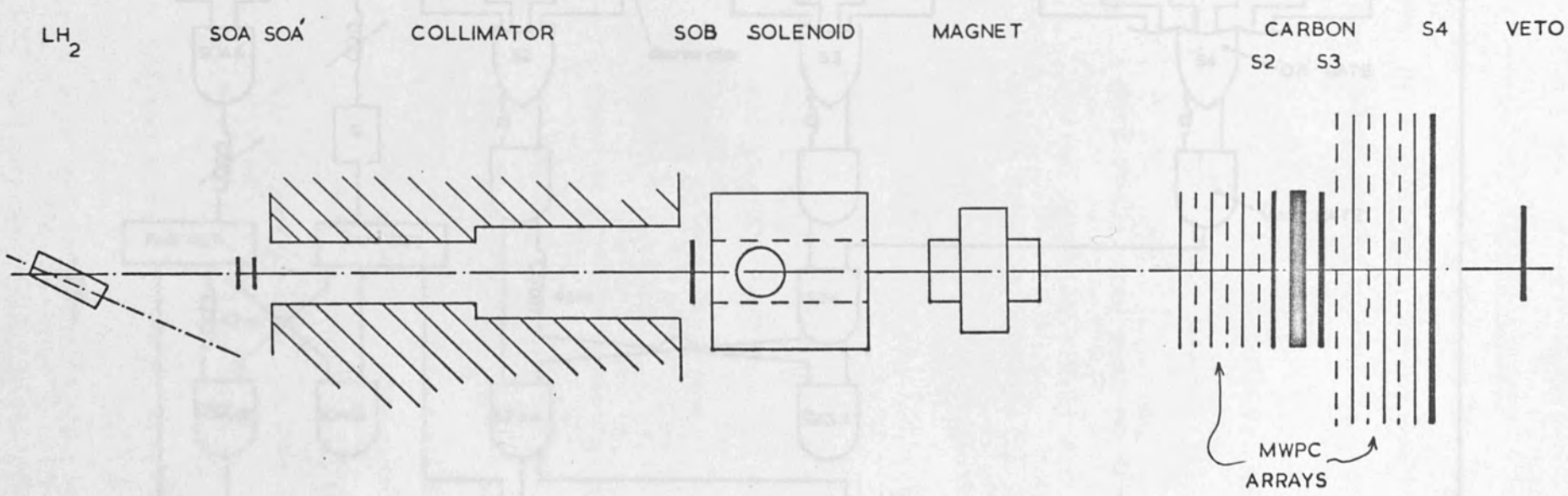

FIGURE 3.6.1.1 SCHEMATIC SETUP FOR POLARIMETER CALIBRATION AT 24° PORT

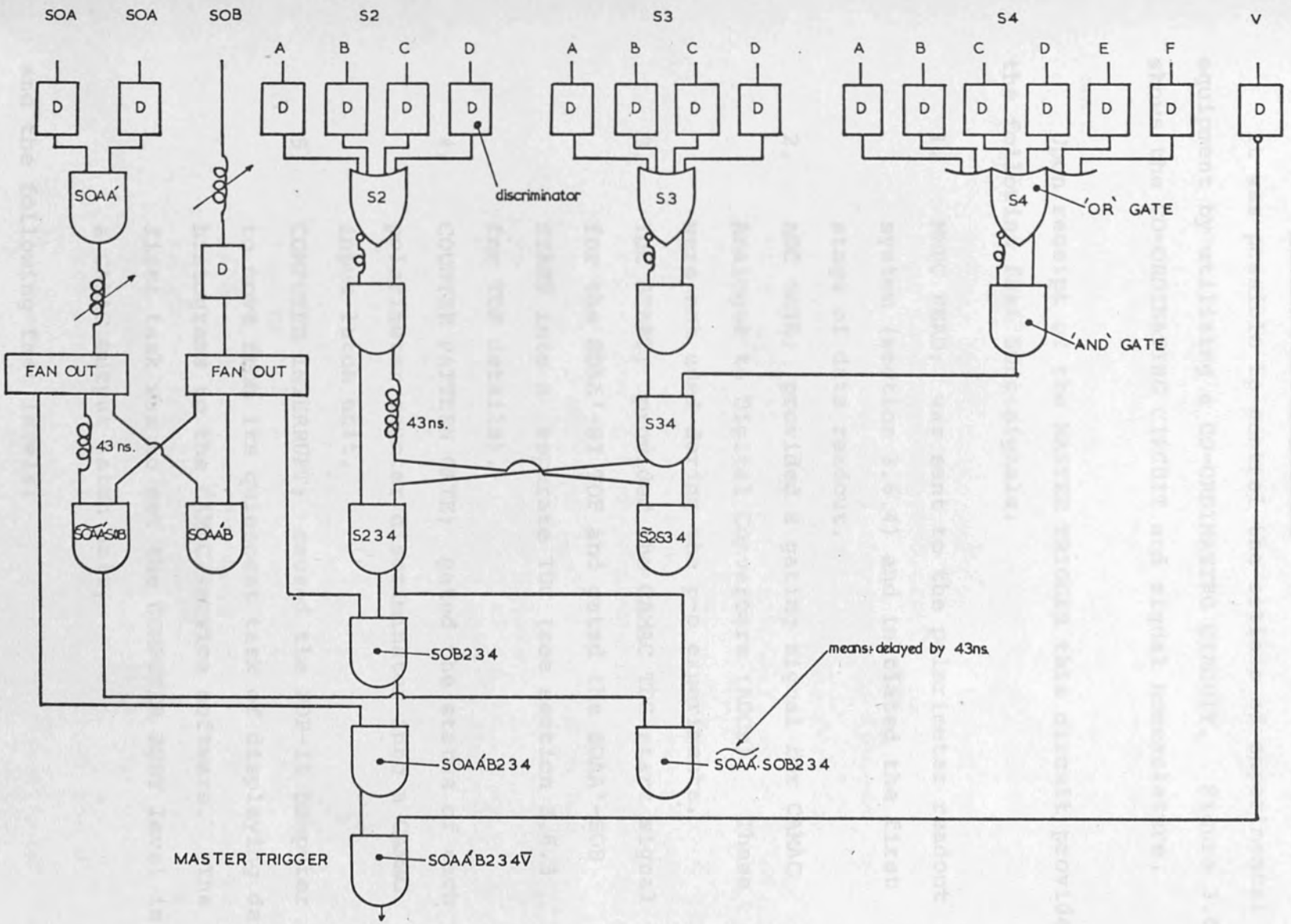

FIGURE 3·6·1·2 MASTER TRIGGER ELECTRONICS SUBSYSTEM

3.6.2 Co-ordinating circuit

It was possible to control the actions of experimental equipment by utilizing a CO-ORDINATING CIRCUIT. Figure 3.6.2.1 shows the CO-ORDINATING CIRCUIT and signal nomenclature.

Upon receipt of the MASTER TRIGGER this circuit provided the following fast 50ns signals:

1. MWPC READ; was sent to the polarimeter readout system (section 3.6.4) and initiated the first stage of data readout.
2. ADC GATE; provided a gating signal for CAMAC Analogue to Digital Converters (ADCs). These were not used during the p-p experiments.
3. TDC START; provided the CAMAC TDC start signal for the SOAA'-S3 TOF and gated the SOAA'-SOB START into a separate TDC (see section 3.6.3 for TOF details).
4. COUNTER PATTERN GATE; gated the status of each polarimeter counter discriminator into a CAMAC input latch unit.
5. COMPUTER INTERRUPT; caused the PDP-11 computer to move from its quiescent task of displaying data histograms to the CAMAC service software. The first task was to set the COMPUTER BUSY level in a CAMAC output latch unit,

and the following fast levels:

1. BUSY and INHIBIT; were used to inhibit CAMAC scalars and a clock during the system deadtime.

A second clock recorded the real time, hence a measure of the system workload was given by the ratio of the live to real time.

The CO-ORDINATING CIRCUIT accepted the following signals in addition to MASTER TRIGGER:

1. COMPUTER CLEAR; originated from a pulsed CAMAC output latch unit. This 50ns signal ensured that the CO-ORDINATING CIRCUIT output levels were asserted until the computer removed slow internal CAMAC inhibits. These fast levels were then removed simultaneously, 100μs after receiving COMPUTER CLEAR.
2. COMPUTER BUSY; was a software controlled level originating in a CAMAC output latch unit. This level held BUSY and INHIBIT levels on for the duration of the system deadtime.
3. EVENT-RATE VETO; a rate meter monitored the MASTER TRIGGER rate for part of the polarimeter calibration experiment. This provided a veto output level whenever the rate being monitored rose or fell through pre-defined levels. Higher rates were vetoed as random MASTER TRIGGERS rose in proportion to the beam current squared, whilst low rates gave an indication that beam conditions were possibly changing. This signal was not used in the p-p work as a smaller hydrogen target gave a lower event rate for the same EPB.
4. BUSY SWITCH; gave a manually controllable busy switch.

5. SPIN BUSY; was asserted by the TRIUMF CONTROL ROOM computer controlling the polarized ion source. The busy level covered the period during which the polarization was changing.

3.6.3 Time-of-flight measurements

Three time-of-flights (TOFs) were monitored during the polarimeter calibration and Wolfenstein parameter experiments, these were:

1. SOAA'-S3; the path length SOAA'-S3 was 7.6m and provided adequate TOF separation for pions and inelastic protons from elastically scattered protons (section 5.1.2).
2. RF-S3; was used to monitor the microstructure of the beam and its phase stability. These quantities were of interest for future neutron experiments (where TOF measurements on neutrons will be made relative to a fixed phase of the RF). As shown in figure 3.6.3.1 the cyclotron radio-frequency (RF) signal was discriminated before forming RF-S3 TOF STOP. Hence this TOF was measured between the S3 signal and a fixed phase (determined by the discriminator setting) of the RF. It was possible for the phase of the beam pulses (with respect to the RF) to change whenever the excitation currents of harmonic or trim coils were varied. This was normally due to operator intervention.
3. SOAA'-SOB; having a path length of 3.6m this TOF served as a check of SOAA'-S3.

Figure 3.6.3.1 shows the basic TOF subsystem.

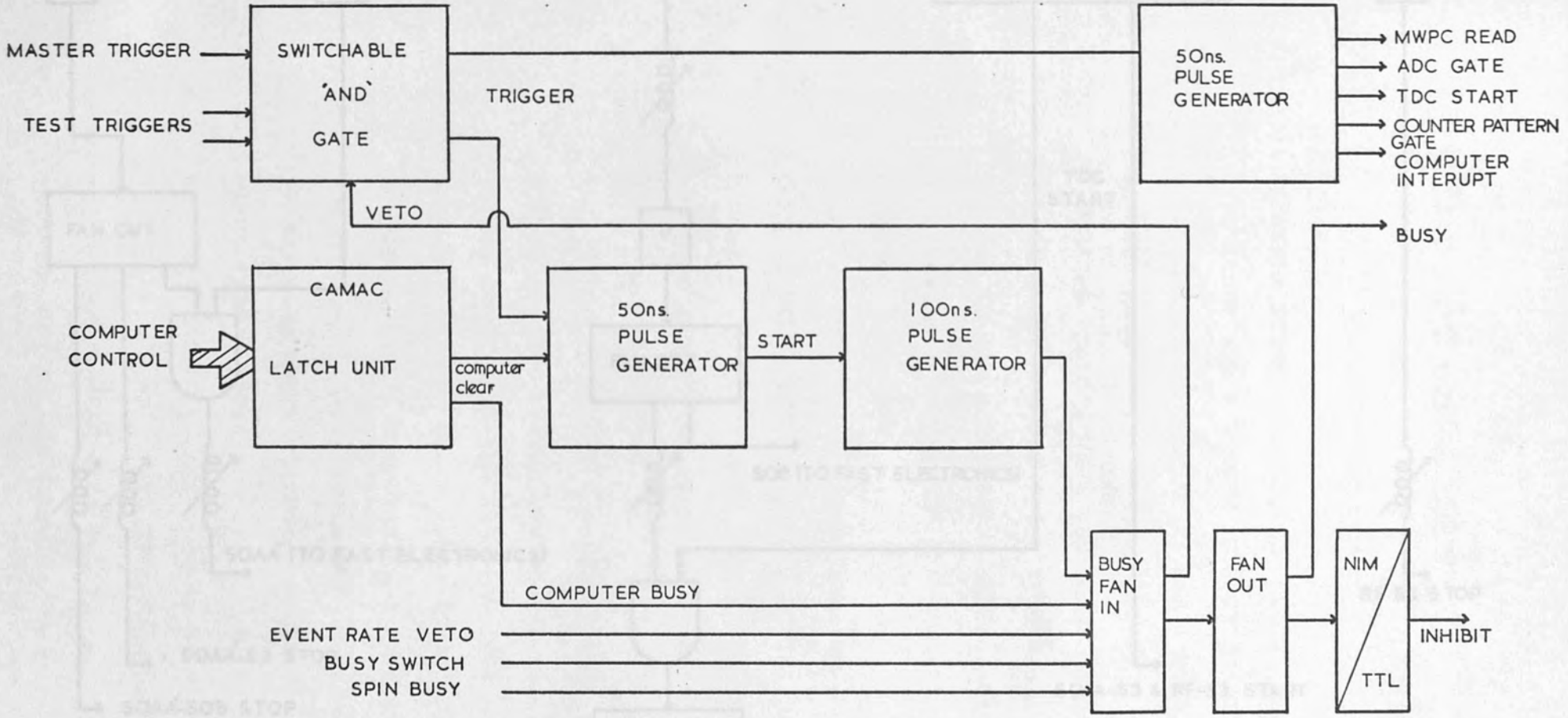

FIGURE 3·6·2·1 COORDINATING CIRCUIT

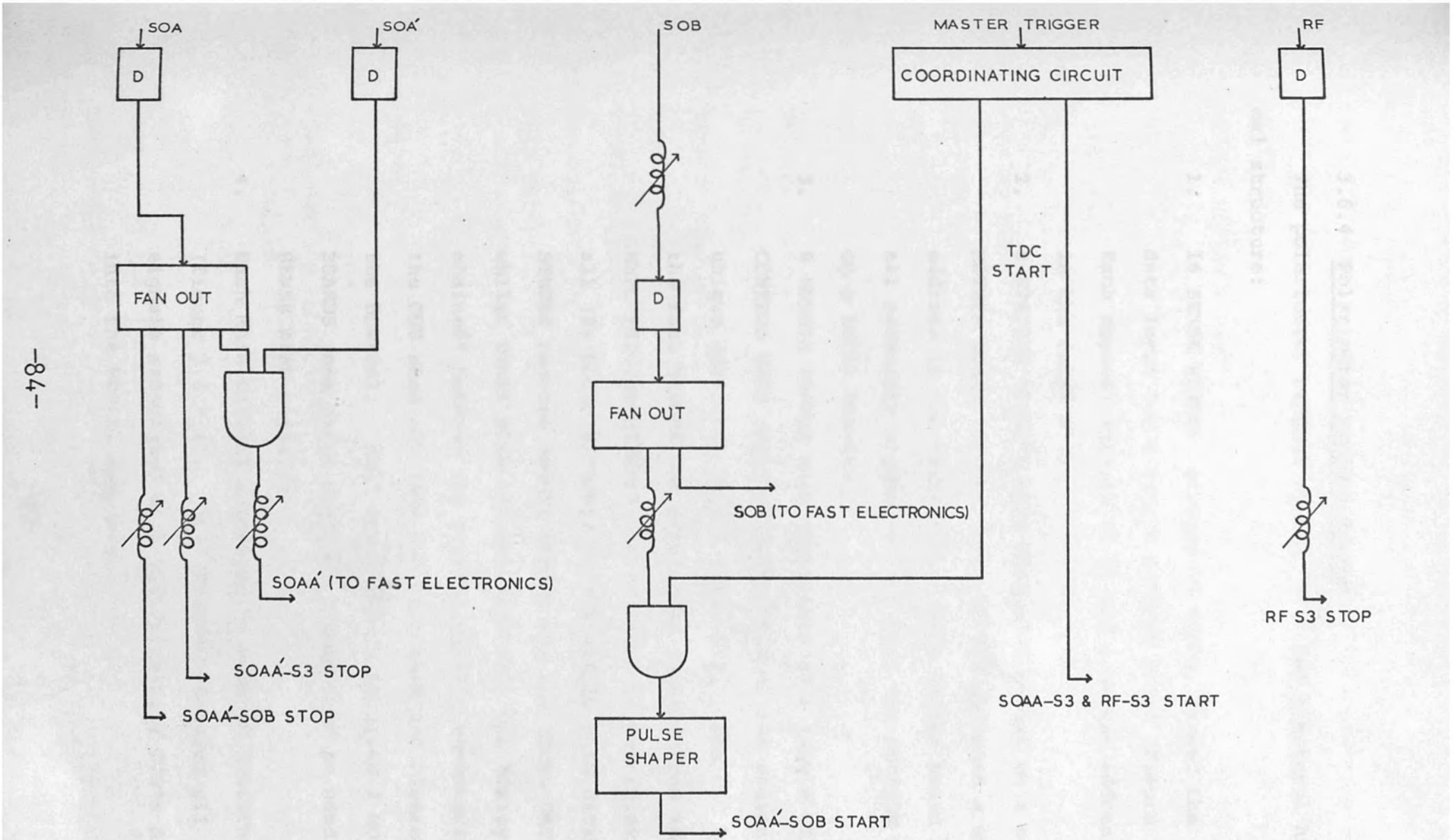

FIGURE 3·6·3·1 TIME OF FLIGHT SUBSYSTEM

3.6.4 Polarimeter readout system

The polarimeter readout system[3.15] had a natural hierarchical structure:

1. 16 SENSE WIRES; grouped in two's, formed the data input for a single STATION BOARD (figure 3.6.4.2). Each channel (groups of 2) had a unique address in the range 0-7.
2. 8 STATION BOARD's were grouped together on a single MOTHER BOARD (figure 3.6.4.3) and assigned a unique address in the range 0-7. This latter board bussed all necessary signals to and from the STATION BOARDs on a LOCAL DATAWAY.
3. 8 MOTHER BOARDS were controlled by a single CHAMBER CONTROL UNIT (CCU) (figure 3.6.4.4) and assigned unique addresses in the range 0-7. The CCU handled the fast STROBE and START SCAN signals from the MWPC TRIGGER CIRCUIT, in addition to multiplexing all (8) LOCAL DATAWAYS onto a single MAIN DATAWAY. STROBE reached MOTHER BOARDS via the LOCAL DATAWAYS whilst START SCAN (became SCAN OUT) was "daisy chained" between the boards, finally re-entering the CCU when all data had been read and cleared (from the boards). Half metre MWPC's required 2 MOTHER BOARDS (one metre chambers required 4) to handle SENSE WIRE signals.
4. Each MAIN DATAWAY connected to a CAMAC INTERFACE (figure 3.6.4.4). The INTERFACE handled all fast signals associated with multiplexing a CCU's data into the PDP-11 computer.

Passage of a charged particle through the polarimeter resulted in pulses forming on sense wires closest to the particle's track. Each signal was amplified and discriminated before firing a monostable of predetermined switching time (figure 3.6.4.2). Simultaneously the scintillator fast electronics (section 3.6.1) decided whether the event was of sufficient interest to warrant readout of the polarimeter data. If the decision was affirmative then readout was initiated by sending MWPC READ from the CO-ORDINATING CIRCUIT to the MWPC TRIGGER CIRCUIT (figure 3.6.4.1). This latter circuit generated and fanned out to 5 CCU's (an 80ns) STROBE followed 50ns later by (a 50ns) START SCAN. STROBE gated the falling monostable edge into a set/reset latch (figure 3.6.4.2), thus making the MWPC data permanent. START SCAN caused the SCAN OUT level to be asserted from each CCU (figure 3.6.4.4). This level propagated through consecutive MOTHER BOARDS, "daisy chained" together, on a CCU. Permanent data held up the progress of this level and gated the status of the complete STATION BOARD's latches onto the LOCAL DATAWAY and thus, via the CCU, onto the MAIN DATAWAY.

The PDP-11 computer interrogated INTERFACE's separately (hence a single CCU). Each computer data transfer from the INTERFACE consisted of a sense wire address from the STATION BOARD holding up SCAN OUT. The boards latches were reset when all activated wire addresses had been read (obviously a maximum of 8). SCAN OUT moved on to the next STATION BOARD (then MOTHER BOARD, etc) finally re-entering the CCU as SCAN IN. Receipt of this latter signal indicated the end of data from a given INTERFACE.

A sense wire address was composed of three principle fields plus a flag BIT to indicate that the address was a valid address.

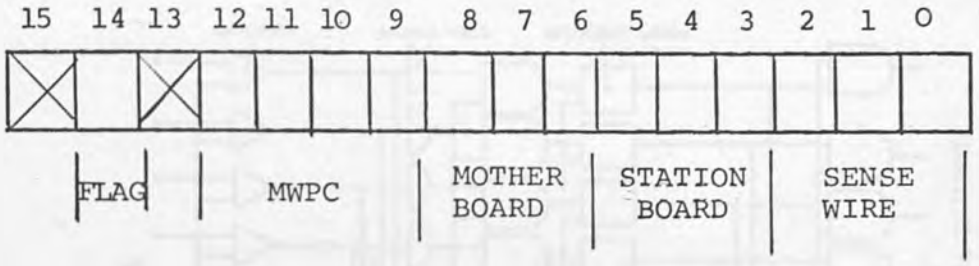

1. SENSE WIRE; was the sense wire address on its STATION BOARD (range 0-7).
2. STATION BOARD; was the station board address on its MOTHER BOARD (range 0-7).
3. MOTHER BOARD; was the mother board address in its CCU (range 0-7).

Wire addresses were interpreted according to the physical arrangement of LOCAL DATAWAYS amongst the CCU's. One further field was added by the computer before the data was output onto magnetic tape. The MWPC number was calculated from the known physical arrangement of MOTHER BOARDS and placed in bits 9-12: the flag bit was cleared, being irrelevant for off-line analysis.

3.7 Data acquisition system

The purpose of any data acquisition system[3.17] in modern Nuclear Physics is to collect sufficient information about each event so that, on the basis of this data alone, "good" events can be selected for further analysis. Due care must be taken to ensure adequate redundancy, though an attempt must be made to minimise the amount of information recorded. The purpose of this section is to show how the individual electronic subsystems (described in section 3.6) combine together to form the data

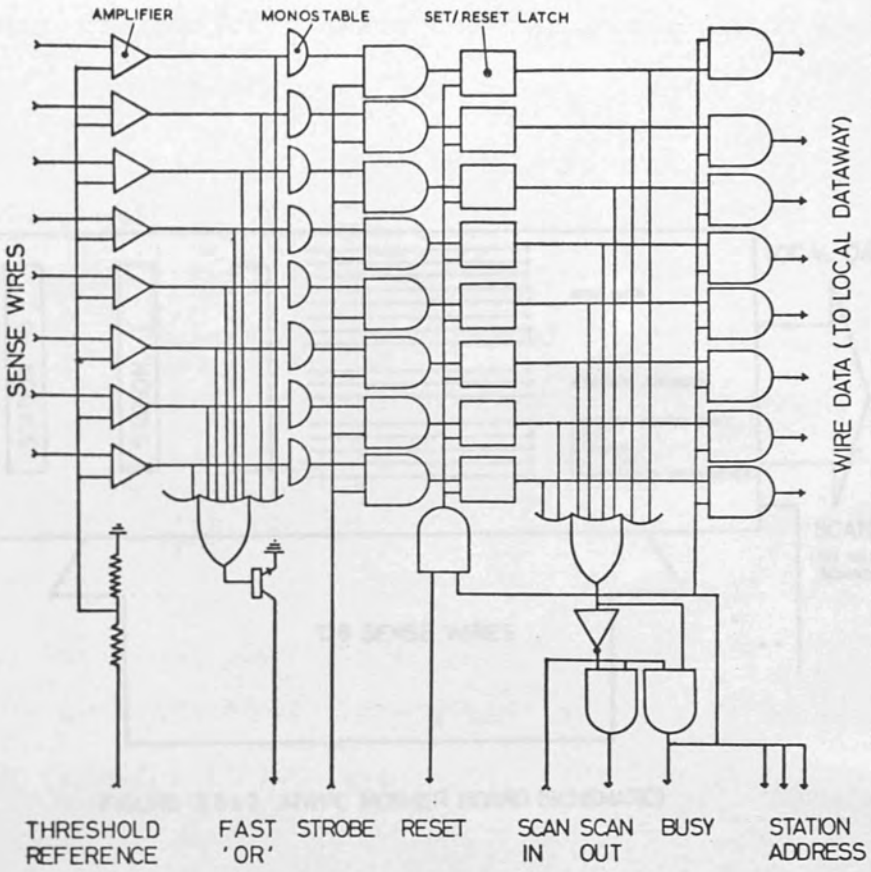

FIGURE 3·6·4·2 STATION BOARD

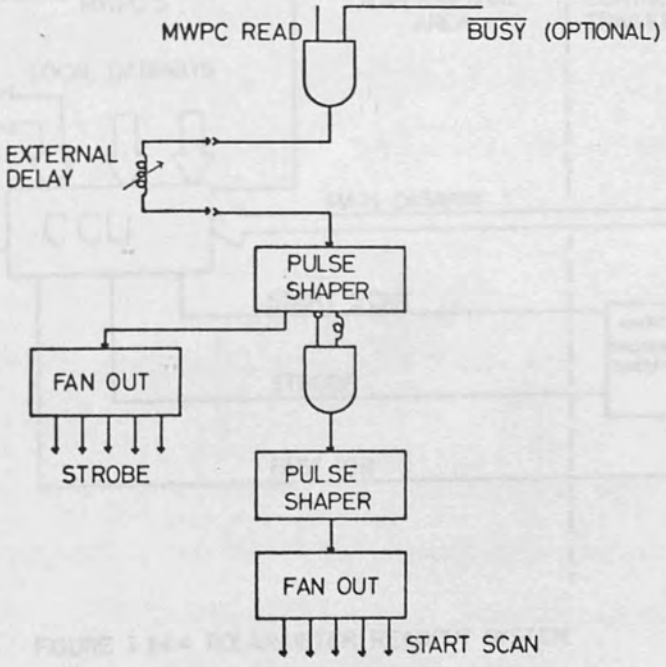

FIGURE 3·6·4·1 MWPC TRIGGER CIRCUIT

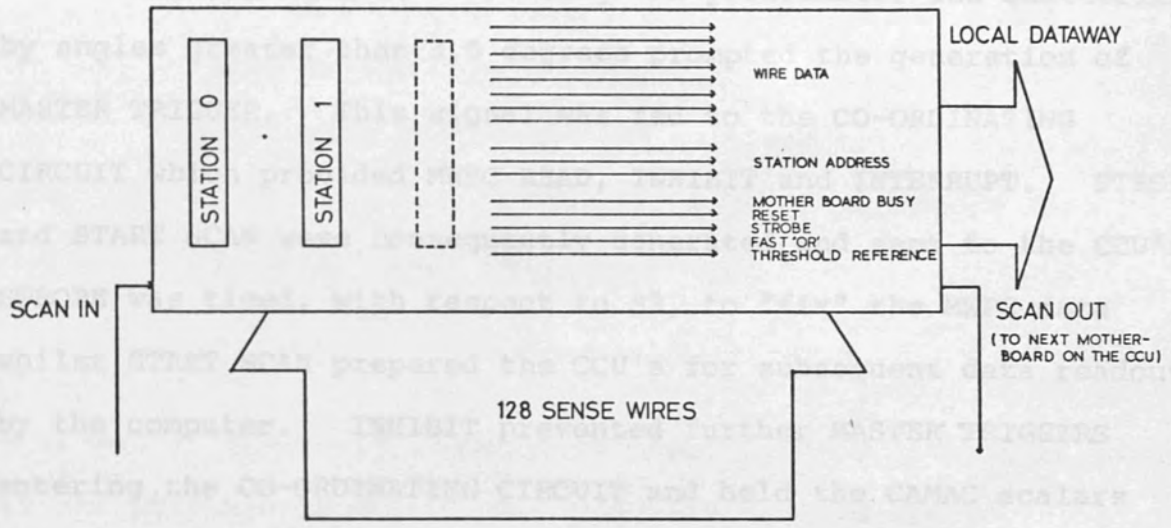

FIGURE 3·6·4·3 MWPC MOTHER BOARD (SCHEMATIC)

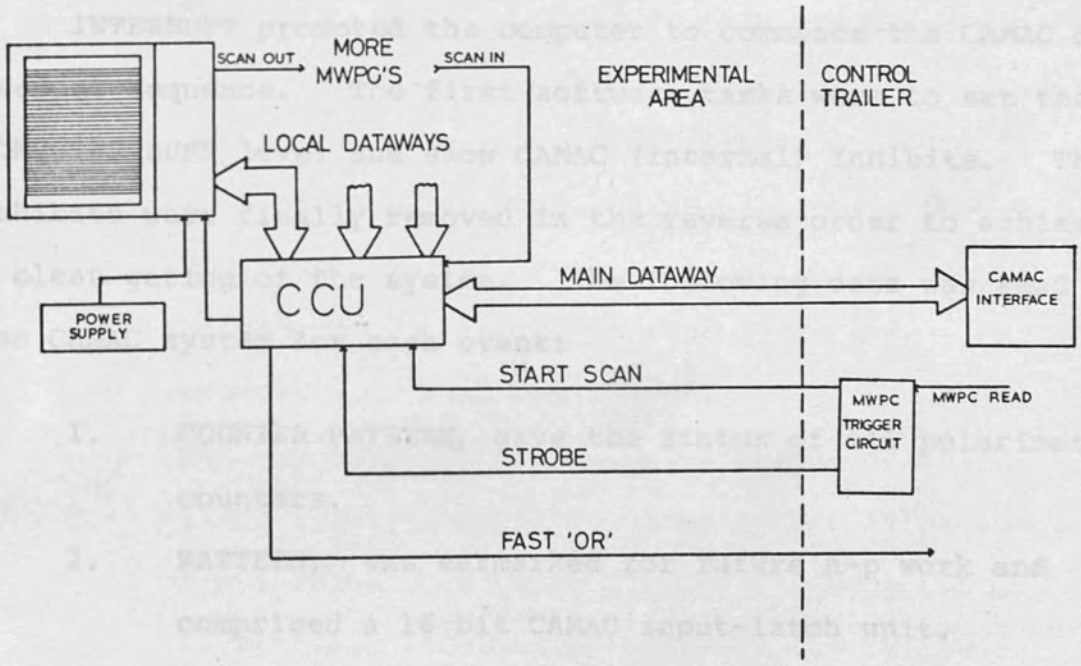

FIGURE 3·6·4·4 POLARIMETER READOUT SYSTEM

acquisition system. Analysis of this (recorded) data is dealt with in Chapter 5 where several minor errors in the data acquisition system are discussed. Figure 3.7.1 illustrates the system whilst figure 3.7.2 shows the electronic units assembled in the BASQUE experimental trailer.

Charged particles traversing the polarimeter and scattering by angles greater than 3.5 degrees prompted the generation of MASTER TRIGGER. This signal was fed to the CO-ORDINATING CIRCUIT which provided MWPC READ, INHIBIT and INTERRUPT. STROBE and START SCAN were consequently generated and sent to the CCU's. STROBE was timed, with respect to S3, to "fix" the MWPC data whilst START SCAN prepared the CCU's for subsequent data readout by the computer. INHIBIT prevented further MASTER TRIGGERS entering the CO-ORDINATING CIRCUIT and held the CAMAC scalars off for the duration of the system deadtime.

INTERRUPT prompted the computer to commence the CAMAC data readout sequence. The first software tasks were to set the COMPUTER BUSY level and slow CAMAC (internal) inhibits. These inhibits were finally removed in the reverse order to achieve a clean gating of the system. The following data was read from the CAMAC system for each event:

1. COUNTER PATTERN; gave the status of all polarimeter counters.
2. PATTERN; was earmarked for future n-p work and comprised a 16 bit CAMAC input-latch unit.
3. REAL and LIVE TIME clocks; monitored the real and live times for the data acquisition system.

4. SCALARS; selected scalars were read for each event enabling the beam intensity and polarization to be continuously monitored. All scalars were read at the end of an experimental run and their values placed onto magnetic tape.

5. ADC's and TDC's; ADC's were earmarked for n-p work, whilst TDC's contained the three monitored TOF's.

6. MWPC data; were the addresses of sense wires activated by the charged particle traversing the polarimeter. A maximum of three addresses were read from each MWPC.

On-line rejection of events was undertaken to remove those events that would "obviously" have to be removed in off-line analysis. It was possible to select the following tests to be performed, on each event, by the computer:

1. TOF CUT; rejected those events outside of an experimentally determined TOF window. Typically a wide acceptance ($\sim$ 12ns) ensured that the elastic peak and some inelastic background were recorded.

2. CLEANING; for each event the polarimeter data consisted of 12 sets (one for each MWPC) of wire addresses. Each set was restricted to contain a maximum of 3 addresses. (More than 3 activated wires in any chamber resulted in bit 14 of the first 3 addresses read being flagged). Each set was classified, in off-line analysis, as follows:

   a) TYPE 0; the set was empty.

   b) TYPE 1; the set had a single address.

c) TYPE 2; the set had two adjacent addresses.

d) TYPE 3; the set had two non-adjacent addresses.

e) TYPE 4; the set had three adjacent addresses.

f) TYPE 5; the set had three addresses group according to the classifications of TYPE 1 and TYPE 2.

g) TYPE 6; the set had three non-adjacent addresses.

h) TYPE 7; the event was not TYPE 0-6 and the three addresses had bit 14 set.

CLEANING ensured that an event was rejected if it did not have at least two TYPE 1 sets, in the X-Z and Y-Z planes, both before and after the carbon scatterer.

3. STRAIGHT TRACK REJECTION; events with a scattering angle of less than 3.5 degrees (adjustable) in both X-Z and Y-Z planes were not recorded. This situation occurred whenever a proton scattered downstream of the last MWPC, missing V, but was undeflected in the carbon analyser.

4. BIT PATTERN; the polarimeter COUNTER PATTERN was examined. Events were rejected if more than one element of any detector was activated. The test was designed to eliminate events in which two or more particles were present in the polarimeter.

Events passing the above tests (if the tests were enabled) were written onto magnetic tape for further off-line analysis. Histograms of their three TOF's, MWPC activated wire numbers, MWPC multiplicities and counter BIT PATTERN were immediately available to experimenters on a TEKTRONIX 4010 visual display unit.

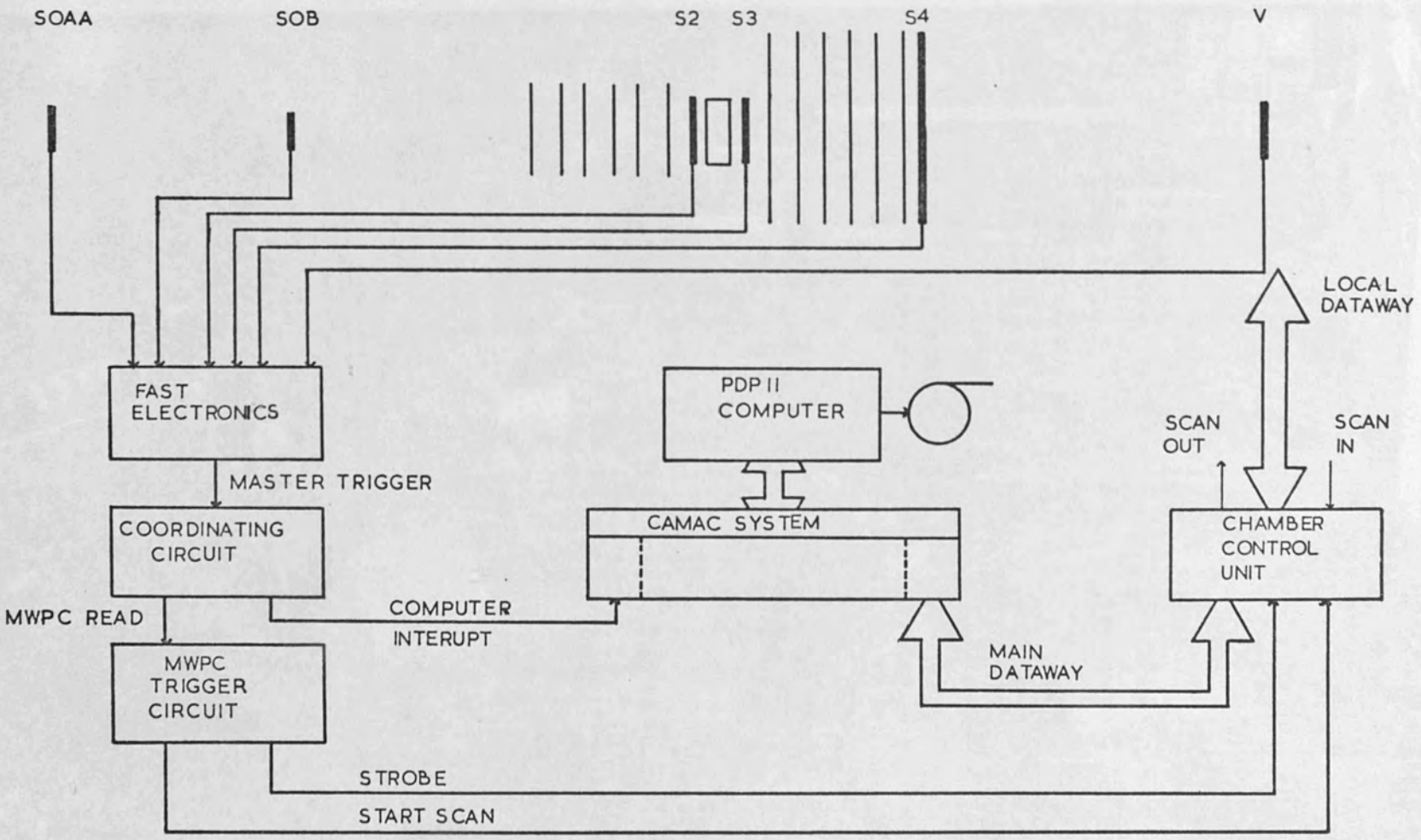

FIGURE 3·7·1 DATA ACQUISITION SYSTEM

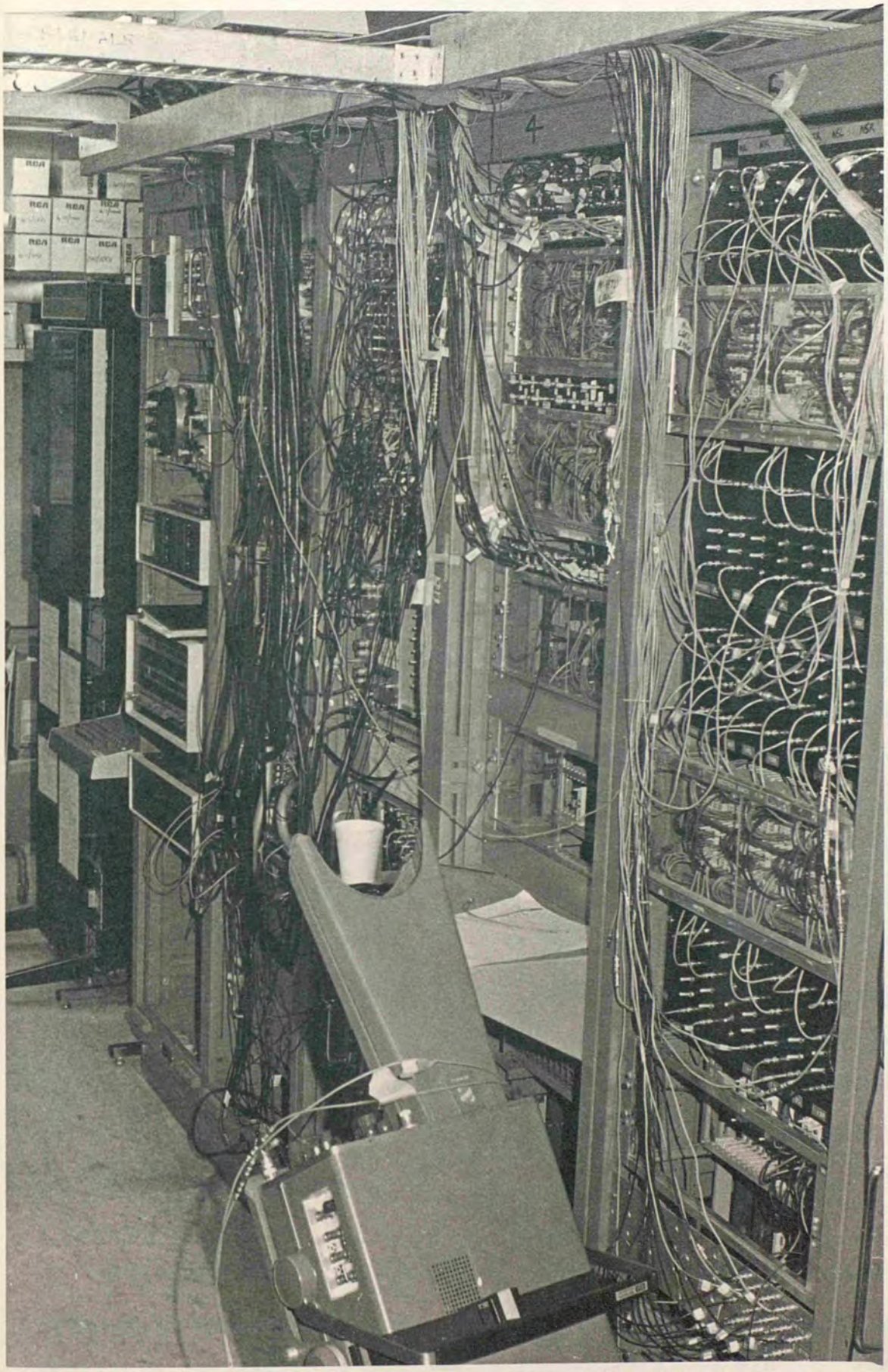

FIGURE 3.7.2 ELECTRONIC SUBSYSTEMS ARRANGED IN BASQUE TRAILER

CHAPTER 4

Experimental Configurations

Three basic experimental arrangements were utilized, a different configuration being needed in each case for the polarimeter calibration, the D and R measurements and the R' experiments The polarimeter calibration (section 4.1) required the superconducting solenoid to be removed from the primary beam-line and placed immediately downstream of the collimator. It was replaced for the R and R' measurements (section 4.2 and 4.3) to enable the beam polarization to be precessed by -90 degrees from the vertical before the hydrogen target. A vertical polarization was required for D measurements hence the solenoid was turned off. The R' measurement (section 4.3) required a spin precession magnet before the polarimeter to rotate the longitudinal component of the scattered beam's polarization into the horizontal plane. All three experiments required the polarimeter to measure transverse polarization components of the secondary beam. The 35 degree bending magnet downstream of the hydrogen target was turned off for the proton work and the primary beam dumped in the zero degree port of the neutron collimator (suitably filled with steel plugs). This expedient prevented precession of the scattered beam's polarization in the magnet's fringe field and allowed protons to pass, undeflected, into the collimator port corresponding to their true laboratory angle of scatter in the hydrogen target.

The polarimeter calibration was performed during the winter of 1976. Section 2.2 discussed the energies and angles at which Wolfenstein parameters were to be measured whilst table 4.2.1

lists the actual experiments (for historical completeness) carried out early in the Spring of 1976. This chapter is devoted to describing the philosophy behind the aforesaid configurations in which beams were prepared with known polarization vectors and specific components of the scattered beam polarization vector were measured. Analysis of these experiments forms the topic of Chapter 5.

4.1 Polarimeter calibration

Figure 4.1.1 illustrates the experimental configuration for the polarimeter calibration. Data were recorded in this configuration using unpolarized primary beam throughout 1975. A gas target was synthesized from the empty target-radiation-shield by sealing the target entry port and pressurizing with hydrogen. Test data and part of the polarimeter calibration at 480 MeV were consequently written onto magnetic tape. These runs proved useful for testing the data acquisition system and debugging off-line software.

The polarimeter calibration was performed in the early months of 1976, after installation of the liquid hydrogen target during Autumn 1975. The target flask was 203mm long by 51mm diameter. With this length target it was impossible to raise the target flask and dummy completely out of the beam-line. A shorter flask was therefore installed for the Wolfenstein parameter measurements.

The 24 degree port was (historically) chosen for the calibration before it was deemed safe to dump the beam in the zero degree port of the collimator. At this angle the magnitude of

p-p polarization has only dropped by 20% (at 500 MeV, the worst energy) from its peak value (15-18 degrees lab in the energy range 200-500 MeV), and the scattered beam would have suffered minimal precession from the vertical, after passing through the edge of the 35 degree bending magnet's fringe field.

The scattered beam was defined by the proton telescope and our solenoid was positioned downstream of the collimator to rotate the resulting polarization by $\pm$ 90 degrees from the vertical. Approximately 800K events were recorded on magnetic tape for the following EPB energies 518, 480, 435, 380, 343, 307, 271, 237 and 209 MeV. Half the data were recorded with the secondary beam polarization oriented along the -X axis (see figure 3.4.1 for the definition of the co-ordinate system) and half along +X. Thus the measured asymmetry in the polarimeter could be averaged over two polarization orientations to remove systematic biases in its determination. The measured analysing power of carbon (A_c) was therefore subject to the 24 degree polarization error, statistical errors and systematic errors. This former quantity will be measured at TRIUMF in a double scattering experiment and will improve the error in the determination of A_c.

Straight tracks in the polarimeter were rejected by positioning a veto counter downstream of the carbon analyser. Protons scattering by angles less than 3.5 degrees, in the carbon, struck the counter and vetoed the event. For the calibration experiment a veto counter was provided by the overlap of the two central counters of the neutron detector (figure 3.4.1). The veto counter was offset from the polarimeter centre line 60mm

to allow for the 7 milliradian steering of the secondary proton beam by the momentum analysing magnet. This latter magnet coupled with a TOF measurement was sufficient to enable elimination of pions above threshold and inelastic protons. Below EPB energies of 271 MeV multiple scattering effects forced the veto counter to be moved from 4m to 2.5 metres from the carbon (Appendix A).

Four tests were performed on each event by the data acquisition computer (section 3.7). Of these CLEANING was later found to have a deleterious effect on the recorded data. It was possible however to extract correct values of A_c after extensive tests showed that the algorithm used to extract asymmetries was insensitive to effects introduced by the CLEANING test.

Implicit in the following sections are the "normal setting up procedures" for our apparatus, viz:

a) cooling and filling the hydrogen target and superconducting solenoid,
b) plateauing all scintillation counters,
c) timing in all signals to form MASTER TRIGGER, positive TOF's etc.
d) timing in the polarimeter STROBE with respect to MASTER TRIGGER and setting MWPC voltages,
e) "tuning beam-line 4A",
f) examining all histograms, provided by the data acquisition computer, for obvious trouble.

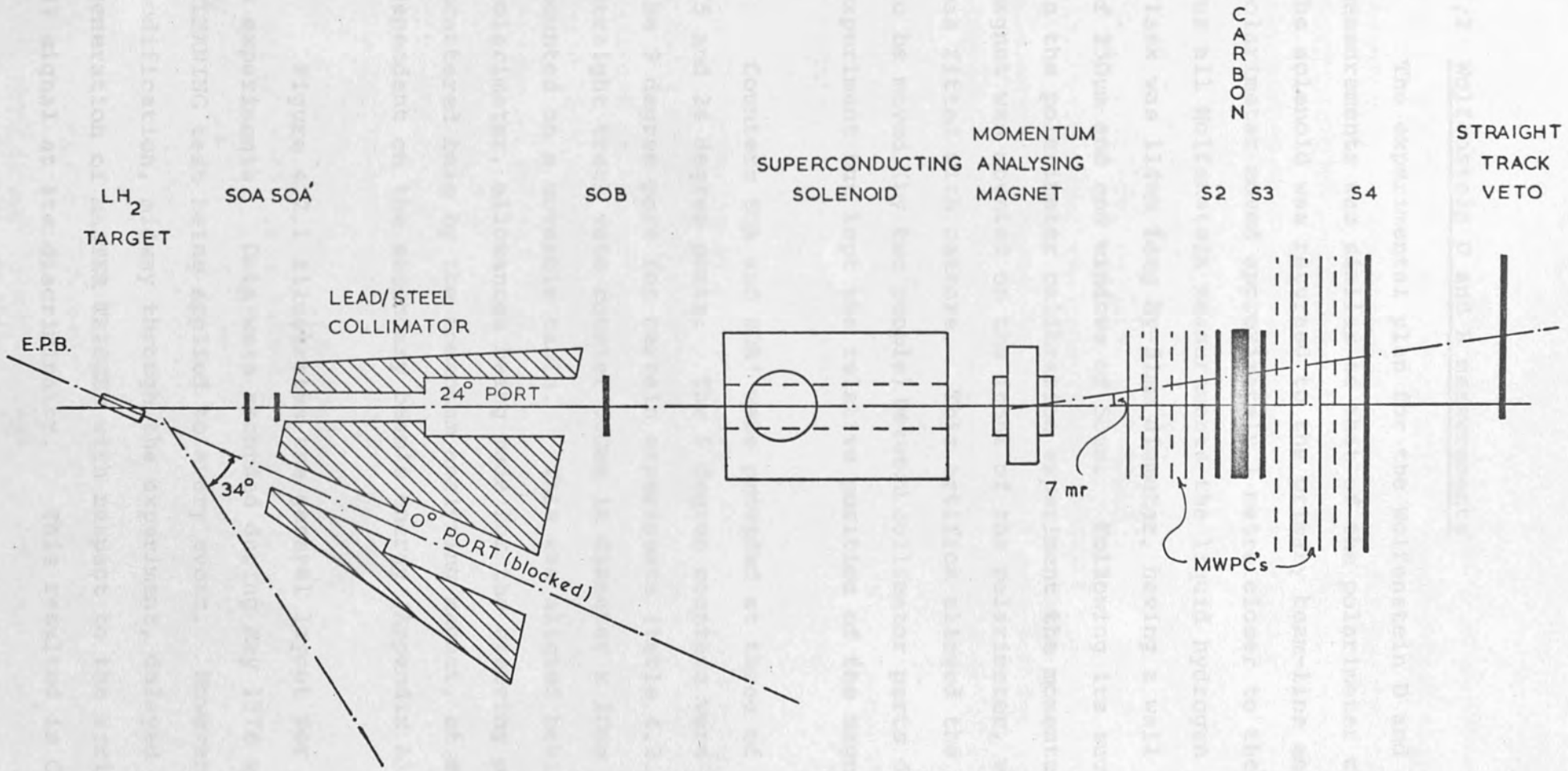

FIGURE 4.1.1 EXPERIMENTAL ARRANGEMENT FOR THE POLARIMETER CALIBRATION

4.2 Wolfenstein D and R measurements

The experimental plan for the Wolfenstein D and R parameter measurements was similar to that of the polarimeter calibration. The solenoid was returned to the primary beam-line and the polarimeter moved approximately 1 metre closer to the collimator. For all Wolfenstein measurements the liquid hydrogen target flask was 114mm long by 51mm diameter, having a wall thickness of 250μm and end windows of 50μm. Following its successful use in the polarimeter calibration experiment the momentum analysing magnet was mounted on the front of the polarimeter, which itself was fitted with castors. This artifice allowed the polarimeter to be moved (by two people) between collimator parts during the experiment but kept the relative position of the magnet unchanged.

Counters SOA and SOA' were provided at three of the 6, 9, 15 and 24 degree ports. The 6 degree counters were moved to the 9 degree port for certain experiments (table 4.2.1). A straight track veto counter 360mm in diameter x 10mm thick was mounted on a moveable table. This was aligned behind the polarimeter, allowances being made for the steering of the scattered beam by the momentum analysing magnet, at a distance dependent on the secondary beam's energy (Appendix A).

Figure 4.2.1 illustrates the general layout for the D and R experiments. Data were recorded during May 1976 without the CLEANING test being applied to every event. However a timing modification, midway through the experiment, delayed the generation of MASTER TRIGGER with respect to the arrival of the S3 signal at its discriminator. This resulted in COUNTER

PATTERN GATE failing to gate the status of polarimeter counter S4A into a CAMAC input latch unit. The on-line test BIT PATTERN therefore rejected all events in which S4A was included in the MASTER TRIGGER coincidence. Fortuitously all essential data were recorded without this test being applied.

Precession of the EPB's polarization by -90 degrees from the vertical was required during the R measurement. Figure 1.3.3 shows that the polarimeter was then used to determine the horizontal component (R) of the final polarization vector in addition to the ever present vertical component (P). The solenoid was switched off for D measurements and the polarimeter determined the vertical component: the horizontal component being inconsistent with zero (section 5.4).

In order to remove possible instrumental biases, parameters D and R were determined from the difference of two asymmetries measured in the polarimeter (see section 1.3 for further details). For R this corresponded to a complete reversal of the measured horizontal polarization component by reversing the sign of the EPB polarization at the target; whilst for D this corresponded to measurements of the asymmetry with D both parallel and anti-parallel to the vertical polarization P (again by reversing the EPB polarization). The direction of the EPB polarization was changed at the polarized ion source for the reasons discussed in section 2.3. Values of P determined from the polarimeter data were therefore subject to possible instrumental asymmetries.

A total of 180K events were recorded for each parameter (EPB energy) and laboratory scattering angle listed in table 4.2.1

Half the data were recorded at each EPB polarization orientation. Twice the normal amount of data were recorded at 518 MeV and 15 degrees enabling the polarimeter calibration to be extended to higher energies (section 5.3).

EPB energy (MeV) \ Lab. scattering angle	6^o	9^o	15^o	24^o
518	D,R	D,R	D,R,R'	D,R
425	D,R	D,R	D,R,R'	D,R
380	D,R	D,R	D,R,R'	D,R
325	-	D,R	D,R,R'	D,R
210	-	D,R	D,R,R'	D,R

TABLE 4.2.1 Wolfenstein parameter measurements 1976 (for historical completeness)

4.3 Wolfenstein R' measurement

Figures 4.3.1 and 4.3.2 show the equipment arranged for R' measurements. These measurements were performed after the Wolfenstein D and R experiments were concluded. The momentum analysing magnet was replaced by the UCLA magnet (section 3.5) which was used to turn the longitudinal polarization component of the secondary beam into the horizontal transverse direction (see figure 1.3.3 for the physical definition of R'). The magnet and polarimeter were fixed to "observe" scattered beam

emerging from the 15 degree port and only the veto counter was moved, backwards for higher energies, along the polarimeter centre line. The solenoid was powered to rotate the EPB polarization by -90 degrees.

Part of the setting up procedure was to vary the precession magnets excitation, sweeping the scattered beam centroid across the face of the veto counter (in the horizontal plane). The final excitation was chosen to minimise the MASTER TRIGGER rate. The beam centroid was then aligned with the centre of the veto to sufficient accuracy (with the veto rejecting the maximum percentage of events its function was fulfilled).

In using this fixed-geometry configuration the chosen magnetic field was generally insufficient to rotate the longitudinal component completely into the transverse orientation. A linear combination of the original horizontal and longitudinal components were therefore measured in the polarimeter. Figure 1.3.3 shows this actually corresponds to a measurement of a linear combination of R and R'.

Data were recorded for two transverse orientations of the EPB polarization. 90K events were recorded for each orientation without employing the CLEANING and BIT PATTERN tests in the data acquisition computer.

FIGURE 4·2·1 EXPERIMENTAL ARRANGEMENT FOR D&R MEASUREMENTS

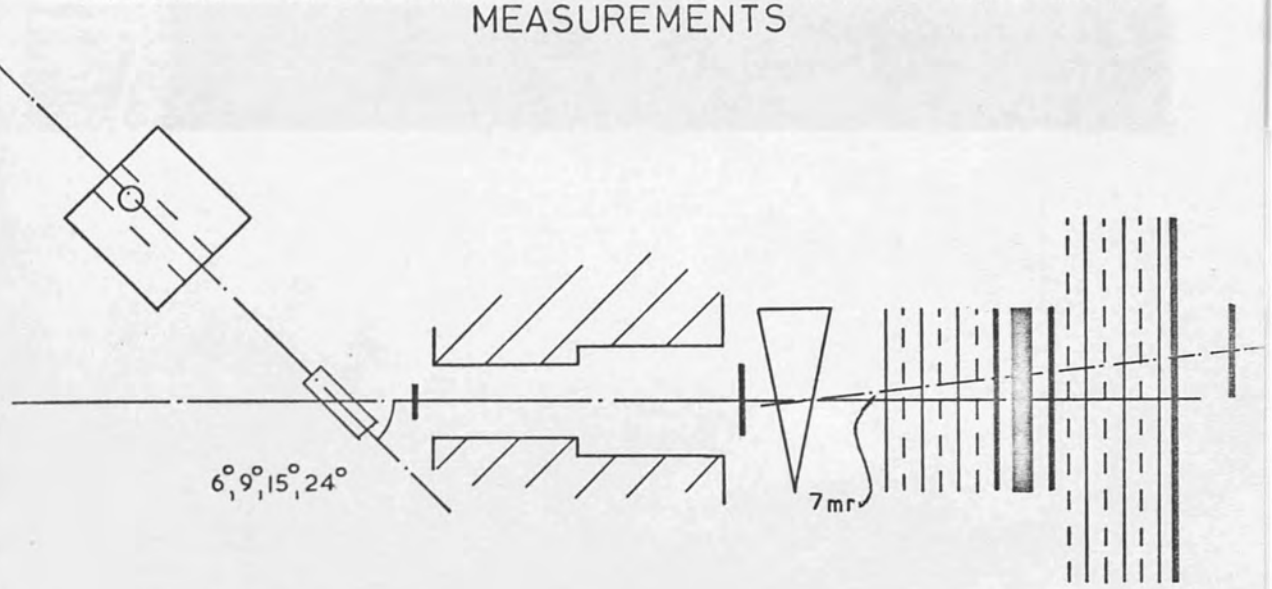

SWEEP MAGNET

SOLENOID LH_2 TARGET SOA'A COLLIMATOR SOB POLARIMETER VETO

UCLA MAGNET

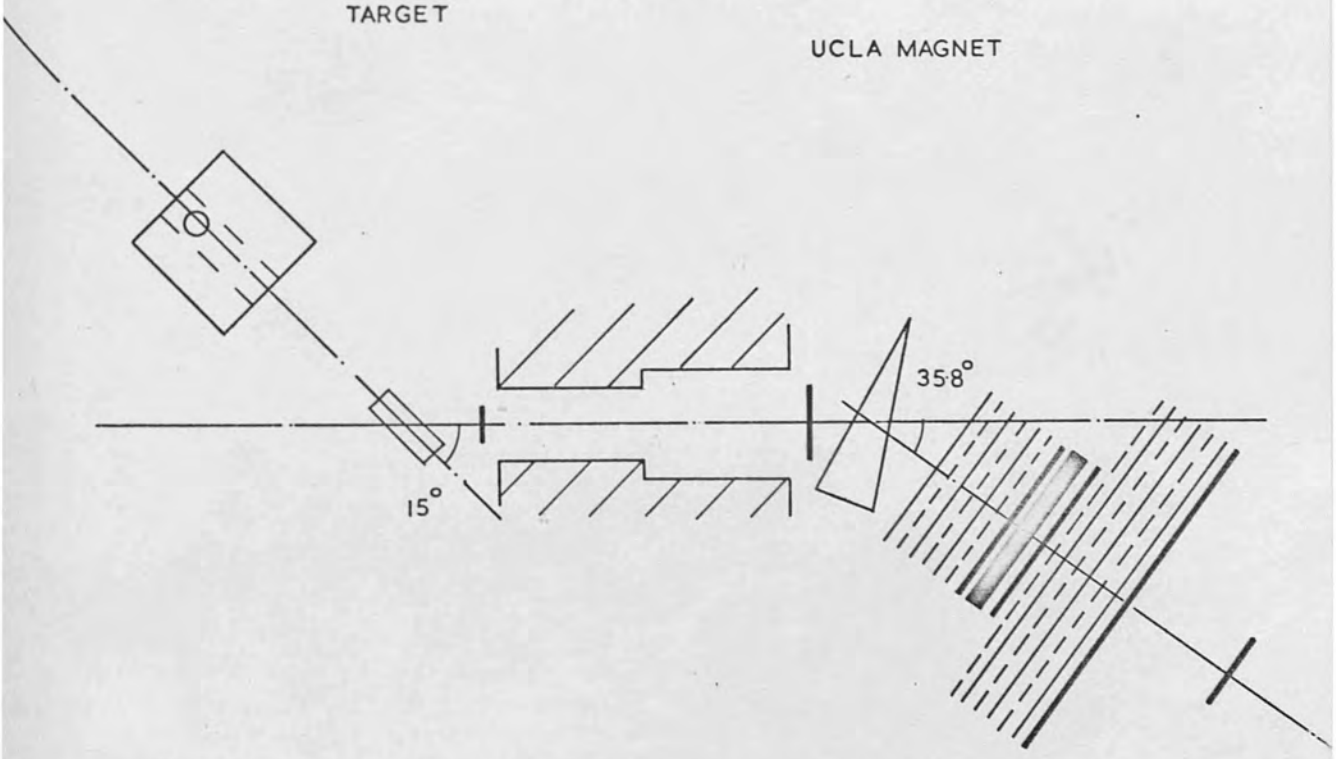

FIGURE 4·3·1 EXPERIMENTAL ARRANGEMENT FOR R' MEASUREMENT

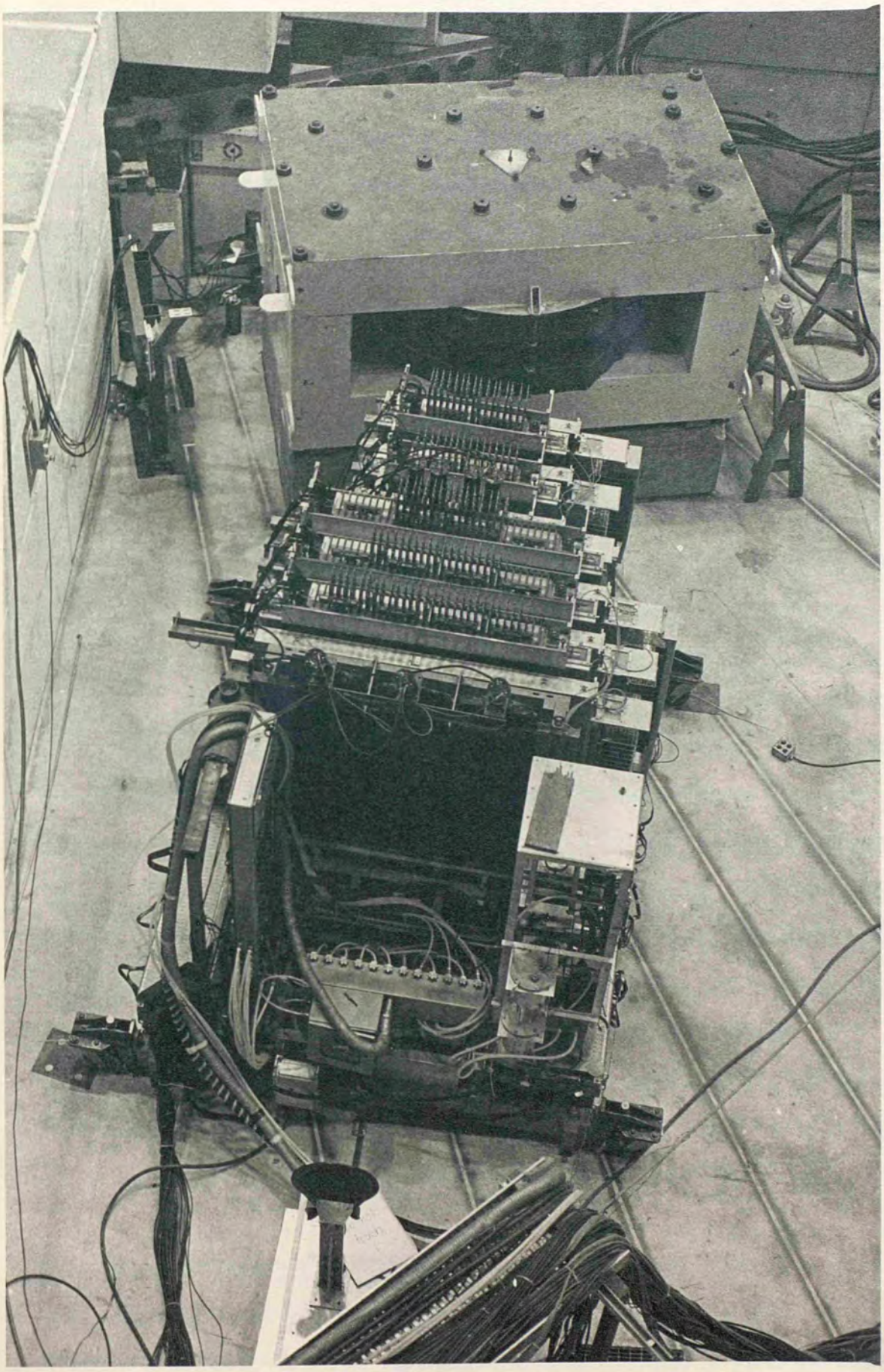

FIGURE 4.3.2 R' MEASUREMENT IN THE PROTON HALL

CHAPTER 5

Data Analysis

This chapter deals with the analysis of the polarimeter calibration and Wolfenstein parameter measurements. The methods used to select "good events" from candidate events were essentially the same for all experiments (section 5.1). The polarimeter data was always reduced to sets of asymmetries (section 5.2). Calibration sets (section 5.3) were used with Wolfenstein parameter sets (section 5.4) to obtain values for the P, D, R and R' parameters. These results were used in a single energy phase shift analysis at 515 MeV (section 5.5) to improve the values and associated error of the p-p isospin one phase shifts (section 2.1).

Bulk data processing was carried out by the author on the Rutherford Laboratory's IBM 360/195 computer during the Spring and Summer of 1976. A simple method of assembling computer jobs with repetitive steps was developed and is explained in Appendix B. A small portion of the data was analysed on the University of British Columbia's IBM 370 computer. This consisted mainly of checks on the data during experimental runs, processing the entire 480 MeV polarimeter calibration data and all 325 MeV Wolfenstein parameter data. This latter processing however was insufficient to ensure completely "clean" data (section 5.3 and 5.4). Final results were available in the Autumn of 1976.

5.1 Data reduction software

The computer software necessary to read raw data files (produced by the PDP-11) and reduce them to θ-ϕ matrices were

written and tested at TRIUMF during 1975 by the author and Mr C Oram (θ-Ø were the scattering and azimuthal angles in the carbon and will be described in section 5.1.2). The complete analysis chains for the polarimeter calibration and Wolfenstein parameter experiments are shown in figures 5.1.1 and 5.1.2 respectively. These chains divided naturally into two parts. Part one required physics input to pre-process the data up to and including the extraction of θ-Ø matrices; for instance establishing "cuts" on the raw data (section 5.1.2). Part two saw the extraction of physics results in the form of values for A_c, P, D, R, R' and a final phase shift analysis utilizing these latter data.

Bulk data processing programs REDUCE 1 and 2 are dealt with in sections 5.1.1 and 5.1.2 (SIEVE being briefly discussed in the former). The mathematics used by ASYMMETRY (to determine asymmetries) are described in section 5.2 (detailed in Appendix F) whilst the fitting of A_c as a function of scattering angle and incident momenta, by program FIT, forms the topic of section 5.3.2. Program ASYMMETRY became a subroutine of DRIP for the Wolfenstein parameter analysis, where A_c was generated from its fitted values, and experimentally determined values of D, R, R' and P were derived. The algorithms used by the phase shift analysis program QUAPS-PP3 are well known in the "phase shift literature"[5.1] and will not be explained in this thesis.

A program of software optimisation was carried out by the author during May 1975, with the aim of reducing computing time requirements. The following salient points emerged:

1. irrelevant subroutine calls had to be removed and FORTRAN code explicitly inserted into the calling program;
2. FORTRAN input/output was replaced by locally written routines transferring unformatted data to and from intermediary tapes. A relative factor of 18 was saved by these modifications alone;
3. extracting fields of known length from a bit-pattern was more speedily accomplished by division (by a factor of 2 for right shifting the entire pattern), multiplication (by a factor of 2 to left shift the pattern and right fill with zeros) and subtraction (to remove the required field) rather than calls to shifting and masking routines. A case in point was program REDUCE 1 where a factor of 7 was saved in total computer processing time by these modifications.

It is the considered opinion of the author that, in fairness to other users, all bulk data processing programs be subjected to computer processing time optimization before being generally used. To this end computer centres need to provide a simple and convenient monitor (program), within which the user's program executes, and whose output indicates those parts of the program which require most computing time.

5.1.1 Track reconstruction in the polarimeter

The polarimeter consisted of a carbon target sandwiched between 6 front and 6 rear MWPCs and associated trigger counters. The chambers divided naturally into four "quadrants". Each quadrant being a triplet of MWPCs determining the X or Y

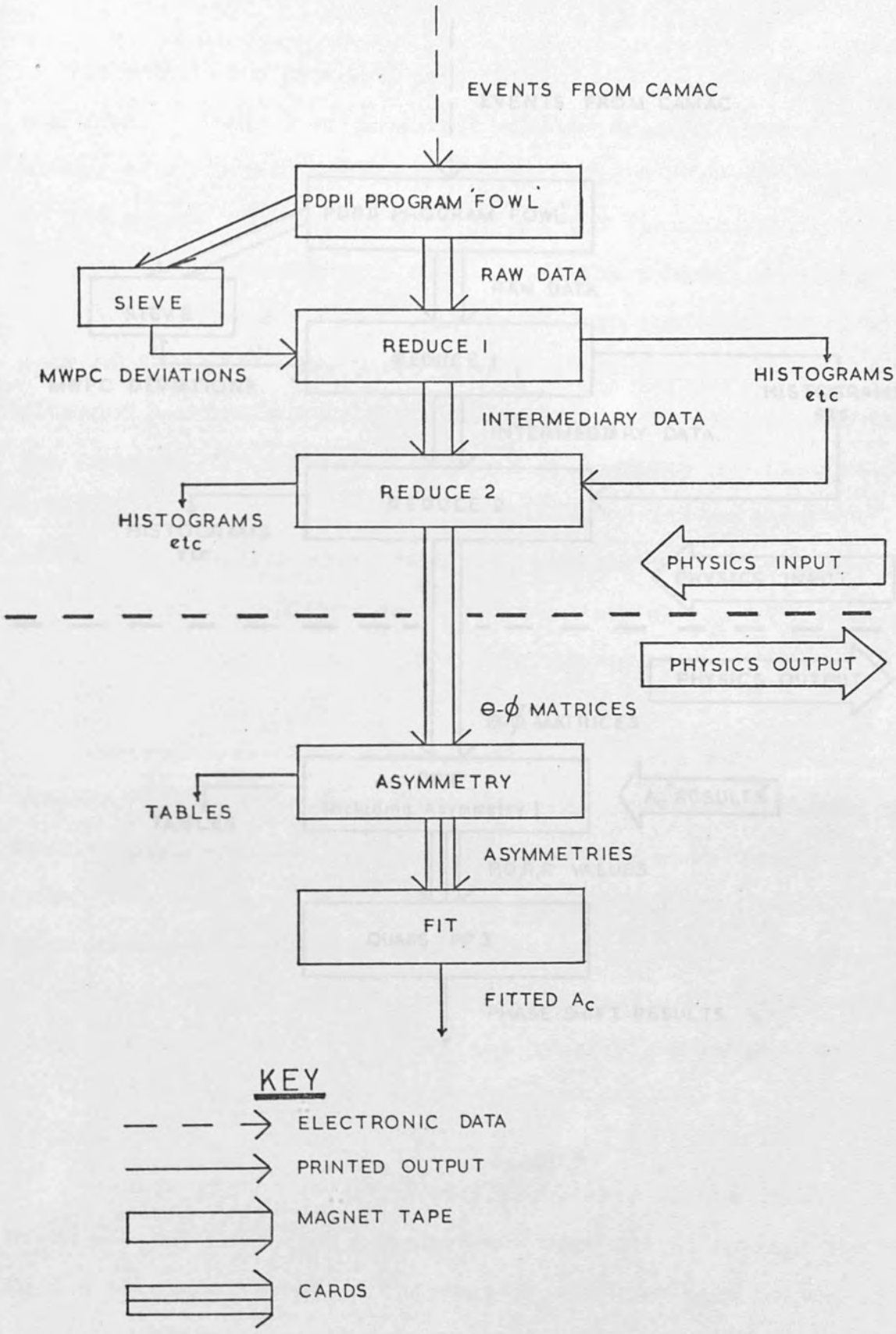

FIGURE 5·1·1 ANALYSIS CHAIN FOR POLARIMETER CALIBRATION

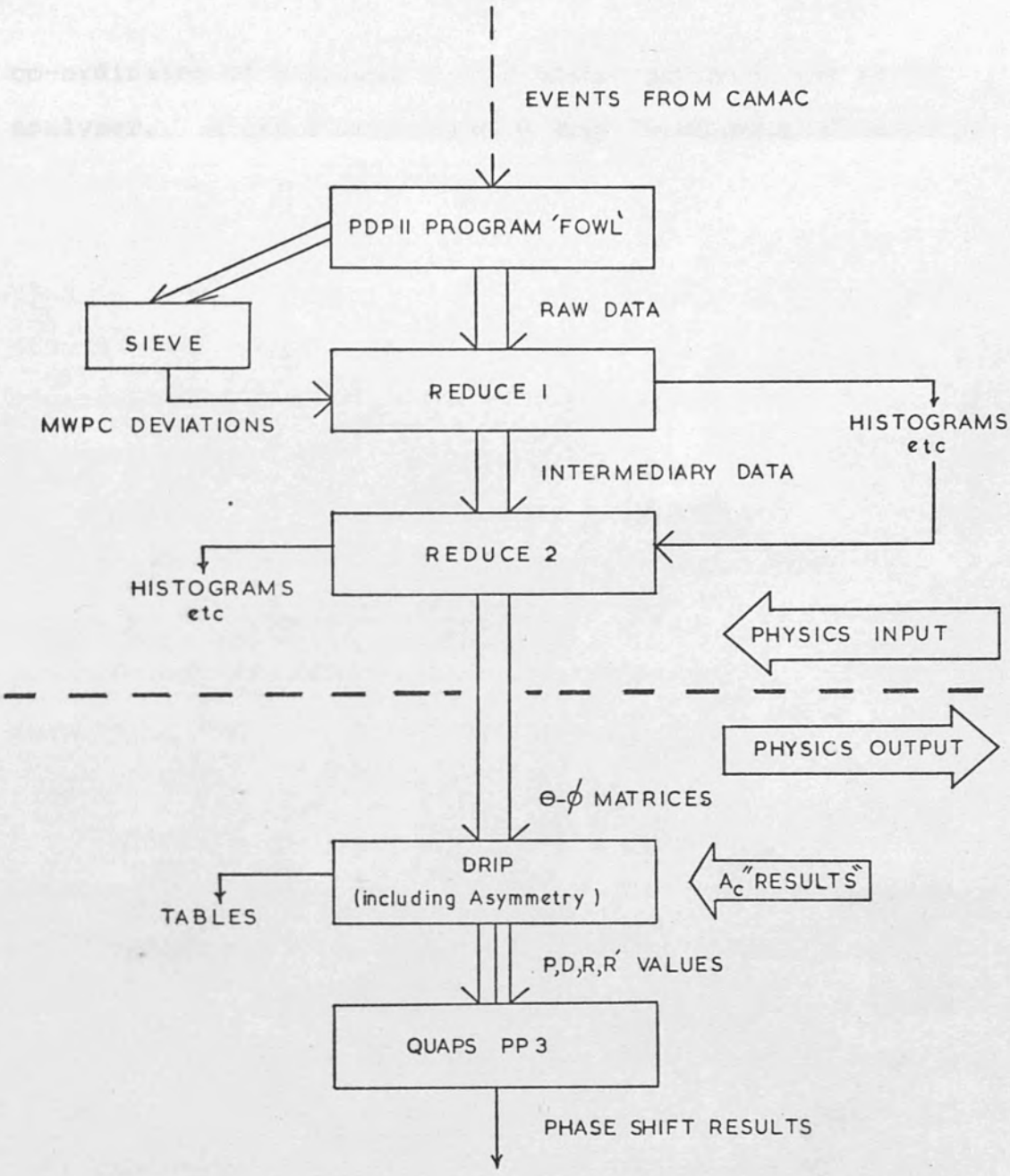

FIGURE 5·12 ANALYSIS CHAIN FOR WOLFENSTEIN PARAMETERS
(Notation as in figure 5·11)

co-ordinates of a proton's path before or after the carbon analyser. X and Y co-ordinates were determined alternately. Groups of activated wires, in any MWPC, were classified according to the scheme proposed in section 3.7 and assigned the co-ordinates of their centroids. With the carbon removed straight tracks were fitted to proton paths through the polarimeter by program SIEVE. Every track gave a residual (defined as the distance between the actual track and the co-ordinate used in the chamber) for each MWPC. The average value of these residuals were used as corrections to the MWPC positions when assigning co-ordinates in REDUCE 1. These values were found to be unchanged to better than 0.04mm over six months of operation despite removal of several MWPCs for repair.

Co-ordinates were "randomized" by adding a random number between $\pm$ 2mm to the co-ordinate determined above (Appendix C). Each triplet was then fitted with a least squares straight line[5.2]; a search being carried out for the straightest line that could be formed from the co-ordinates, subject to a maximum χ^2 value of 6.06mm^2 for the track's residuals. Two chamber fits were acceptable if no data was available from the third, but the fit was required to be unique.

Program REDUCE 1 performed a first pass on the data. Each event was unpacked from the raw data tape and an attempt was made to fit straight tracks to the polarimeter data both before and after the carbon analyser. Successful events were written to an intermediary data tape for subsequent analysis. Histograms and dot plots (synonymous with scatter plots and two dimensional

histograms) of beam profiles, TOF's and their correlations were produced by the program. Their use will be explained in the next subsection where the "second pass" program REDUCE 2 is fully discussed.

5.1.2 Event selection

Program REDUCE 2 selected "good" events for the asymmetry determination from the intermediary tape containing all event candidates. Cuts (placing limits on the range of a measured parameter) were applied to candidate's parameters to select events for further analysis. Limits were taken from the printed output of REDUCE 1. A logical division of the applied cuts into internal and external was apparent. External cuts were:

1. rejection of events appearing not to come through the collimator. Allowing for geometrical and multiple scattering effects the front 6 MWPCs were calculated to have a resolution of typically 30mm, for secondary beam protons of 380 MeV, at SOAA'. The low random MASTER TRIGGER rate ($\sim$ 1%) was entirely attributable to the high rate in SOAA'. The number of random triggers caused by protons completely missing these counters was therefore of the same order as the error on the former measured quantity. Tracks appearing to come from positions up to 2.5 times the resolution distance off the counters' edges were included as "good" events coming through the collimator (figure 5.1.2.1). A similar criteria was applied at SOB.

2. rejection of events scattering on or after the momentum analysing magnet. The exact physical location and aperture of this magnet were known. Events appearing to come through the magnet's yoke (or around) were rejected: regarded as having scattered between the magnet and the front 6 MWPCs;

3. rejection of events far from the elastic TOF peak. This eliminated pions from the two-body reaction $pp \rightarrow d\pi^+$ and inelastic protons from $pp \rightarrow np\pi^+$ and $pp\pi^o$ (above 290 MeV).

The elastic TOF peak had a full width at 2-3% full height of 6ns (figure 5.1.2.2). Inelastic protons were removed by a TOF cut on the high side of the elastic peak but a combined TOF and momentum cut was necessary to completely eliminate pions. Figure 5.1.2.3 shows the number of events plotted as a function of their TOF and bend angle in the momentum analysing magnet (proportional to the reciprocal of their momentum). Obviously a linear TOF cut on the low side of the elastic peak coupled with one on the bend angle removed two-body pions. Three-body pions from $pp \rightarrow np\pi^+$ lay on the indicated dotted locus , well clear of the elastic peak for equal TOFs.

Multiple scattering effects in the secondary beam-line smeared the proton and pion angles of incidence on the polarimeter. At 518 MeV (primary beam energy) the secondary beam at 24 degrees was observed to have a full width at 1% maximum of 24 milliradians (mr). This comprised a 10mr acceptance through the proton telescope added in quadrature to a multiple scattering and polarimeter resolution of $\sim$ 4.5mr. Being lighter pions had

a multiple scattering angle seven times that of protons with the same velocity, but were deflected by a factor 7 more in the momentum analysing magnet. Hence the proton peak (with centroid at 7mr and half width 12mr) overlapped the deflected pion peak (with centroid at 49mr and half width 33mr) at the $\sim$ 1% maximum height level. Assuming normally distributed peaks the percentage of three-body pions under the proton peak was 0.15% (of the total pions). This was insignificant as the recorded number of three-body pions was $\sim$ 100. Asymmetries were found to be essentially unchanged after varying the TOF cuts by 10%. Figure 5.1.2.4 shows the time-of-flight per metre for the reactions discussed above. Internal cuts formed the CONE test and required:

1. rejection of events if, after rotating the outgoing track about the incoming track to form a cone, part of the cone fell inside the veto counter (V) or outside S2, the carbon, S3 or S4. Symmetrizing the (azimuthal angle) ϕ distribution was required by the method of moments; chosen to determine the polarimeter asymmetry (section 5.2);
2. rejection of events with $\theta < 0.25$ degrees. Unscattered events (that missed the veto counter) passed to this stage of the analysis as they were too complex for the on-line computers straight track facility to reject, during the experimental run. In actuality events with $\theta \leq 3.5$ degrees were rejected by the presence of the veto counter in test (1) (this latter figure obviously depended on the location and shape of the veto counter).

Angles Θ and $\emptyset$ were calculated for events not rejected by the aforesaid cuts. If $\underline{k}_i$ was the incident direction-vector (obtained from polarimeter data) and $\underline{k}_f$ the outgoing, then the polar scattering angle Θ was determined from

$$\cos(\Theta) = \underline{k}_i \cdot \underline{k}_f / |\underline{k}_i||\underline{k}_f|$$

and the azimuthal angle $\emptyset$ from

$$\cos(\emptyset) = - \hat{\underline{j}} \cdot \underline{k}_i \times \underline{k}_f / |\underline{k}_i \times \underline{k}_f|$$

where $\hat{\underline{j}}$ was a unit vector in the Y direction. This definition implied $\emptyset = 0$ was to the left for particles entering the polarimeter, but $\emptyset$ was further required to increase for positive (right hand screw) rotations about the Z axis. The calculated values of Θ and $\emptyset$ were binned in a Θ-$\emptyset$ matrix which was:

a) 0.5 x 0.1 degrees in Θ and $\emptyset$ respectively for the polarimeter calibration;

b) 0.5 x 0.972 degrees in Θ and $\emptyset$ respectively for the Wolfenstein experiments.

The former size was historical and originated during early software testing; the latter size was chosen as being closer to the actual polarimeter resolution of these quantities (Appendix C). These matrices were stored on tape for further analysis (section 5.2), though at RHEL card decks were simultaneously produced.

Program REDUCE 2 provided histograms and dot plots to allow the effectiveness and interelation of applied cuts to be determined. It was always necessary to ensure that cuts did not bias the Ø distribution.

The preceding general philosophy for applying cuts to event candidates was maintained throughout the polarimeter calibration and Wolfenstein parameter measurements. Minor deviations are noted in section 5.3 for the former and 5.4 for the latter.

5.2 Polarimeter asymmetry

Program ASYMMETRY was written to determine the asymmetry in the polarimeter from the Θ-Ø matrices produced by REDUCE 2. Figure 5.2.1 shows a typical Ø distribution integrated over all Θ whilst 5.2.2 shows an entire Θ-Ø matrix (both from REDUCE 2).

Matrices pertaining to a given parameters measurement were added by ASYMMETRY to give a total matrix for each of the two possible "polarization orientations". In the polarimeter calibration experiment this corresponded to different states of the solenoid (precession by $\pm$ 90 degrees), whilst for the Wolfenstein parameter measurements different EPB polarization orientations (0 or 180 degrees for D; $\pm$ 90 degrees for R and R').

Each Θ bin was separately fitted by moments to the functional form:

$$f(\Theta_j,\Phi_i) = N(\Theta_j)\ \{1+\sum_{n=1} a_n(\Theta_j)\cos(n\Phi_i)+\sum_{n=1} b_n(\Theta_j)\sin(n\Phi_i)\} \quad \ldots\ (5.2.1)$$

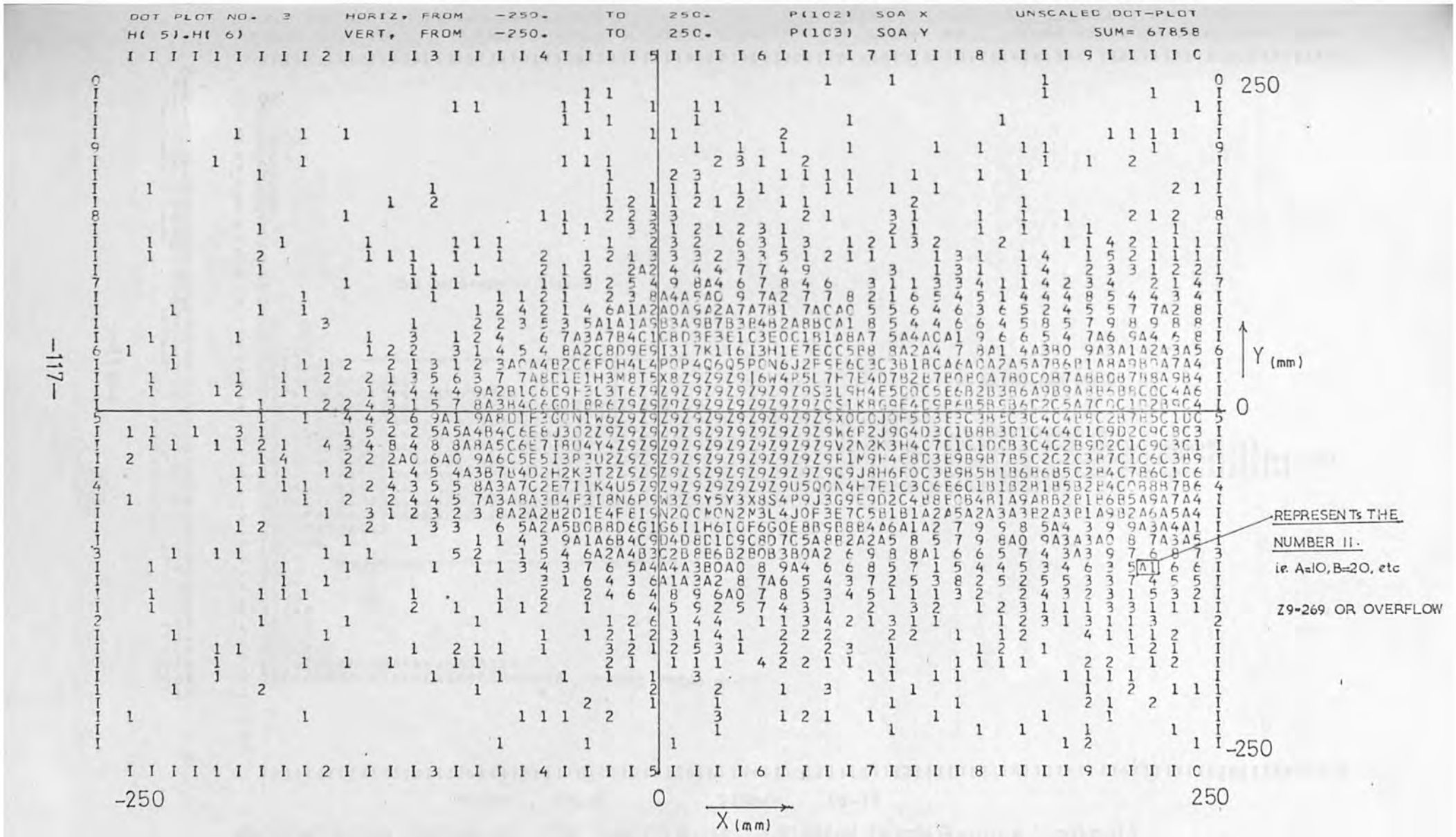

FIGURE 5·1·21 SECONDARY BEAM PROFILE AT SOA,Å (518MeV, 24 lab., Reduce 1 output)

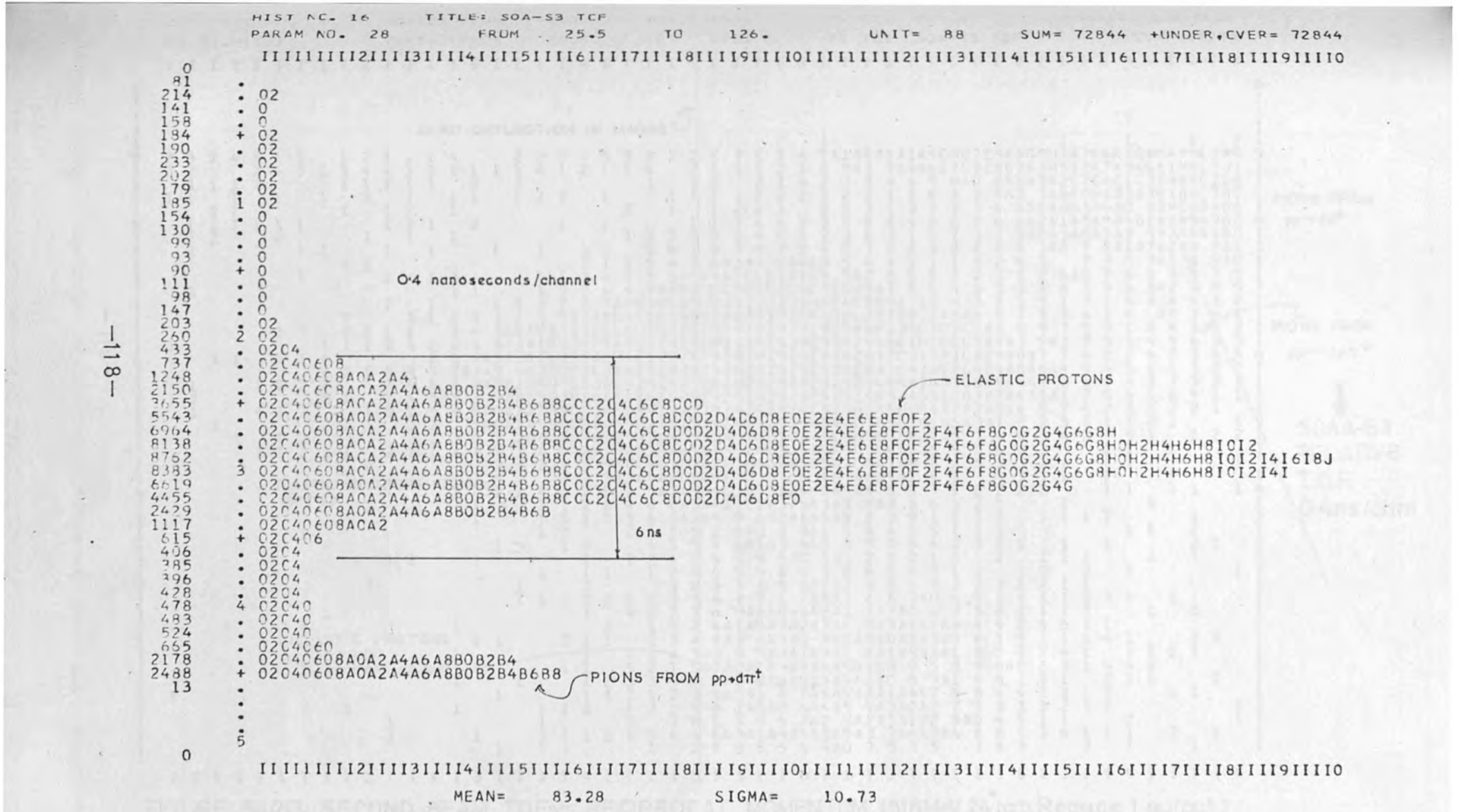

FIGURE 5·1·2·2 SOAA′-S3 TOF SPECTRUM (518MeV, 24°lab, Reduce 1 output)

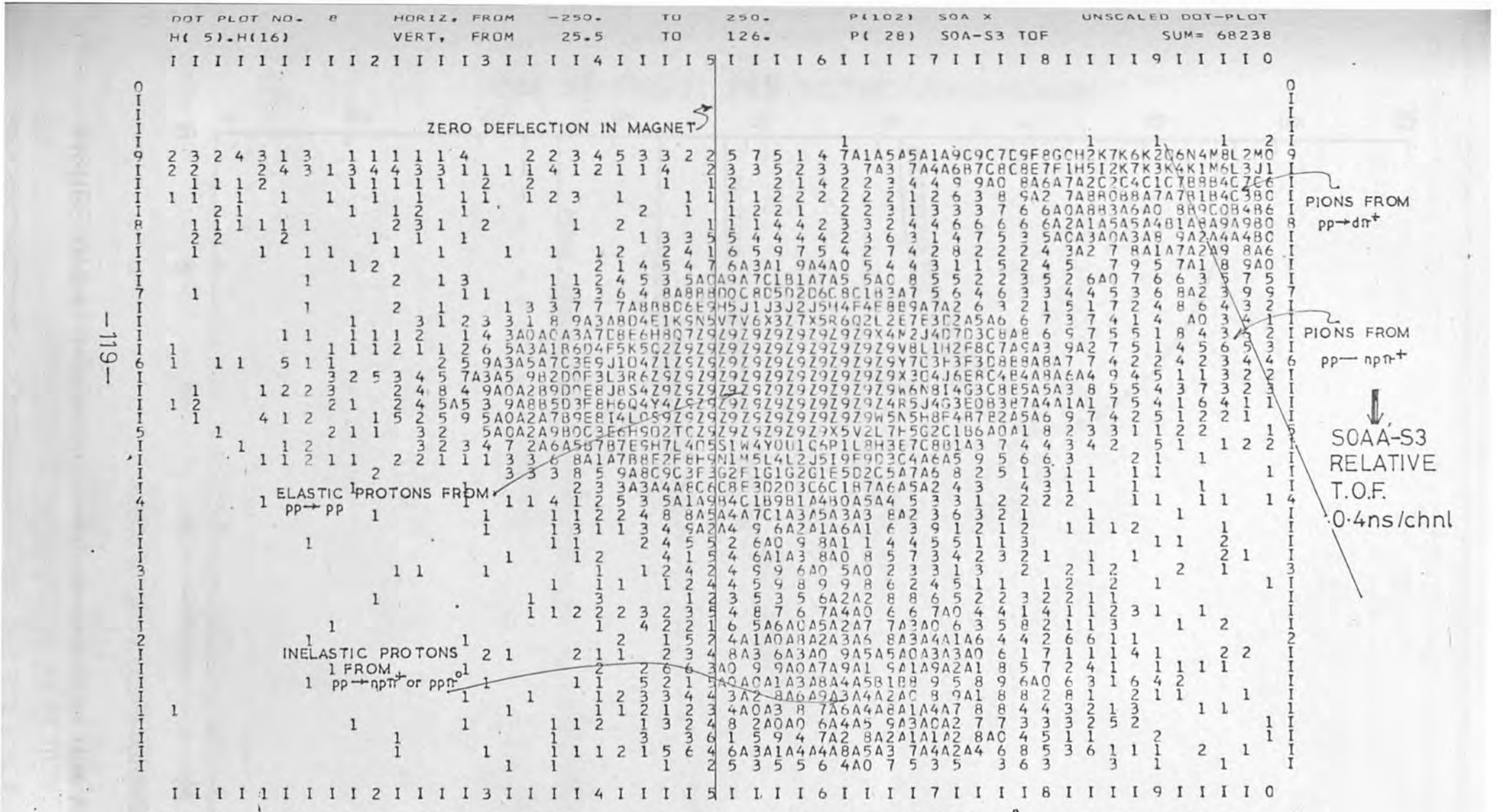

FIGURE 5·1·2·3 SECOND BEAM TOF vs. RECIPROCAL MOMENTUM (518MeV, 24° lab, Reduce 1 output)

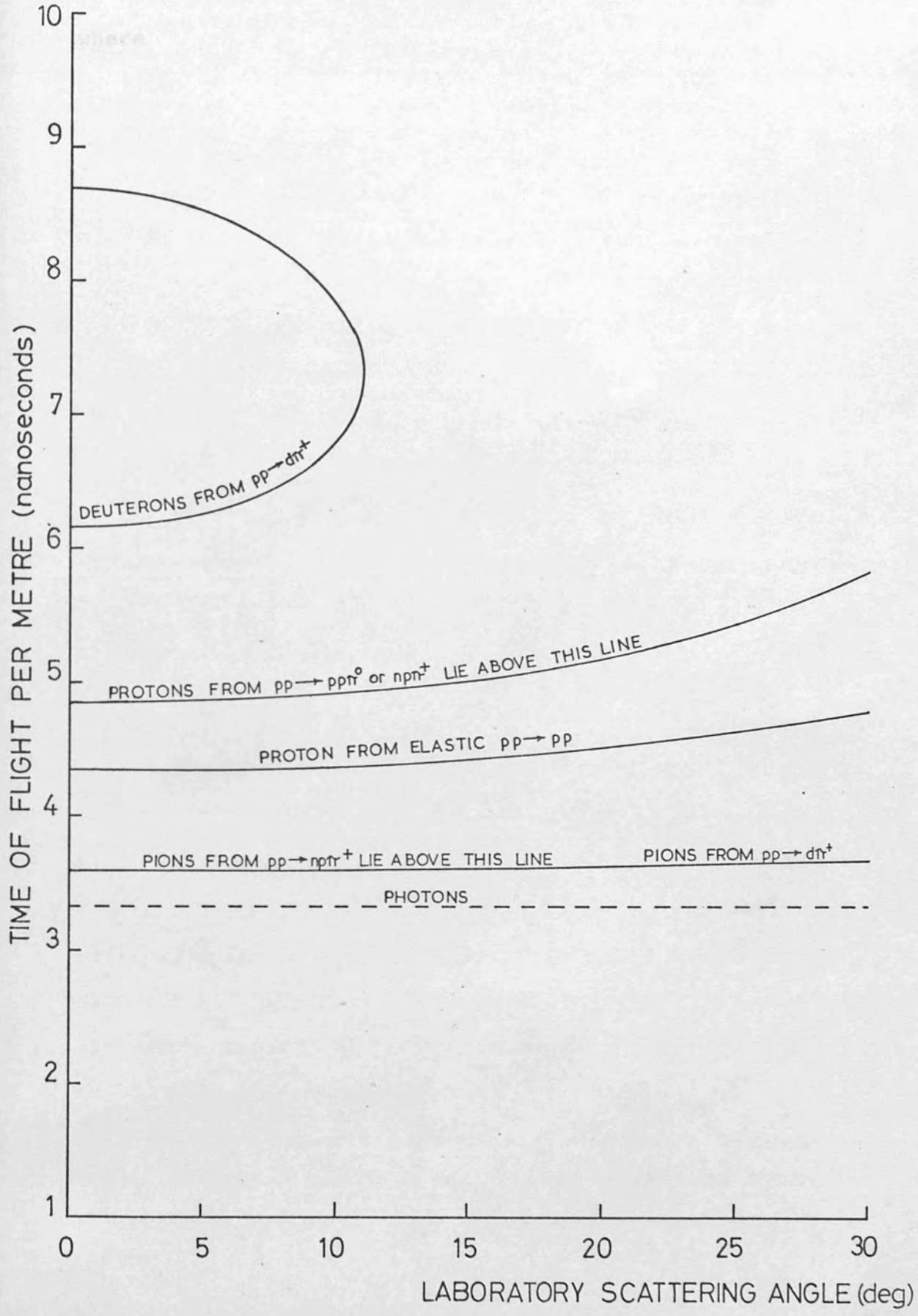

FIGURE 5·1·2·4 THEORETICAL TOF vs. LAB. SCATTER ANGLE FOR ELASTIC & INELASTIC REACTIONS (518 MeV)

where

$f(\theta_j,\phi_i)$ was the number of events in the i^{th} ϕ bin of the j^{th} θ bin (i=1, ..., 50; j=1, ..., 16).

$N(\theta_j)$ was the total number of events in the j^{th} θ bin.

ϕ_i was the centre of the i^{th} ϕ bin: $\phi_i = \frac{360}{50}(i-0.5)$ degrees.

θ_j was the centre of the j^{th} θ bin: $\theta_j = 2(j+1)$ degrees.

It follows that the coefficients ($a_n(\theta_j)$ and $b_n(\theta_j)$) and their errors ($\delta a_n(\theta_j)$ and $\delta b_n(\theta_j)$) were given by (Appendix F):

$$a_n(\theta_j) = \overline{2\cos(n\phi_i)},\quad \delta a_n(\theta_j) = \sqrt{\frac{2+a_{2n}(\theta_j)-a_n^2(\theta_j)}{N(\theta_j)}} \quad \ldots\ (5.2.2)$$

$$b_n(\theta_j) = \overline{2\sin(n\phi_i)},\quad \delta b_n(\theta_j) = \sqrt{\frac{2-a_{2n}(\theta_j)-b_n^2(\theta_j)}{N(\theta_j)}} \quad \ldots\ (5.2.3)$$

The definition of ϕ implied that a secondary beam with vertical polarization, giving rise to a left-right asymmetry, produced $a_1 \neq 0$ whilst a horizontal polarization giving an up-down asymmetry produced $b_1 \neq 0$ (for all θ_j). Higher coefficients should have been consistent with zero (see section 1.3 for the predicted variation of f with ϕ); that they were not as explained in the two following sections where the polarimeter calibration and Wolfenstein parameter analyses are discussed.

Values of a_1 and/or b_1 from a particular experiment were

found to be insensitive to the precise cuts applied to raw data. Time-of-flight and incident angle cuts were simultaneously modified by typically 10% without producing changes greater than 0.005 in the coefficients. Elastically scattered protons were therefore being well identified by the procedures of section 5.1.2. The number of events accepted through the analysis chain was obviously more sensitive to the precise cuts.

5.3 Polarimeter calibration

The polarimeter calibration data was fully analysed (section 5.3.2) before final Wolfenstein parameter values were deduced. The methods employed in reducing the former data to sets of asymmetries were also applied to the latter and have been described in sections 5.1 and 5.2. This section develops the final "tools" (sections 5.3.1 and 5.3.3) necessary to extract the calibration results presented in section 5.3.4. They are logically grouped into this section being developed during the calibration analysis, from originally simple ideas, on the basis of seeing intermediate results. This "feedback loop" approach to analysis smoothed off the "rough edges" on all methods before their full power was confidently brought to bear on the Wolfenstein parameter data (section 5.4).

Calibration data recorded for an EPB energy of 518 MeV were found to give values of A_c at variance with those obtained during the p-p measurements under the same conditions. Wolfenstein D and R experiments (at 24 degrees) permitted a determination of A_c using the reliable value of P at this angle (section 5.4). Both the shape and magnitude of the calibration estimates for

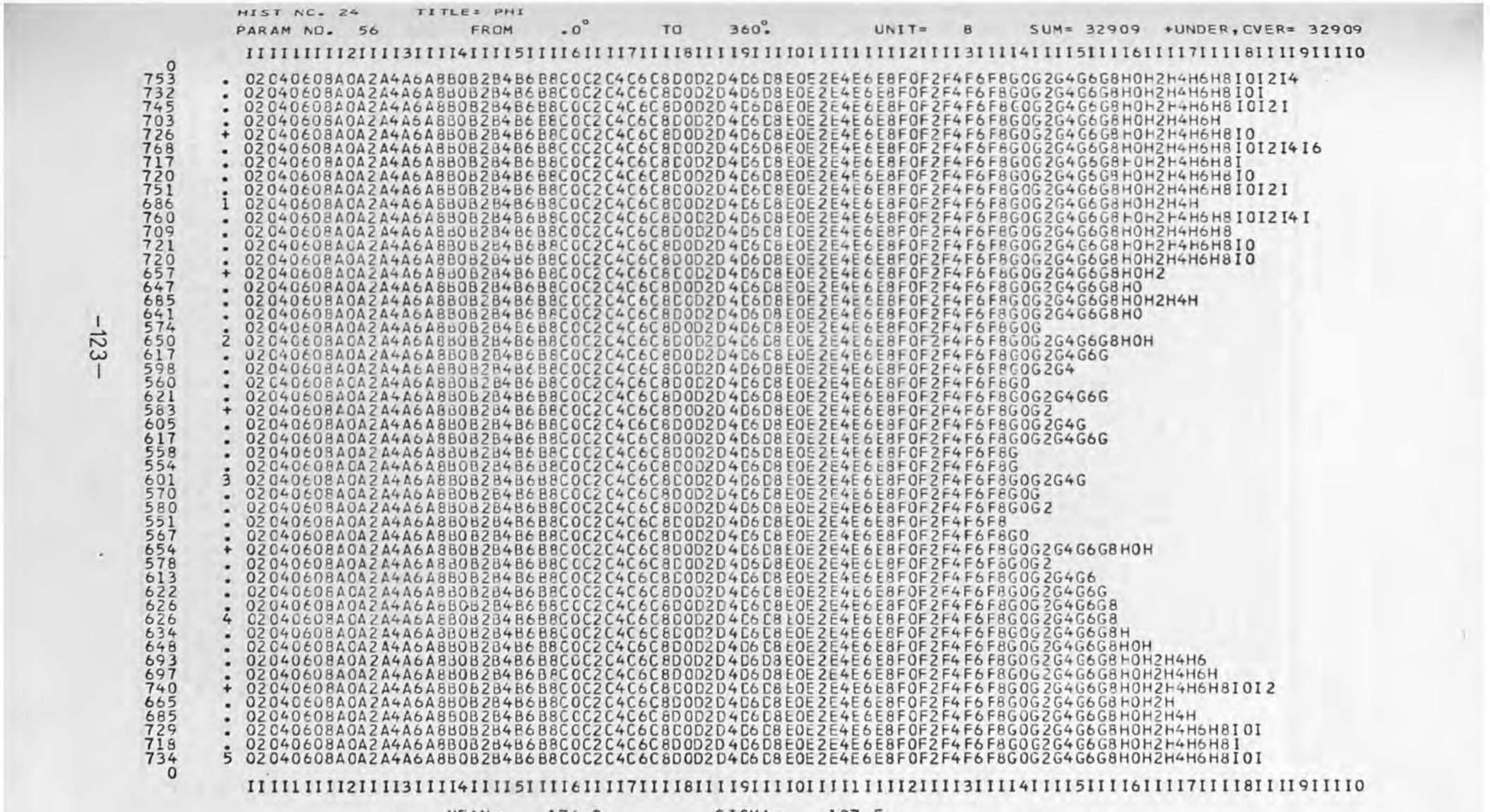

FIGURE 5·2·1 TYPICAL Ø HISTOGRAM INTEGRATED OVER ALL Θ (518 MeV, 24° lab, Reduce 2, output)

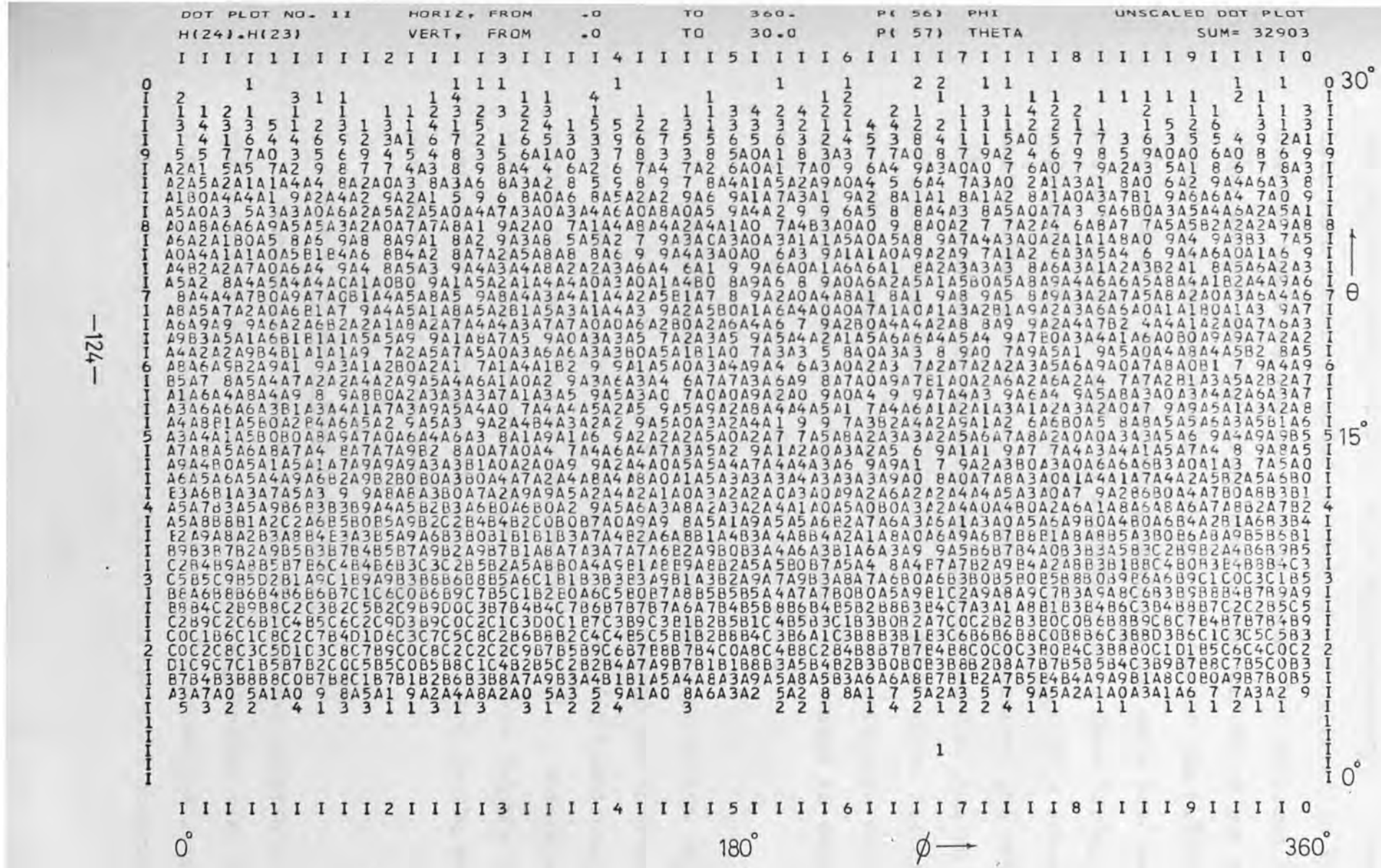

FIGURE 5·2·2 θ-φ MATRIX PRESENTED BY REDUCE 2 (518MeV, 24° lab)

θ > 14 degrees disagreed with predictions from equation 5.3.2.1 but p-p data were found to be in full agreement. These latter data were therefore added to that of the calibration for θ < 14 degrees (reducing the statistical error) but replaced it at all other angles (giving larger than normal errors as p-p measurements were recorded with only one quarter of the calibration statistics). As a further precaution one more precise calibration point was added by recording extra data during the p-p experiment at 15 degrees lab and 518 MeV. This extended the calibration to 1023 MeV/c (at the carbon centre) and was fitted well by our empirical formula; supporting the premise that 24 degree data had been incorrect (a fault which has never been traced). Accurate values of P at 15 degrees were obtained from the scintillation counter experiment discussed in section 5.4.6 and used to normalize data at this angle.

Final values for the analysing power of carbon (A_c) were particularly smooth as a function of energy and scattering angle (θ) in the carbon, despite an annoying experimental error during the data acquisition (section 5.3.2). Accurate values for A_c over the momentum range 486-1023 MeV/c (at the carbon centre) were determined and subsequently used in the Wolfenstein parameter experiments (section 5.4).

5.3.1 Primary beam polarization

Section 3.2.5 described the geometrical construction of the primary beam monitor. The monitor provided (see table 3.2.5.1) four-fold coincidences L' (left forward scatter) and R' (right forward scatter) in addition to two-fold coincidences

LF' (left forward), LR' (left recoil), RF' (right forward) and RR' (right recoil) from each telescope. Due to high rates in its constituent telescopes it was necessary to correct the coincidence L' (and R' similarly) for random coincidences. If the live time for a particular experiment was T then average rates were given by L = L'/T, LF = LF'/T etc. and the random rate contribution (L_R) to L was determined from

$$L_R = \tau(LF-L)(LR-L) \qquad \ldots. \ (5.3.1.1)$$

(similarly for R_R). L_R and R_R were then used to form the true asymmetry ($_T$) from formula (3.2.5.3) viz.

$$\varepsilon_T = \frac{(L-L_R) - (R-R_R)}{(L-L_R) + (R-R_R)} \qquad \ldots. \ (5.3.1.2)$$

(where τ was the resolving time of the system, determined by the 43 nanosecond period between beam pulses at TRIUMF). Corrections to the asymmetry were typically in the range 0.001-0.003.

A larger and more important correction to the asymmetry was that due to background from carbon in the CH_2 target. A CH_2 target 0.8255mm thick, with density 0.935g/cm^3, had a carbon composition corresponding to a surface density of 0.06615g/cm^2. This was experimentally compared with a 0.3mm carbon target having a surface density 0.06386g/cm^2 (i.e. ratio 1.036). Denoting the rate (corrected for randoms) of left forward scatters from hydrogen in the CH_2 target by L^H and that from carbon by L^C (similarly for R), then the asymmetry determined from the CH_2 target was given by

$$\varepsilon_{CH_2} = \frac{(L^H + L^C) - (R^H + R^C)}{(L^H + L^C) + (R^H + R^C)} \quad \ldots\ (5.3.1.3)$$

denoting $\varepsilon_H = \frac{L^H - R^H}{L^H + R^H}$, $\varepsilon_C = \frac{L^C - R^C}{L^C + R^C}$, $I_C = L^C + R^C$,

$I_{CH_2} = I_C + L^H + R^H$

we find after rearranging (5.3.1.3)

$$\varepsilon_H = \frac{\varepsilon_{CH_2} - \frac{I_C}{I_{CH_2}} \varepsilon_C}{(1 - \frac{I_C}{I_{CH_2}})} \quad \ldots\ (5.3.1.4)$$

The scattering intensities I_{CH_2} and I_C were determined relative to a beam monitor formed from the 24 degree proton telescope; whilst ε_{CH_2} and ε_C were measured by inserting CH_2 and carbon targets respectively into the beam monitor. Table 5.3.1.1 presents the results between 210 and 516 MeV, a line drawn by eye through these points was used for all other energies.

The primary beam polarization (P^b) was finally determined after dividing the corrected asymmetry (ε_H) by the polarization ($P_{26}(E_b)$) for free p-p scattering at energy E_b and laboratory angle 26 degrees. One final correction was necessary however to allow for the possibility of a non zero ε_H being recorded for zero EPB polarization. Denoting the true asymmetries for spin up, down and off by ε_+, ε_- and ε_o respectively we find beam polarizations given by:

$$P^b_{\pm} = (\varepsilon_{\pm} - \varepsilon_o)/P_{26}(E^b) \quad \ldots\ (5.3.1.5)$$

P_{26} was taken from a smooth curve drawn through values predicted by single energy phase shift analyses at 210, 325, 380, 425 and 515 MeV.

Primary beam energy (MeV)	I_C/I_{CH_2} (%)	$\varepsilon_H/\varepsilon_{CH_2}$ ($\pm$ 0.008)
210	4.22	1.031
325	8.4	1.050
427	10.9	1.056
480	12.3	1.057
516	12.1	1.056

TABLE 5.3.1.1 Carbon background correction to beam monitor asymmetry.

5.3.2 Analysis of data

Data were originally recorded at each of 9 EPB energies with the solenoid rotating the secondary beam polarization by $\pm$ 90 degrees from the vertical. Empty target runs were used. to correct the summed target-full asymmetry sets for the presence of the steel target flask, in the manner described by section 5.3.3. An up-down asymmetry was expected in the polarimeter ($b_1 \neq 0$); that other coefficients were non zero arose from the use of CLEANING during data acquisition. As discussed in section 3.7 CLEANING required at least two out of every three MWPCs before and after the carbon to have a single hit in the chamber. The test was designed to minimise the number of straight tracks written to the output tape and maximise

the number of events fitted by REDUCE 1. However the number of doubles (two hits) in a chamber increased dramatically with the track angle of incidence. This results in

1. $a_1 \leq 0$; the secondary beam centroid made an angle of $\sim$ 7 milliradians, with respect to the polarimeter axis, left of centre;
2. $a_2 \neq 0$; implied a difference in efficiency between X and Y determining chambers;
3. $a_4 \neq 0$; the corners of 1 metre MWPCs received highly inclined tracks. Large inefficiencies resulted for angles of scatter greater than 16 degrees giving $a_4 > 0$. This coefficient was found to be a very sensitive monitor of chamber performance and became large before other coefficients were noticeably non-zero.

Assuming chamber performance remained constant over the time taken to record data for both polarization orientations then averaging the two asymmetry sets removed instrumental biases to first order. Extensive tests with calibration data (recorded without CLEANING) and p-p data showed that CLEANING did not bias the estimate of b_1, after averaging, to better than 1% confidence level at 387 MeV (primary beam energy and 24 degrees lab.) where the effect was largest.

The 9 final asymmetry sets $\varepsilon(E_i,\theta_j)$ (i=1, ..., 9: j=1, ..., 16) for EPB calibration energies E_i were individually divided by the relevant polarization $P_{24}(E_i)$ of the secondary

beam at 24 degrees to give 9 sets of carbon analysing power $A_c(p_i,\theta_j)$ viz.

$$A_c(p_i,\theta_j) = \varepsilon(E_i,\theta_j)/P_{24}(E_i)$$

$P_{24}(E_i)$ was taken from a smooth curve drawn through phase shift predictions of P at 24 degrees lab (section 5.4), p_i was the proton momentum at the carbon and θ_j the centre of the j^{th} θ bin. The energy and angular dependence of A_c were fitted (in program FIT) by an empirical formula:

$$A_c(p,\theta) = \frac{A(p)p_T}{1 + B(p)p_T^{\,2} + C(p)p_T^{\,4}} \quad \ldots\ (5.3.2.1)$$

where the momentum transfer (p_T) was given by

$$p_T = pR \sin(\theta)/\hbar$$

R = 2.747 fermi was the carbon nuclear radius, $\hbar$ = 197.31 MeV.fm and A, B, C were fitted power series in p as follows:

define $Q = 0.001\ p$

then
$$A = 9.5619\ Q^3 - 23.089\ Q^2 + 18.025\ Q - 4.1589$$
$$B = 2.7193\ Q^2 - 4.1305\ Q + 1.5182$$
$$C = 2.3973\ Q^4 - 6.7215\ Q^3 + 6.5337\ Q^2 - 2.5185\ Q + 0.3176$$

$\ldots\ (5.3.2.2)$

Values of A_c between calibration points were derived from this formula with a linear interpolation of the error from the nearest calibration points.

Statistical accuracy of the calibration (table 5.3.4.1) ranged from 1.5% at the highest energy to 5% at the lowest. A statistical analysis of the changes (Δa_1, Δa_2, Δa_4) in the coefficients a_1, a_2 and a_4 between solenoid +& - runs gave an indication for instrumental noise in the polarimeter. The level was found to be of the order 0.84 of statistics from the more precise data above 307 MeV EPB energy. The average statistical accuracy over this energy region was 1.45%, so the noise level was given by 1.45 x 0.84 = 1.21%. Adding this in quadrature with the purely statistical errors gave the bracketed values in column 8 of table 5.3.4.1; from which interpolated errors on A_c are quoted for the p-p experiments (table 5.4.1).

5.3.3 Empty target correction

A certain (unknown) fraction of primary beam protons scattering from the steel target flask were accepted through the complete analysis chain. These protons had a polarization differing from that of pure p-p elastic scattering at 24 degrees and therefore modified the measured polarimeter asymmetry. It was possible to remove the contribution to the asymmetry from these protons by recording data with the target emptied of hydrogen. In actuality a "chinese copy" (dummy) of the target was used to speed up the process of changing from full to empty target during the experiments; dummy and empty target were compared in a separate experiment. The number of events accepted from the empty target was measured to be 1.027 ± 0.007 of those from the dummy. This factor was negligible for the calibration experiment but was important for the Wolfenstein parameter measurements at smaller angles.

The simplest way to have done the empty target subtraction would have been to simply scale the empty target asymmetries and subtract the results individually from each θ_j bin (j=1, ..., 16), viz.

$$\varepsilon_H(\theta_j) = \frac{\varepsilon_F(\theta_j) - \frac{I_F}{I_E}\frac{N_E(\theta_j)}{N_F(\theta_j)}\varepsilon_E(\theta_j)}{1 - \frac{I_F}{I_E}\frac{N_E(\theta_j)}{N_F(\theta_j)}} \quad \ldots\ (5.3.3.1)$$

(a proof of which appears in Appendix G); where for the target full experiment I_F was the primary beam intensity, $N_F(\theta_j)$ and $\varepsilon_F(\theta_j)$ were the number of events and asymmetry respectively for the θ_j bin (similarly for I_E, $N_E(\theta_j)$, $\varepsilon_E(\theta_j)$) and $\varepsilon_H(\theta_j)$ was the asymmetry due to hydrogen in the target. The ratio I_F/I_E was often large and statistics on $N_E(\theta_j)$ usually low. This method would therefore have introduced unnecessary noise into the shape of ε_H as a function of θ.

Assuming that both the shape of A_c and N_F as functions of θ were the same for target full and empty experiments the ratio of polarizations (in these experiments) R was given by

$$R = \bar{\varepsilon}_E/\bar{\varepsilon}_F \quad \ldots\ (5.3.3.2)$$

where

$$\bar{\varepsilon}_E = \sum_j N_E(\theta_j)\ \varepsilon_E(\theta_j)/\sum_j N_E(\theta_j) \quad \ldots\ (5.3.3.3)$$

(similarly for $\bar{\varepsilon}_F$) and the fractional background from the empty target (B) was given by

$$B = \frac{I_F}{I_E}\,\frac{N_E}{N_F} \qquad \ldots\ (5.3.3.4)$$

where $$N_E = \sum_j N_E(\theta_j) \qquad \ldots\ (5.3.3.5)$$

(similarly for N_F). It follows therefore that R and B were statistically better measures of (all) $\varepsilon_E(\theta_j)/\varepsilon_F(\theta_j)$ and $I_F\ N_E(\theta_j)/I_E\ N_F(\theta_j)$ respectively. Using these in equation (5.3.3.1)

$$\begin{aligned}\varepsilon_H(\theta_j) &= \varepsilon_F(\theta_j)(1-BR)/(1-B)\\ &\simeq \varepsilon_F(\theta_j)(1-B(1-R)) \qquad \ldots\ (5.3.3.6)\end{aligned}$$

to first order in B.

The error in the average asymmetry for target full ($\delta\bar{\varepsilon}_F$) is certainly bounded by (section 5.2)

$$\delta\bar{\varepsilon}_F \leq \sqrt{\frac{2}{N_F}} \qquad \ldots\ (5.3.3.7)$$

and for target empty

$$\delta\bar{\varepsilon}_E \leq \frac{I_F}{I_E}\,\frac{N_F}{N_E}\sqrt{\frac{2}{N_E}} = B\sqrt{\frac{2}{N_E}} \qquad \ldots\ (5.3.3.8)$$

Adding these in quadrature the error in $\bar{\varepsilon}_H$ is certainly less than

$$\delta\bar{\varepsilon}_F \sqrt{\frac{\frac{2}{N_F} + B^2\,\frac{2}{N_E}}{\frac{2}{N_F}}}$$

i.e. $$\delta\bar{\varepsilon}_H \leq \delta\bar{\varepsilon}_F \sqrt{1 + B^2\ N_F/N_E} \qquad \ldots\ (5.3.3.9)$$

This correction was of the order 1-10%, which was small compared with the factor previously introduced to cover instrumental noise. Table 5.3.3.1 contains the essential data necessary for the empty target subtraction.

5.3.4 Presentation of calibration results

The calibration of our polarimeter was essentially a high statistics experiment measuring the analysing power of carbon, for protons, as a function of their laboratory scattering angle (Θ) and incident energy. A_c was determined (finally) at 10 points over the momentum range 487-1023 MeV/c (at the carbon centre) with no restriction on the inelasticity of the scatter. General characteristics of A_c in this momentum range are:

1. as a function of scattering angle (Θ) in the carbon A_c rises from zero at 0 degrees, passes through a maximum then decreases (out to 30 degrees);
2. the maximum moves to smaller angles ($\lesssim$ 8 degrees) as the momentum increases;
3. values of the maximum rise to a peak of $\sim$ 0.7 at 663 MeV/c then decrease;
4. the "peak" (described in 1) narrows as the momentum increases.

Figure 5.3.4.1 shows graphs of A_c as a function of Θ for the 10 (final) calibration momenta. Indicated errors are purely statistical and do not include the possible 6% systematic uncertainty from p-p polarization at 24 degrees; the solid line represents fitted values. Statistical error on the average analysing power ($\bar{A}_c$) are given in table 5.3.4.1 along with the

TABLE 5.3.3.1 Empty target subtraction data.

Proton Energy at LH_2 target (MeV)	Solenoid ($\pm$ 90°)	N_F	N_E	I_F/I_E	$\bar{\varepsilon}_F$	$\bar{\varepsilon}_E$	$\delta\bar{\varepsilon}_H/\delta\bar{\varepsilon}_F$ (%)	$\delta\bar{\varepsilon}_H/\bar{\varepsilon}_H$
514	+	214901	550	6.22	.1462	.0373	1.0492	2.19
514	-	227995	301	14.14	.1547	.0619	1.1250	2.15
476	+	223825	643	1.31	.1436	.1555	1.0033	2.69
476	-	205803	669	1.15	.1342	.0404	1.0032	2.33
429	+	209627	412	1.76	.1397	.0592	1.0032	2.22
429	-	208889	427	1.80	.1509	-.0154	1.0032	2.05
380	+	223111	149	5.54	.1672	.1219	1.0108	1.81
380	-	205135	89	8.25	.1703	-.2095	1.0160	1.86
337	+	201445			.1623	.0616*	1.0476	2.03
337	-	202050	122	6.13	.1864	.0043	1.0095	1.71
300	+	161131	37	10.87	.1604	.1864	1.0142	2.22
300	-	164144	52	11.61	.1804	.0859	1.0430	2.02
264	+	93110	35	7.90	.1390	.1185	1.0119	3.37
264	-	99286	70	3.78	.1737	.2020	1.0142	2.62
228	+	143143	64	6.14	.0796	-.1238	1.0081	4.74
228	-	209269	57	7.66	.1386	-.0375	1.0079	2.24
200	+	218344	230	2.24	.0528	.0303	1.0026	5.76
200	-	219579	136	3.06	.0625	.1189	1.0068	4.86

*interpolated from nearest energies

precise energies, target empty-full ratios and 24 degree polarization used in deriving A_c from raw asymmetries. Indications are that, within statistical error, A_c was well determined over the entire energy range and insensitive to cuts removing pions and inelastic protons from the raw data (above EPB energies of 290 MeV).

The values of A_c reported here overlap the recent small angle Geneva measurements of Aebischer et al[5.3] at our two highest energies and their two lowest. The Geneva group determined A_c when the proton was allowed either unlimited inelasticity in its carbon scatter or an inelasticity limited to a known energy loss in a range-energy telescope. Plotted in figure 5.3.4.1 are their values at 399 MeV, with inelasticity $\lesssim$ 16 MeV, and 462 MeV, with inelasticity $\lesssim$ 38 MeV, and the unlimited inelasticity data of the same energies (measured at front face of carbon). Our results lie clearly between these two measurements but are in closer agreement with the unlimited inelasticity values than the limited inelasticity. Aebischer provides references for other measurements in this energy region; a study of which clearly implies that values derived with unlimited inelasticity are very dependent on the experimental procedure.

For the Wolfenstein parameter analysis A_c was determined over this momentum range from the empirical formula (5.3.2.1) using the fitted coefficients (5.3.2.2). The error was linearly interpolated to intermediate energies from the nearest calibration points.

EPB energy (MeV)	Energy at centre of LH_2 target (MeV)	Energy at solenoid (MeV)	Momentum at solenoid (MeV/c)	Energy at front face of carbon (MeV)	Energy at centre of carbon (MeV)	Momentum at centre carbon (MeV/c)	Statistical error on A_c (+ noise) (%)	Target empty/ full ratio (%)	p-p polarization at 24° lab.†
520.14	514.57	403.16	958.66	400.78	387.36	936.42	1.53(1.95)	1.70	0.419
481.88	476.10	373.80	917.13	371.28	357.36	893.45	1.56(1.97)	0.40	0.406
435.20	429.16	336.36	862.72	333.70	318.95	836.78	1.51(1.93)	0.36	0.390
386.95	380.56	298.37	805.53	295.50	279.32	775.97	1.30(1.77)	0.36	0.372
344.02	337.23	262.95	750.79	259.89	242.38	716.62	1.32(1.79)	0.37	0.357
307.42	300.18	232.84	700.79	229.55	210.59	662.95	1.50(1.93)	0.31	0.343
273.34	264.58	203.55	650.67	199.99	179.12	606.78	3.00(3.23)	0.29	0.327
236.52	228.07	173.00	595.44	169.06	145.36	542.11	3.49(3.69)	0.24	0.307
210.08	200.99	149.91	551.15	145.60	118.81	486.88	5.31(5.45)	0.20	0.289
*518.35	515.31	518.10	1113.8	462.35	449.92	1023.06	1.24(1.73)	1.60	0.497

†smooth curve drawn by eye through the phase shift predictions of section 5.5 (following method of section 5.4)

*15 degree lab scattering angle, solenoid in primary beam-line, different length LH_2 target

TABLE 5.3.4.1 Polarimeter calibration data

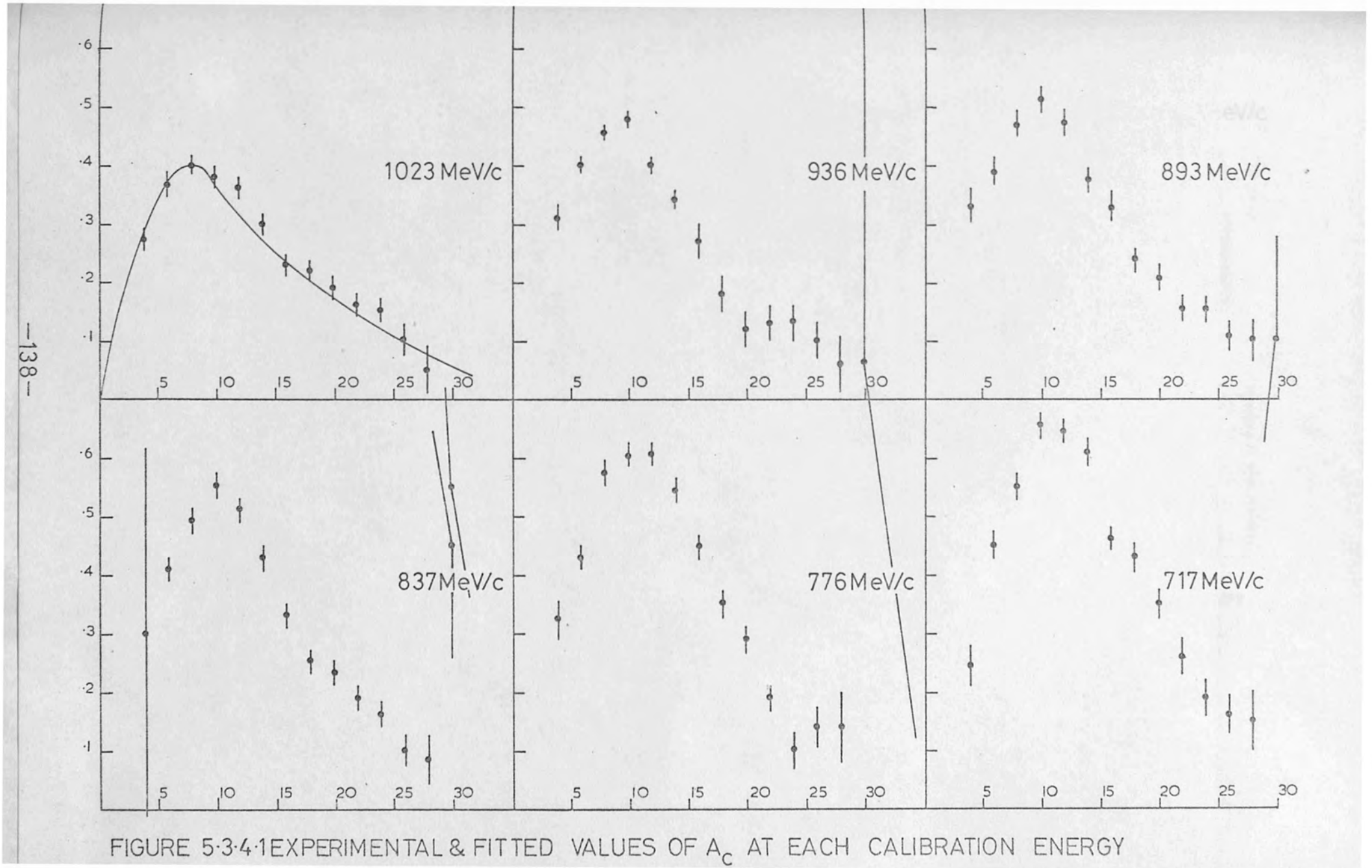

FIGURE 5·3·4·1 EXPERIMENTAL & FITTED VALUES OF A_c AT EACH CALIBRATION ENERGY

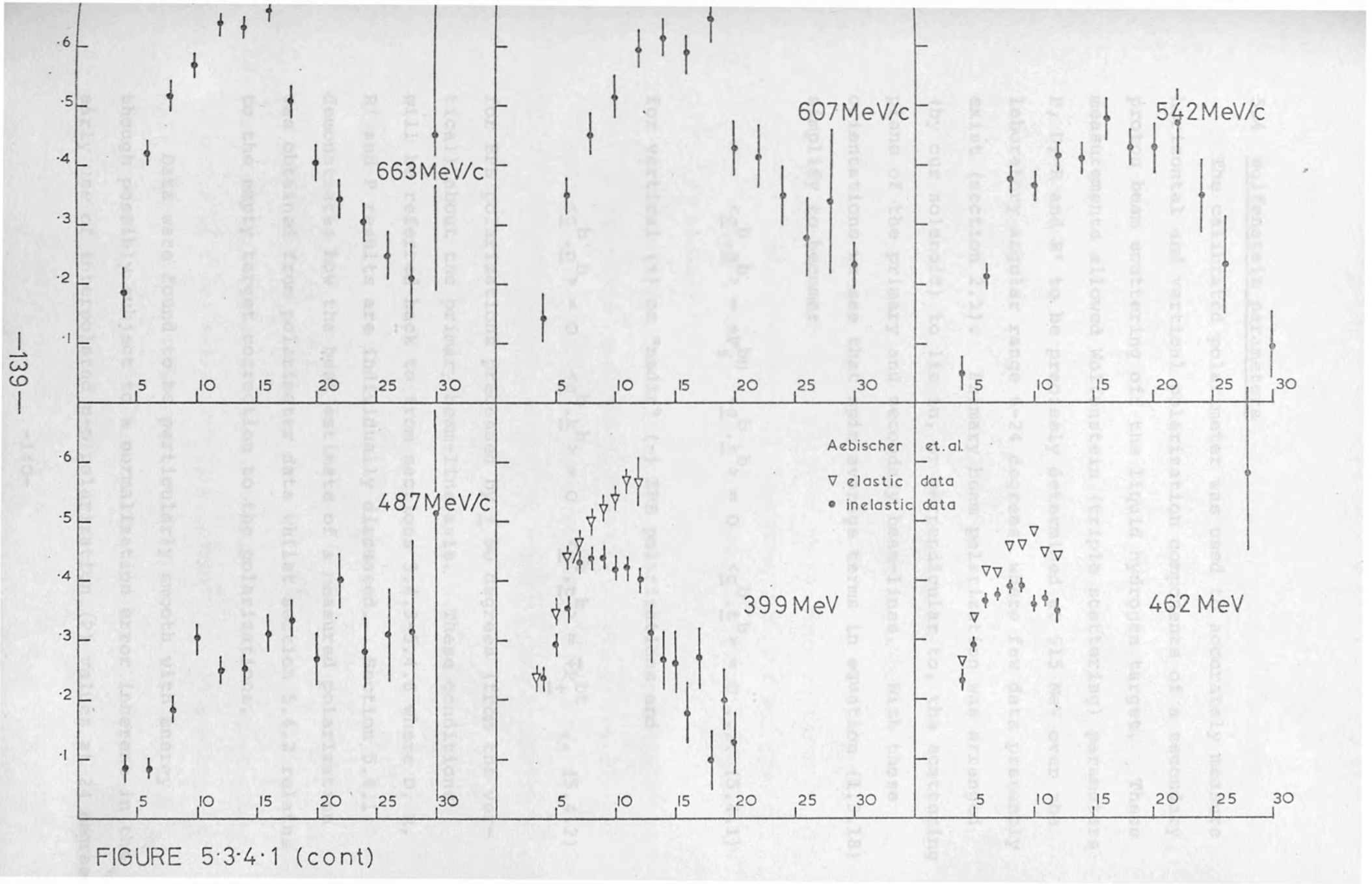

FIGURE 5·3·4·1 (cont)

5.4 Wolfenstein parameters

The calibrated polarimeter was used to accurately measure horizontal and vertical polarization components of a secondary proton beam scattering off the liquid hydrogen target. These measurements allowed Wolfenstein (triple scattering) parameters P, D, R and R' to be precisely determined at 515 MeV over the laboratory angular range 6-24 degrees, where few data presently exist (section 2.1). Primary beam polarization was arranged (by our solenoid) to lie in, or perpendicular to, the scattering plane of the primary and secondary beam-lines. With these orientations we see that spin average terms in equation (1.3.18) simplify to become:

$$\langle \underline{\sigma}^b . \underline{n}^b \rangle = \pm P_{\pm}^{bn} \quad \langle \underline{\sigma}^b . \underline{k}^b \rangle = 0 \quad \langle \underline{\sigma}^b . \underline{t}^b \rangle = 0 \quad \ldots\ldots (5.4.1)$$

for vertical (+) or "nadir" (-) EPB polarizations and

$$\langle \underline{\sigma}^b . \underline{n}^b \rangle = 0 \quad \langle \underline{\sigma}^b . \underline{k}^b \rangle = 0 \quad \langle \underline{\sigma}^b . \underline{t}^b \rangle = \mp P_{\pm}^{bt} \quad \ldots\ldots (5.4.2)$$

for EPB polarizations precessed by $\pm$ 90 degrees (from the vertical) about the primary beam-line axis. These conditions will be referred back to from sections 5.4.3-5.4.6 where D, R, R' and P results are individually discussed. Section 5.4.1 demonstrates how the best estimate of a measured polarization was obtained from polarimeter data whilst section 5.4.2 relates to the empty target correction to the polarizations.

Data were found to be particularly smooth with energy though possibly subject to a normalization error inherent in the early use of interpolated p-p polarization (P) values at 24 degrees

(calibration) and 26 degrees (beam-line monitor) from contemporary phase shift solutions. A double scattering experiment, to be performed early in 1977, will reduce normalization errors in P to the 1% level, but for the purpose of this thesis the "most reliable" values were obtained by a bootstrapping procedure involving our p-p data at all energies. The following procedure was iterated:

a) plot the predictions for P at 24 and 26 degrees lab from single energy phase shift solutions at 210, 320, 380, 425 and 515 MeV
b) from a smooth curve drawn by eye through these predictions extract the the values of P for the 10 EPB energies at which the polarimeter was calibrated;
c) refit the calibration data to give A_c over the momentum range 486-1023 MeV/c (at the carbon centre);
d) use the new interpolated values of A_c and P_{26} to obtain estimates of P, D, R and R' from asymmetry data;
e) incorporate the results of (d) into single energy phase shift analyses at 210, 320, 380, 425 and 515 MeV.

Convergence to a solution was fast: two iterations of the procedure gave stable values for P which were subsequently used to arrive at final values for P, D, R and R'. This procedure will not be discussed further in the "results' sections" but must be borne in mind when each parameter is compared with existing data. A normalization error on P affects values calcu-

lated for D, R, R' and P but can be carried through the phase shift analysis.

Data at all energies and angles were subjected to statistical tests to assess their reliability as a whole. A vertical instrumental asymmetry of -0.0153 ± 0.0074 was found from a consideration of the mean vertical asymmetries recorded during the D experiment (should be zero) and the difference between measured values of R and R' for two EPB spin orientations. The difference between vertical asymmetries in the D experiment for spin up and down was, however, found to be 0.0049 ± 0.0076 and thus consistent with zero; giving rise to the opinion that systematic errors in measurements recorded with two spin orientations were small and the quoted errors are thus purely statistical (P accepted) setting aside for the moment possible common normalization errors, which can be carried through a phase shift analysis. D, R and R' data were not affected by this bias as they were protected by taking data for two secondary beam polarizations, and forming the unbiased difference of the polarizations so recorded. Data for P were affected however and to cover this uncertainty the magnitude of the bias was added in quadrature with the statistical and A_c variances to give the final quoted error.

The MASTER TRIGGER timing change, discussed in section 4.2, did not affect data recorded at 515 MeV. Only target empty runs at other energies were biased by the on-line computer test BIT PATTERN. It was possible to correct for this mistake by simulating the effect on "good" target full data and applying a correction factor to the (distorted) asymmetries.

. At 6 degrees lab the nuclear diffractive cross-section peak of steel greatly enhanced the background from the empty target and gave rise to an empty/full ratio of typically 18%. The peak was so sharp that at 9 degrees the ratio had dropped to a tolerable level of 4.5%. Results at 6 degrees therefore had a larger error than originally hoped for (insufficient dummy target data were recorded) and an extra measurement at the 9 degree port was deemed necessary to restore the stated aims of the experiment (section 2.1). Data relevant to the evaluation of all Wolfenstein parameters are collected into table 5.4.1. The secondary beam at 6 and 9 degrees passed through 80mm and 60mm of carbon respectively to degrade their energies into the range over which the polarimeter had been calibrated.

5.4.1 Measurement of polarization

The calibrated polarimeter was a flexible tool for determining the sign and magnitude of horizontal and vertical polarization components of any secondary (scattered) beam. Following an experiment the normal data analysis chain (figure 5.1. 2) provided horizontal and vertical asymmetry sets, for both target full and empty runs, from which the unknown polarizations were to be determined (for continuity the target empty subtraction and error calculations are dealt with in section 5.4.2). Denoting the horizontal or vertical asymmetries (possibly averaged over two experiments) by $\varepsilon(\theta_j)$ (j=1, ..., 16) it was required to form the best estimate ($\overline{P}$) of the incident polarization from this set. Each asymmetry, after division by the calibration value $A_c(\theta_j)$, gave an estimate ($P(\theta_j)$) of the required polarization with statistical uncertainty $\delta P(\theta_j)$ viz.

Cyclotron energy	518.35 MeV
Energy at solenoid	518.10 MeV
Momentum at solenoid	1113.80 MeV/c
Energy at hydrogen target centre	515.31 MeV
Energy at centre of UCLA magnet (R')	464.13 MeV
Momentum at centre of UCLA magnet (R')	1042.27 MeV/c

Lab scatter angles (degrees)	Energy at carbon front face (MeV)	Energy at centre carbon (MeV)	Momentum at centre carbon (MeV/c)	p-p polarization at 515 MeV	Interpolated $\bar{A}_C$ error (%)	True lab scatter angle (degrees)	CM scatter angle (degrees)	Secondary beam energy degrader thickness
6	464.89	452.48	1026.53	0.289±0.015	1.734	5.976	13.48	80mm
9	465.55	453.14	1027.43	0.399±0.011	1.734	8.970	20.22	60mm
15	462.35	449.92	1023.06	0.497±0.007	1.734	14.945	33.54	none
15 (R')	461.88	449.44	1022.41					
24	401.06	387.78	937.02	0.419±0.004	1.950	23.977	53.31	none
26	518.35	518.10	1113.80	0.367±0.004	-	26.000	57.74	none

TABLE 5.4.1 Primary and secondary beam characteristics for the p-p experiments

$$P(\theta_j) = \varepsilon(\theta_j)/A_c(\theta_j) \qquad \ldots. \ (5.4.1.1)$$

and $$\delta P(\theta_j) = \delta\left(\frac{\varepsilon(\theta_j)}{A_c(\theta_j)}\right) = \frac{\delta\varepsilon(\theta_j)}{A_c(\theta_j)} \qquad \ldots. \ (5.4.1.2)$$

The best estimate for the polarization was taken to be that value ($\overline{P}$) which minimised a goodness of fit χ^2 function defined by[5.6, 5.7]:

$$\chi^2 = \sum_j \left(P(\theta_j)-\overline{P}\right)^2 / \left[\delta P(\theta_j)\right]^2 \qquad \ldots. \ (5.4.1.3)$$

If $N(\theta_j)$ was the number of events in the θ_j bin then from formula (5.3.3.7)

$$\left[\delta\varepsilon(\theta_j)\right]^2 = \delta^2\varepsilon(\theta_j) = 2/N(\theta_j)$$

hence $$\chi^2 = \sum_j N(\theta_j)\, A_c^2(\theta_j)\left(P(\theta_j)-\overline{P}\right)^2/2$$

Minimising with respect to $\overline{P}$ we find

$$\overline{P} = \sum_j N(\theta_j)\, A_c^2(\theta_j) P(\theta_j) / \sum_j N(\theta_j) A_c^2(\theta_j) \ .. \ (5.4.1.4)$$

and inserting the value for $P(\theta_j)$ we obtain the best estimate of the polarization to be:

$$\overline{P} = \frac{\sum_j N(\theta_j)\, A_c(\theta_j)\, \varepsilon(\theta_j)}{\sum_j N(\theta_j)\, A_c^2(\theta_j)} \qquad \ldots. \ (5.4.1.5)$$

5.4.2 Empty target subtraction

Using the notation of section 5.3.3 formula (5.3.3.1) becomes

$$\varepsilon_H(\theta_j) = \frac{\varepsilon_F(\theta_j) - B\varepsilon_E(\theta_j)}{1-B} \quad \ldots\ (5.4.2.1)$$

Averaging each side by the method deduced in section 5.4.1 we find the required polarization generated by scattering from hydrogen in the target is given by

$$\overline{P}_H = (\overline{P}_F - B\overline{P}_E)/(1-B) \quad \ldots\ (5.4.2.2)$$

The statistical error squared $(\delta^2\overline{P}_H)$ in $\overline{P}_H$ is therefore

$$\delta^2\overline{P}_H = (\delta^2\overline{P}_F + B^2\delta^2\overline{P}_E)/(1-B)^2 \quad \ldots\ (5.4.2.3)$$

where the statistical error squared $(\delta^2\overline{P}_F)$ in $\overline{P}_F$ is given from formula (5.4.1.5) as

$$\delta^2\overline{P}_F = 2/\sum_j N_F(\theta_j)\ A_c^2(\theta_j) \quad \ldots\ (5.4.2.4)$$

and similarly for $\overline{P}_E$.

The factor

$$Q(\theta_j) = N_F(\theta_j)\ A_c^2(\theta_j) \quad \ldots\ (5.4.2.5)$$

is historically known as the Quality Factor. Maximising the Quality Factor, by suitably choosing the scattering medium, obviously minimises the final error on the measured polarization (other experimental conditions remaining constant).

A correction to B was necessary at 6 and 9 degrees lab. The ratio of events from the empty and dummy targets was

1.027 $\pm$ 0.007 and became significant when the empty/full ratio rose above 4%. Denoting the number of events from the (true) empty target by N_E^T we find

$$N_E^T = 1.027\ N_E$$

and the modified B (B') was given by

$$B' = \frac{B}{1.027} \quad \ldots\ (5.4.2.6)$$

5.4.3 D parameter results

The D parameter was determined after arranging the EPB polarization to be perpendicular to the scattering plane, of the primary and secondary beams, and measuring the vertical polarization of the secondary beam. Conditions (5.4.1) therefore held and equation (1.3.18) became (using $P_{\pm} = P_{\pm}^{bn}$)

$$P_{\pm}^s = \frac{P_{\pm} D\ P_{\pm}}{1 \pm PP_{\pm}}\ n^s \quad \ldots\ (5.4.3.1)$$

where P is the analysing power of hydrogen.

Evidence for an instrumental asymmetry in the vertical plane implied that D had to be evaluated from a difference of the two measured polarizations in the polarimeter (lest there be a horizontal asymmetry as well). We find

$$P_+^s - P_-^s = \frac{P + DP_+}{1 + PP_+} - \frac{P - DP_-}{1 - PP_-} \quad \ldots\ (5.4.3.2)$$

cancels the bias and solving for D

$$D = \frac{\{ P_+^s - P_-^s + \frac{P}{1-PP_-} - \frac{P}{1+PP_+} \}}{\{ \frac{P_+}{1+PP_+} - \frac{P_-}{1-PP_-} \}} \qquad \ldots\ (5.4.3.3)$$

where the "best values" for P were taken from a phase shift analysis at 515 MeV and are listed for each angle in table 5.4.1.

Solving equations (5.4.3.1) for P allows an estimate of this parameter to be made in section 5.4.6 from

$$P = \frac{\{ \frac{P_+^s}{P_+} - \frac{P_-^s}{P_-} \}}{\{ \frac{1}{P_+} + \frac{1}{P_-} - (P_+^s - P_-^s) \}} \qquad \ldots\ (5.4.3.4)$$

Final results for D have been collected into table 5.4.3.1 and are compared with predictions from phase shift analyses at 515 MeV before and after the inclusion of (all) data presented in this thesis (figures 5.4.3.1 and 5.4.3.2 respectively).

5.4.4 R parameter results

Wolfenstein parameter R was determined by rotating the vertical EPB polarization into the scattering plane of the primary and secondary beams and measuring the horizontal polarization of the secondary beam. Conditions (5.4.2) therefore held and equation (1.3.18) became (using $P_{\underline{+}} = P_{\underline{+}}^{bt}$)

$$P_{\underline{+}}^s = P_{\underline{n}}^s \mp R P_{\underline{+}}\, \underline{t}^s \mp R' P_{\underline{+}}\, \underline{k}^s \qquad \ldots\ (5.4.4.1)$$

Only (the transverse) components in the $\underline{n}^s$ (vertical) and $\underline{t}^s$ (horizontal) planes were measured by the polarimeter. Denoting these by $V_{\underline{+}}$ and $H_{\underline{+}}$ respectively we see that

Lab scatter angle (degrees)	EPB spin (±)	I_F/I_E	N_E/N_F (%)	N_F	D	Statistical error on D	Error from A_c	Error from P	Total error
24	+	1.73380	0.67	40302	0.680	0.019	0.010	0.002	0.022
24	-	2.21496	0.84	38435					
15	+	3.22600	1.65	75684	0.680	0.015	0.008	0.005	0.018
15	-	7.60264	2.13	71296					
9	+	2.6205	4.18	28739	0.660	0.028	0.009	0.007	0.030
9	-	2.9565	5.17	22791					
6	+	37.5136	19.35	30262	0.638	0.090	0.010	0.005	0.091
6	-	34.4295	23.97	27742					

TABLE 5.4.3.1 Data used in evaluating the D parameter at 515 MeV

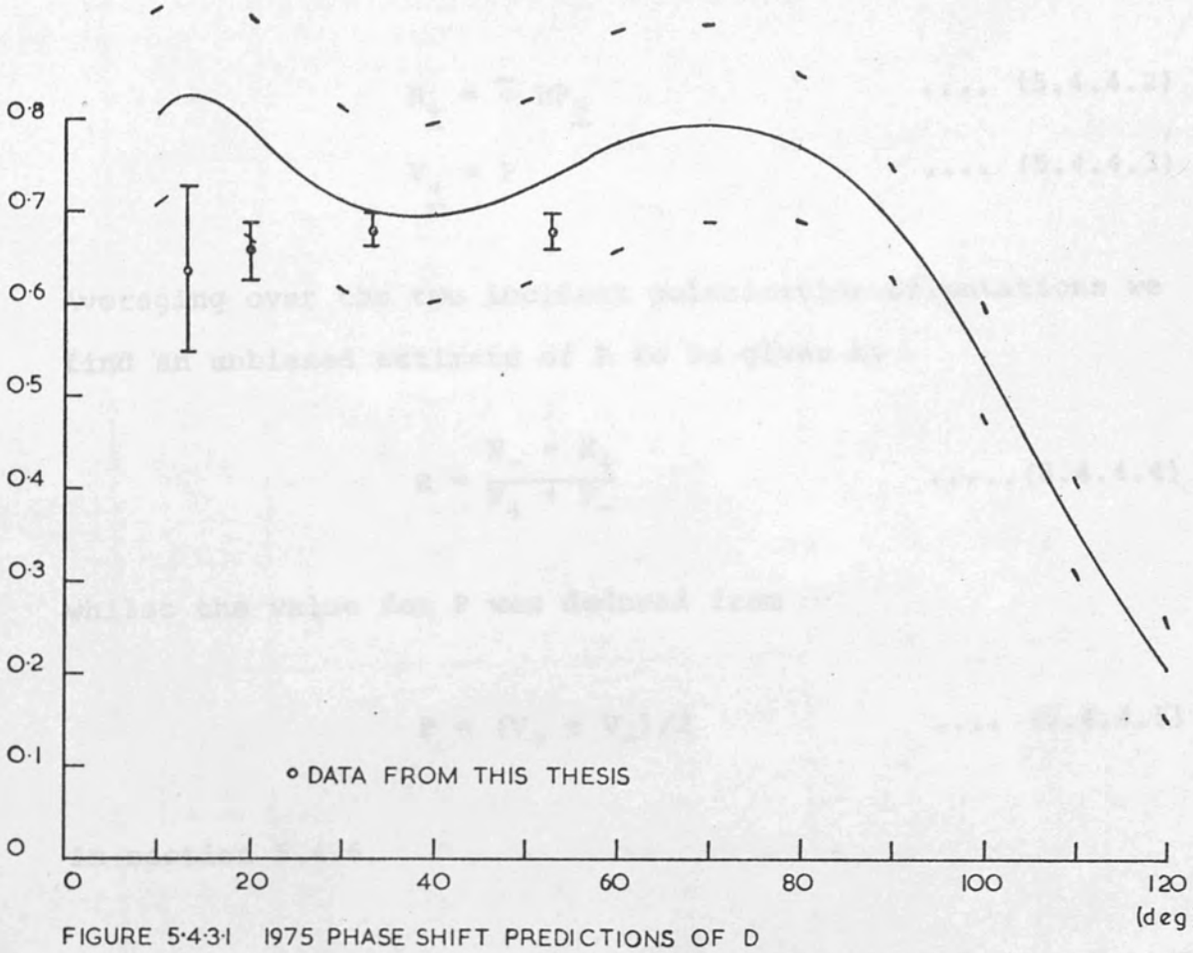

FIGURE 5·4·3·1 1975 PHASE SHIFT PREDICTIONS OF D

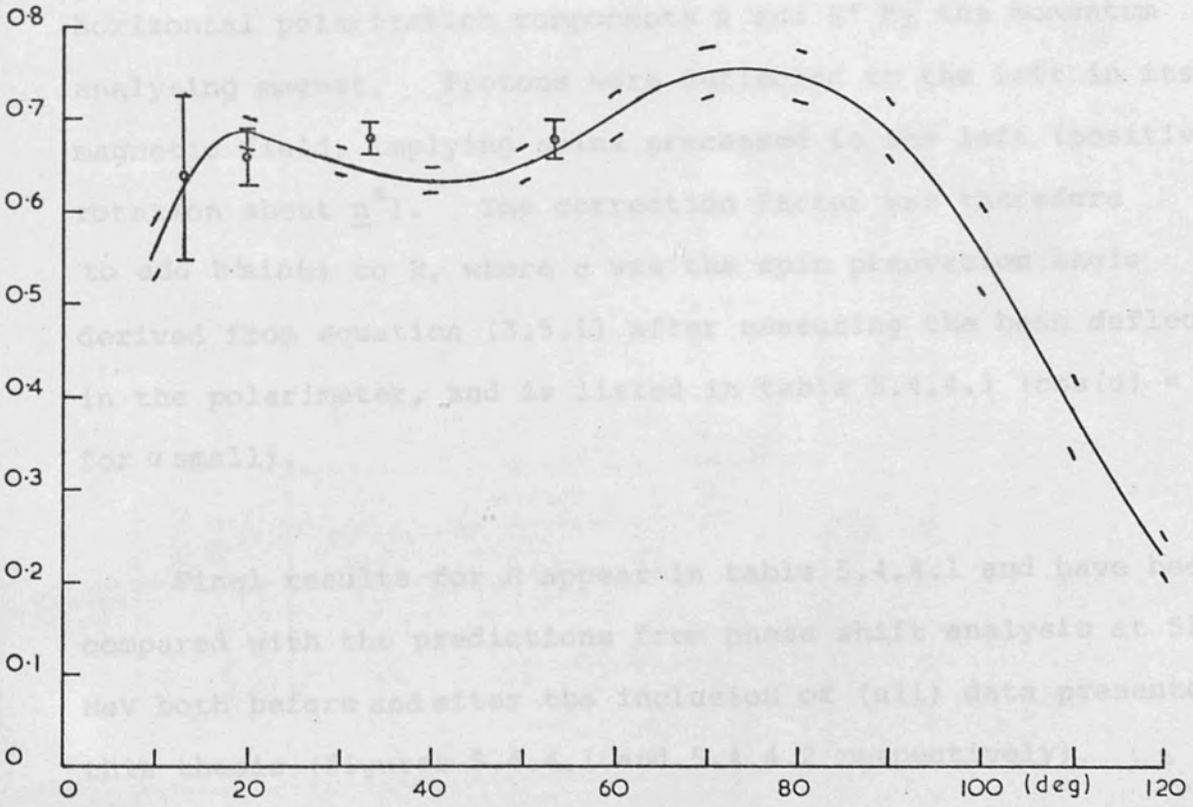

FIGURE 5·4·3·2 1976 PHASE SHIFT PREDICTIONS OF D, INCORPORATING DATA FROM THIS THESIS

$$H_{\pm} = \mp RP_{\pm} \quad \text{.... (5.4.4.2)}$$

$$V_{\pm} = P \quad \text{.... (5.4.4.3)}$$

Averaging over the two incident polarization orientations we find an unbiased estimate of R to be given by

$$R = \frac{H_- - H_+}{P_+ + P_-} \quad \text{.....(5.4.4.4)}$$

whilst the value for P was deduced from

$$P = (V_+ + V_-)/2 \quad \text{.... (5.4.4.5)}$$

in section 5.4.6.

It was necessary to correct the value of R for mixing of horizontal polarization components R and R' by the momentum analysing magnet. Protons were deflected to the left in its magnetic field, implying spins precessed to the left (positive rotation about $\underline{n}^S$). The correction factor was therefore to add R'sin(α) to R, where α was the spin precession angle derived from equation (3.5.1) after measuring the beam deflection in the polarimeter, and is listed in table 5.4.4.1 ($\cos(\alpha) \simeq 1$ for α small).

Final results for R appear in table 5.4.4.1 and have been compared with the predictions from phase shift analysis at 515 MeV both before and after the inclusion of (all) data presented in this thesis (figures 5.4.4.1 and 5.4.4.2 respectively).

Lab. scatter angle (degrees)	EPB spin (±)	I_F/I_E	N_E/N_F (%)	N_F	"raw" R	magnet correction to R	corrected R	statistical error on R	Error from A_c	Total error
24	+	3.51193	0.76	40163	0.431	0.016	0.447	0.022	0.0074	0.023
24	-	3.67601	0.81	41096						
15	+	5.14399	1.38	77380	0.376	-0.002	0.374	0.016	0.0059	0.018
15	-	4.52805	1.25	77573						
9	+	5.02624	4.46	49461	0.356	-0.010	0.346	0.026	0.0056	0.027
9	-	3.0286	5.33	24142						
6	+	30.01693	16.66	31356	0.443	-0.008	0.435	0.067	0.0070	0.068
6	-	26.49016	17.79	29045						

TABLE 5.4.4.1 Data used in evaluating the R parameter at 515 MeV

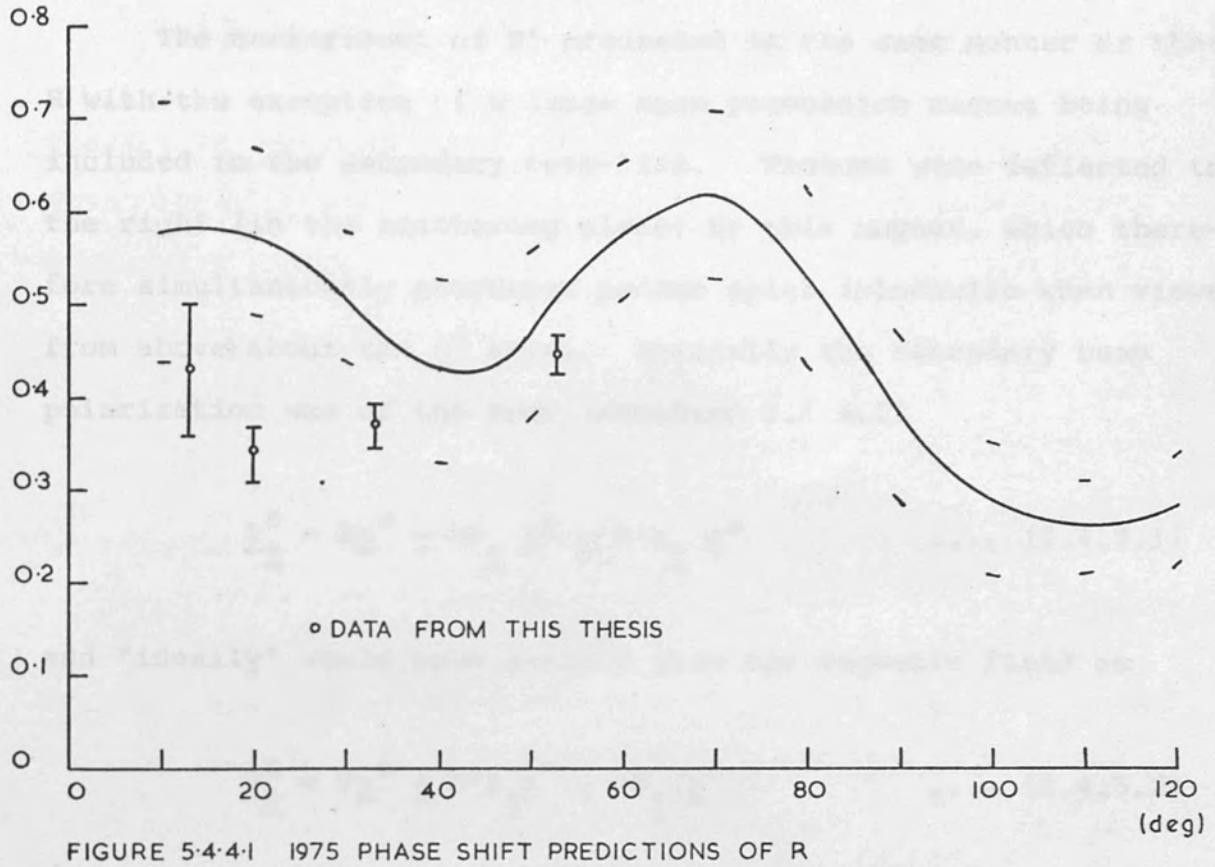

FIGURE 5·4·4·1 1975 PHASE SHIFT PREDICTIONS OF R

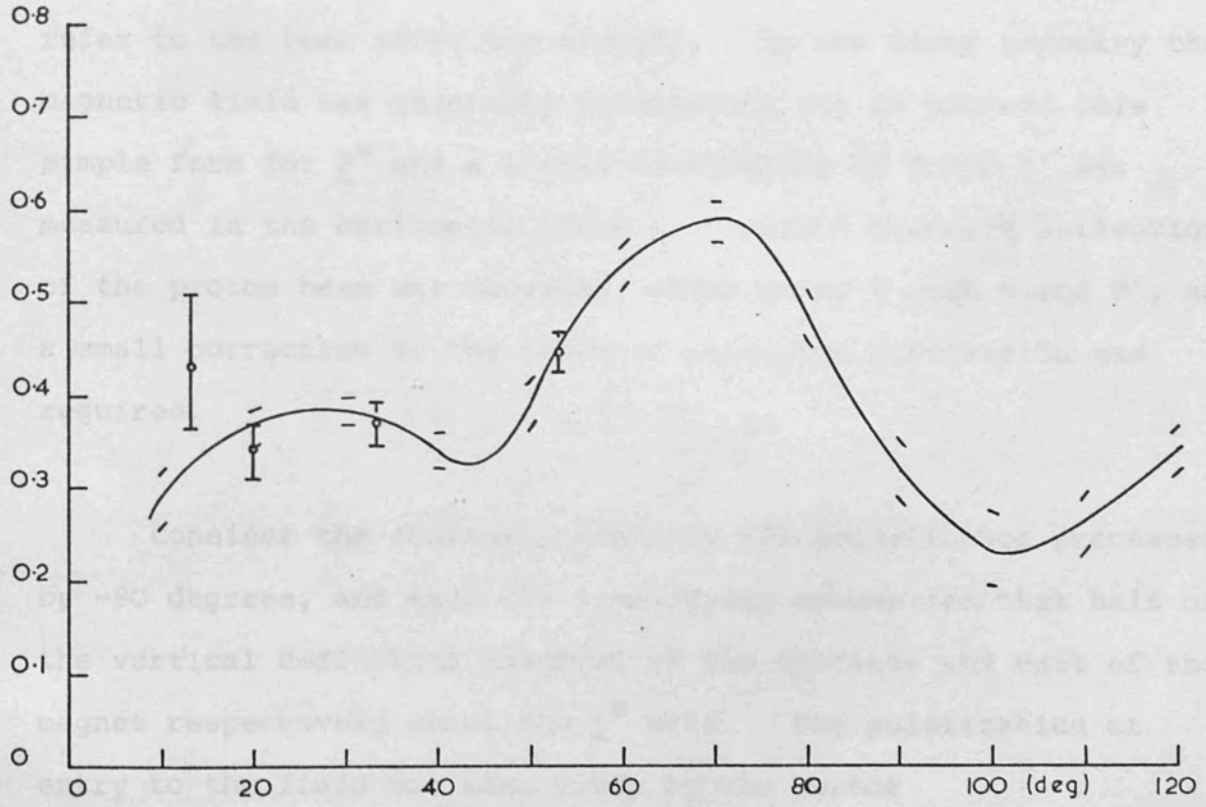

FIGURE 5·4·4·2 1976 PHASE SHIFT PREDICTIONS OF R, INCORPORATING DATA FROM THIS THESIS

5.4.5 R' parameter results

The measurement of R' proceeded in the same manner as that of R with the exception of a large spin precession magnet being included in the secondary beam-line. Protons were deflected to the right (in the scattering plane) by this magnet, which therefore simultaneously precessed proton spins (clockwise when viewed from above) about the $\underline{n}^S$ axis. Initially the secondary beam polarization was of the form (equation 5.4.4.1)

$$\underline{P}^S_{\mp} = P\underline{n}^S \mp RP_{\pm}\,\underline{t}^S \mp R'P_{\pm}\,\underline{k}^S \qquad \ldots\ (5.4.5.1)$$

and "ideally" would have emerged from the magnetic field as

$$\underline{P}^S_{\mp} = P\underline{n}^S \pm R'P_{\pm}\underline{t}^S \mp RP_{\pm}\,\underline{k}^S \qquad \ldots\ (5.4.5.2)$$

(where the unit vectors are oriented in the usual sense but now refer to the beam after the magnet). In our fixed geometry the magnetic field was generally incorrectly set to achieve this simple form for $\underline{P}^S$ and a linear combination of R and R' was measured in the horizontal plane. A slight downward deflection of the proton beam was observed, which mixed P with R and R', and a small correction to the measured parameter combination was required.

Consider the configuration with EPB polarization precessed by -90 degrees, and make the simplifying assumption that half of the vertical deflection occurred at the entrance and exit of the magnet respectively about the $\underline{t}^S$ axis. The polarization at entry to the field was then given by the vector

$$\underline{P}^S = \{P\cos(\alpha) - R'P_{-}\sin(\alpha)\}\ \underline{n}^S + RP_{-}\ \underline{t}^S + \{P\sin(\alpha) + R'P_{-}\cos(\alpha)\}\ \underline{k}^S$$

where α is one half of the total vertical precession angle. This vector precesses in the field about the $\underline{n}^S$ axis, mixing horizontal components, to become

$$\underline{P}^S = \{P\cos(\alpha)-R'P_{-}\sin(\alpha)\}\ \underline{n}^S + \{RP_{-}\cos(\beta) - [P\sin(\alpha)+R'P_{-}\cos(\alpha)] \times \sin(\beta)\}\ \underline{t}^S + \{RP_{-}\sin(\beta) + [P\sin(\alpha)+R'P_{-}\cos(\alpha)] \times \cos(\beta)\}\ \underline{k}^S$$

at exit, where β is the horizontal precession angle. The final vertical deflection again led to mixing of the vertical and longitudinal components giving

$$\underline{P}^S = \{[P\cos(\alpha)-R'P_{-}\sin(\alpha)]\cos(\alpha) - [RP_{-}\sin(\beta)+P\sin(\alpha)\cos(\beta)+R'P\cos(\alpha)\cos(\beta)]\sin(\alpha)\}\ \underline{n}^S + \{RP_{-}\cos(\beta) - P\sin(\alpha)\sin(\beta) - R'P_{-}\cos(\alpha)\sin(\beta)\}\underline{t}^S + \{[P\cos(\alpha)-R'P_{-}\sin(\alpha\ ]\ \sin(\alpha)+[RP_{-}\sin(\beta) + P\sin(\alpha)\cos(\beta)+R'P_{-}\cos(\alpha)\cos(\beta)]\cos(\alpha)\}\ \underline{k}^S \quad \ldots\ (5.4.5.3)$$

Angle β was known from the precise arrangement of equipment (figure 4.3.1) whilst α was determined from the vertical angle of incidence of the secondary beam on the polarimeter. If we use equation (3.5.1) to determine precession angles from measured bend angles then the ratio of horizontal to vertical bend angle (ω=0.019) is given by the ratio of precession angles

$$\omega = 2\alpha/\beta$$

The final result for R' is presented in table 5.4.5.1 and is compared with predictions from phase shift analyses at 515 MeV before and after the inclusion of (all) data presented in this thesis (figures 5.4.5.1 and 5.4.5.2 respectively).

Lab scatter angle (degrees)	EPB spin (±)	I_F/I_E	N_E/N_F	N_F	R'	Error from $\bar{A}_c$	Total error
15	+	5.1136	0.71	42566	0.067	0.002	0.021
15	-	4.7975	0.60	42866			

TABLE 5.4.5.1 Data used in evaluating R' parameter at 515 MeV

5.4.6 P parameter results

Estimates of the P parameter were obtained from data recorded during the following experiments:

a) Wolfenstein D parameter; using equation (5.4.3.4)
b) Wolfenstein R parameter; using equation (5.4.4.5)
c) Wolfenstein R' parameter; using equation (5.4.5.3)
d) Wolfenstein D, R and R'; using the number of "good events", for each EPB polarization, passing through the analysis chain
e) a scintillation counter measurement, performed during August, at the 9, 15 and 24 degree collimator ports for an EPB energy of 518 MeV.

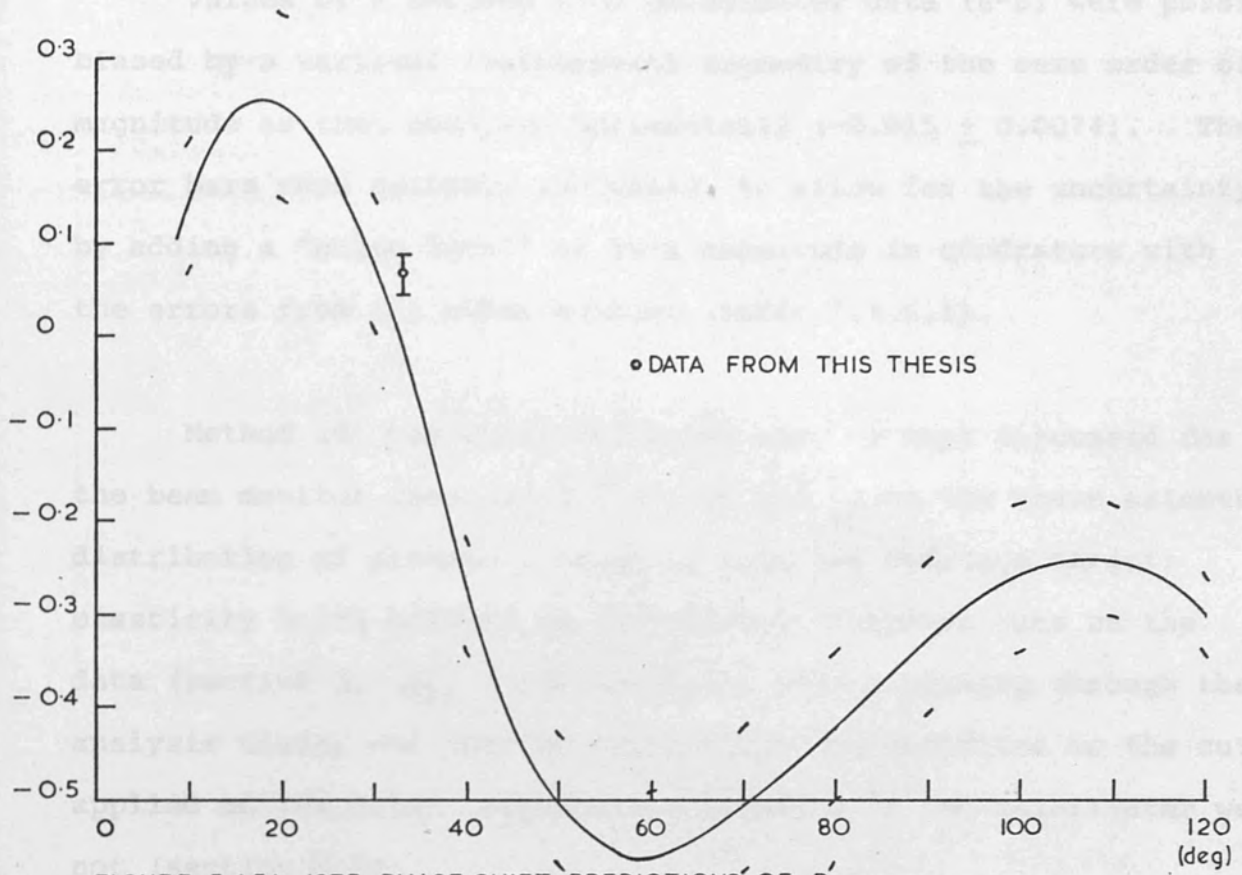

FIGURE 5·4·5·1 1975 PHASE SHIFT PREDICTIONS OF R′

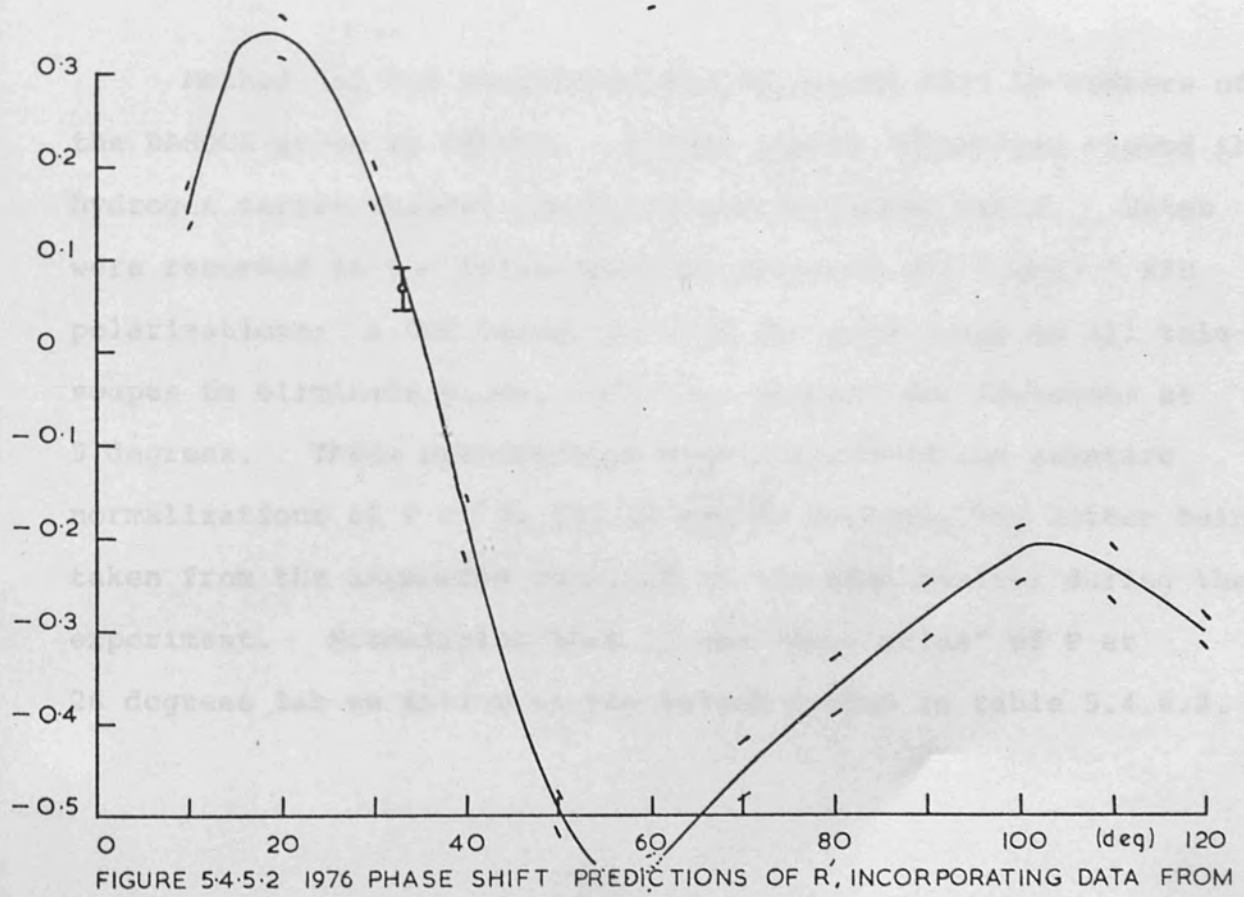

FIGURE 5·4·5·2 1976 PHASE SHIFT PREDICTIONS OF R′, INCORPORATING DATA FROM THIS THESIS

Values of P derived from polarimeter data (a-c) were possibly biased by a vertical instrumental asymmetry of the same order of magnitude as that observed horizontally (-0.015 ± 0.0074). The error bars were suitably increased, to allow for the uncertainty, by adding a "noise level" of this magnitude in quadrature with the errors from all other sources (table 5.4.6.1).

Method (d) was essentially the same as that discussed for the beam monitor (section 3.2.5) and relied on the known azimuthal distribution of protons scattering from the hydrogen target: elasticity being assured by the off-line computer cuts on the data (section 5.1.2). The number of events passing through the analysis chain, and used by the method, was sensitive to the cuts applied on the data; asymmetries recorded in the polarimeter were not (section 5.2).

Method (e) was undertaken during August 1975 by members of the BASQUE group at TRIUMF. Three proton telescopes viewed the hydrogen target through the 9, 15 and 24 degree ports. Rates were recorded in the telescopes for vertical and "nadir" EPB polarizations; a TOF being recorded for each event in all telescopes to eliminate pions, inelastic protons and deuterons at 9 degrees. These measurements accurately fixed the relative normalizations of P at 9, 15, 24 and 26 degrees, the latter being taken from the asymmetry recorded in the beam monitor during the experiment. Normalizing then to the "best value" of P at 26 degrees lab we arrive at the values quoted in table 5.4.6.2.

Lab scatter angle (degrees)	Statistical error on P	Including error from $\overline{A}_c$	Including 0.0153 "noise"	Best value for P	Total error
24	0.0116*	0.0138	0.021	0.417	0.023
	0.0067†				
15	0.0082	0.0118	0.019	0.512	0.02o
	0.0082				
9	0.0152	0.0168	0.023	0.435	0.024
	0.0196				
6	0.043	0.0430	0.046	0.328	0.045

*methods (a-c) †method (d)

TABLE 5.4.6.1 Data used in evaluating the P parameter at 515 MeV

Table 5.4.6.1 lists the values for P derived from methods (a)-(d) and table 5.4.6.2 those from (e). These values are compared with predictions from phase shift analysis at 515 MeV before and after the inclusion of (all) data presented in this thesis (figures 5.4.6.1 and 5.4.6.2 respectively).

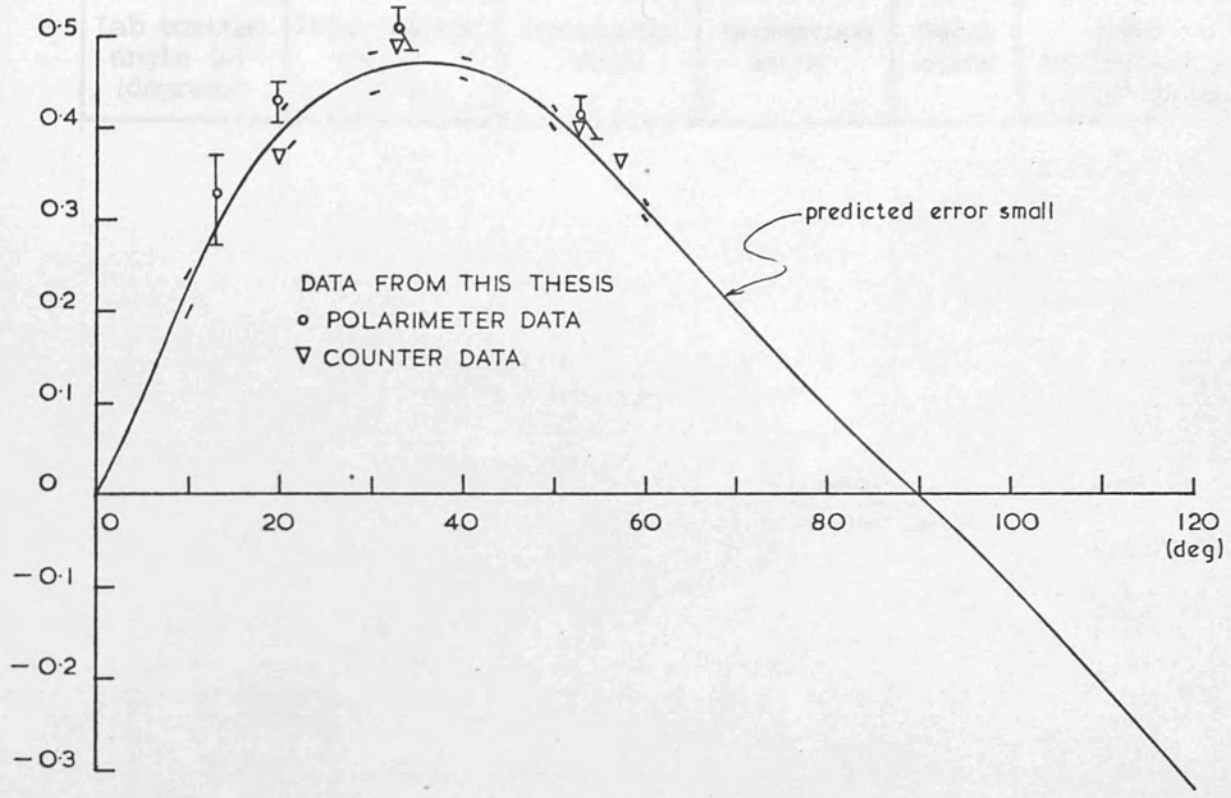

FIGURE 5·4·6·1 1975 PHASE SHIFT PREDICTIONS FOR P

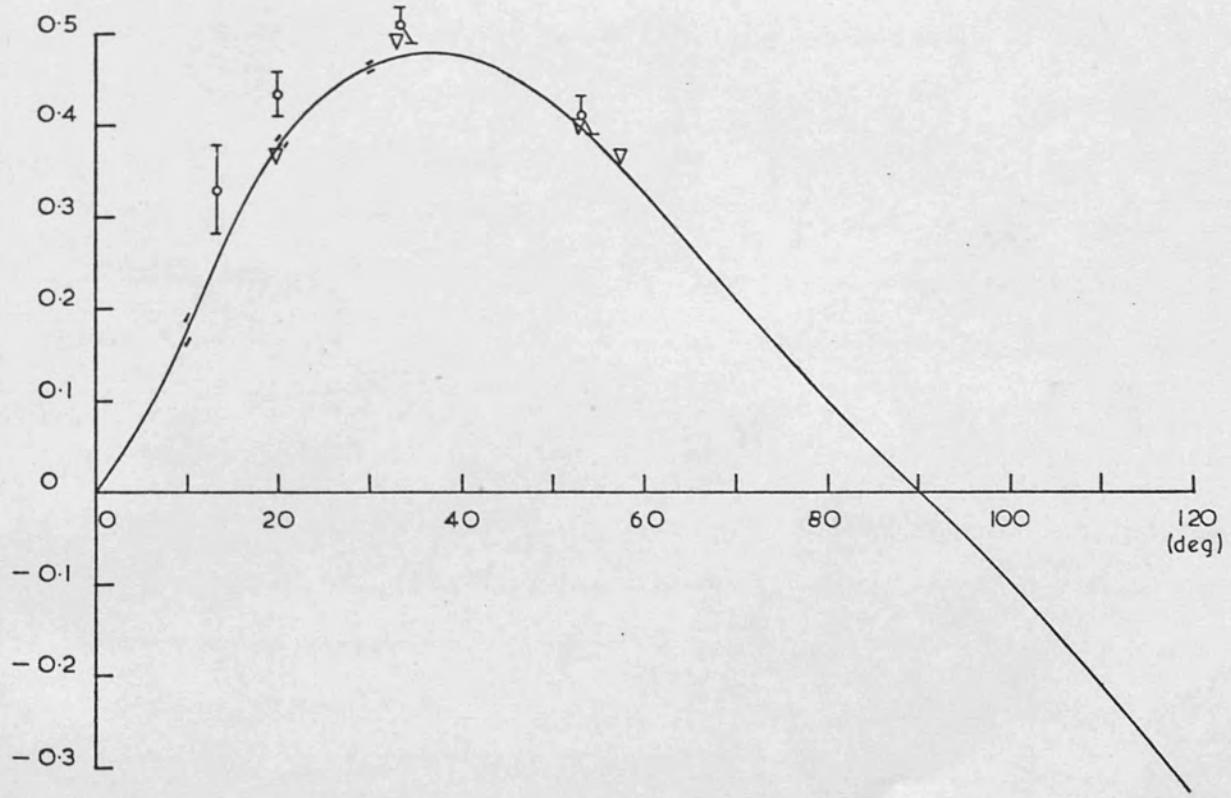

FIGURE 5·4·6·2 1976 PHASE SHIFT PREDICTIONS OF P, INCORPORATING DATA FROM THIS THESIS

Lab scatter angle (α) (degrees)	Polarization ratio P(α)/P(26)	Systematic error	Background error	Total error	P(α) normalised to 26° value
26	1.000	-	-	-	0.367±0.0021
24	1.079	0.018	0.007	0.019	0.396±0.0070
15	1.333	0.018	0.015	0.018	0.489±0.0066
9	1.000	0.050	0.023	0.055	0.367±0.0184

TABLE 5.4.6.2 . Relative values of P at 515 MeV normalized to 26 degrees (from a counter experiment)

5.5 Phase shift analysis at 515 MeV

The Wolfenstein parameter results reported in this thesis have been incorporated into the data base of an isovector phase shift analysis at 515 MeV. World p-p elastic scattering data over the energy range 500-540 MeV have been collated from the compilations of Bystricky[2.7] and MacGregor[2.6]. In addition the recent Maryland cross-section measurements[2.13] and Geneva small angle polarization results[1.27] have been included. Phases (given by the list 1.2.8) were found that minimized a χ^2 goodness of fit function[5.1] using interpolated values from Arndt's latest energy dependent analysis[1.32] as reasonable starting values in the search. Some thought was given to the number of free parameters to allow in the minimization procedure. Phases up to and including $\delta(^3H_6)$ were varied or fixed at their OPEC values in the solutions 1-5 discussed below. The π^oNN coupling constant ($g^2 = 13.85 \pm 0.65$) was taken as the value obtained by Bugg[5.4] from recent phase shift analyses at 210,

325 and 380 MeV, incorporating the data of table 4.2.1. Inelasticity in $\delta(^1D_2)$ was allowed.

Individual solutions and the conditions under which they were obtained are now discussed. The main features of these solutions are listed in table 5.5.1 for completeness.

Solution 1: the world data (W) were incorporated into a solution in which all parameters were allowed to vary. The minimization procedure was forced to halt by choosing suitably large convergence criteria for the phases. Correlations between all phases were extremely large at the minimum and the phases poorly defined.

Solution 2; as (1) but g^2 was fixed at 13.85 and $\bar{\varepsilon}_4$ constrained to its OPEC value. All phases changed appreciably from (1); some by as much as two standard deviations. χ^2 increased dramatically for the "loss" of two parameters. Correlations were still large and phases ill determined. Changes ($\sim$ 1 degree) in the phases were noted for small χ^2 changes during the minimization procedure. In this sense the solution was ill defined; the parameter space being very "flat" near the minimum. Freeing g^2 or $\bar{\varepsilon}_4$ decreased the accuracy of the results whilst fixing any of the H waves individually distorted the solution. These phases, and the observables they predict , have been used throughout this thesis as the pre-1976 phase shift solution.

Solution 3; results from this thesis (T) were added to the data base and a solution found with all phases free. χ^2 rose from 128 for solution (1) to 159 for the addition of 17 data, which

is entirely reasonable. g^2 was predicted to be 8.44 $\pm$ 4.34; one standard deviation below the value determined by Bugg. $\bar{\varepsilon}_4$ was close to its OPEC value of -2.314. Phase shift errors decreased by a factor of 2 and correlation coefficients followed the same trend. The solution was well defined.

Solution 4; as (3) but the value of g^2 was fixed at the more precise value of 13.85 and $\bar{\varepsilon}_4$ was again found to be close to its OPEC value. χ^2 rose by 2.2 for the "loss" of one parameter. The only remaining large (> 0.5) off diagonal elements of the error matrix were between the large phase $^3P_0$ and $^1S_0$, $^3P_1$.

Solution 5; as (4) but $\bar{\varepsilon}_4$ was fixed at its OPEC value, χ^2 increased by 0.8 for the loss of one degree of freedom. Phases were more accurately determined, $\sim$ 0.25 x solution (1) and correlations were at most $\sim$ 0.1. $\delta(^3H_5)$ and $\delta(^3H_6)$ were close to their OPEC values. Fixing the former (at OPEC) gave a χ^2 increase of 2.15 and virtually the same solution; fixing the latter gave a χ^2 increase of 12.26 and distorted the solution. It was considered better to leave the solution "a little too free" rather than achieve greater precision with a possible loss of accuracy.

A well defined solution (5) now exists with a χ^2 of 162 for 113 data and 14 free parameters where previously a poorly defined minimum existed. No other solutions were found within $\pm$ 5 degrees, starting from 20 sets of phases randomly distributed uniformly over this interval. A vast reduction in phase errors has been achieved (table 5.5.1), after the inclusion of the

results T, and Wolfenstein parameters P, D, R, A, R' are now predicted (table 5.5.2) to the accuracy of this experiment ($\pm$ 0.025) up to 70 degrees CM, except possibly in the region < 10 degrees CM. A' is still a suitable candidate for measurement at all angles. The achieved reduction in phase errors is seen to be better than that predicted in section 2.2 (table 2.2) especially in the large low partial waves.

Solution (2) "gave" easily to fit the data set T, illustrating how ill constrained the former solution was by W, with a χ^2 of 1.33 per point and a common normalization of 1.026. The new phases follow the general trend of the high accuracy low energy phases (LEP)[1.32, 5.4], and low accuracy high energy phase (HEP)[1.30, 5.5] with a few notably exceptions. $\delta(^3F_3)$ is strongly positive and at variance with both LEP and HEP: $\delta(^3F_4)$ continues to increase and calls into question the HEP solution at 630 MeV: both $\delta(^3H_4)$ and $\delta(^3H_6)$ are more negative than suggested by a reasonable interpolation from LEP and HEP and $\bar{\varepsilon}_2$ more positive. Solution (5) is plotted in figure 5.5.1 along with the most recent energy independent phase shift analyses of Bugg at 210, 325, 380 and 425 MeV.

TABLE 5.5.1 Phase shift solutions at 515 MeV

Soln. No.	PHASE SHIFTS (SPECTROSCOPIC NOTATION) AND THEIR ERROR													
	$^3P_0$	$^1S_0$	$^3P_1$	$^3P_2$	$\bar{\varepsilon}_2$	$^3F_2$	$^1D_2$	$^3F_3$	$^3F_4$	$\bar{\varepsilon}_4$	$^3H_4$	$^1G_4$	$^3H_5$	$^3H_6$
1	-15.9 4.7	-21.3 5.7	-34.8 3.8	22.9 1.01	-4.40 3.11	-2.50 1.57	10.0 5.60	6.50 1.74	4.60 1.22	-1.99 2.54	-3.89 0.95	6.34 3.4	-1.34 2.07	-0.87 0.82
2	-20.17 5.16	-29.35 6.13	-34.44 3.95	20.63 1.43	1.69 2.06	-0.79 1.52	12.80 2.80	3.83 1.76	5.07 0.77	(-2.31)	-2.08 1.24	3.23 1.24	-1.39 1.10	-0.28 0.75
3	-18.44 2.37	-23.65 2.16	-34.34 1.21	20.98 0.89	3.19 0.73	-1.18 0.97	15.78 1.08	2.00 0.63	4.86 0.57	-2.44 0.66	-3.02 0.61	4.27 0.84	-1.96 0.45	-1.04 0.42
4	-15.90 1.83	-22.08 1.57	-35.42 0.92	21.63 0.62	2.32 0.54	-0.76 0.70	14.93 0.96	2.52 0.47	5.20 0.42	-1.85 0.50	-3.18 0.48	5.04 0.56	-1.79 0.41	-0.88 0.36
5	-17.68 0.85	-22.67 1.44	-34.67 0.91	21.33 0.45	2.67 0.44	-0.97 0.64	15.58 0.70	2.38 0.45	5.00 0.34	(-2.31)	-3.13 0.51	4.78 0.49	-1.83 0.41	-0.94 0.38

Soln No.	Predicted χ^2 for T (17 points)	χ^2 contribution from T	Predicted normalization of T	Largest χ^2 per point	Soln χ^2	Comments	π^0NN g^2	Data base
1	454.13	-	-	-	128.9	all waves free	40.94 7.87	W
2	358.33	-	-	-	151.8	g^2, $\bar{\varepsilon}_4$ fixed	(13.85)	W
3	-	19.59	1.024	5.480	159.2	all waves free	8.44 4.34	W+T
4	-	22.13	1.025	5.933	161.4	g^2 fixed	(13.85)	W+T
5	-	22.62	1.026	5.166	162.2	g^2, $\bar{\varepsilon}_4$ fixed	(13.185)	W+T

T ≡ Data from this thesis; W ≡ World data; (...) ≡ fixed at OPEC

Angle (CM DEG.)	$\frac{\delta\sigma(\theta)}{\sigma(\theta)}$	δP	δD	δR	δA	$\delta R'$	$\delta A'$	δC_{KP}	δC_{NN}
10	0.036	0.010	0.028	0.030	0.018	0.019	0.045	0.011	0.034
20	0.023	0.009	0.017	0.021	0.023	0.024	0.023	0.016	0.030
30	0.019	0.005	0.016	0.014	0.021	0.020	0.017	0.011	0.027
40	0.012	0.006	0.014	0.021	0.024	0.021	0.035	0.010	0.017
50	0.010	0.004	0.018	0.020	0.021	0.021	0.031	0.010	0.018
60	0.009	0.002	0.023	0.022	0.023	0.017	0.018	0.018	0.023
70	0.011	0.004	0.027	0.025	0.030	0.030	0.029	0.030	0.031
80	0.010	0.003	0.030	0.027	0.025	0.031	0.024	0.040	0.048
90	0.017	0.000	0.036	0.034	0.019	0.030	0.021	0.045	0.057
100			0.044	0.037	0.028	0.034	0.028		
110			0.041	0.030	0.035	0.029	0.029		
120			0.026	0.023	0.027	0.017	0.027		
130			0.018	0.029	0.019	0.007	0.034		
140			0.023	0.030	0.019	0.015	0.036		
150			0.025	0.023	0.027	0.020	0.024		
160			0.019	0.018	0.045	0.021	0.015		
170			0.047	0.010	0.063	0.039	0.007		

TABLE 5.5.2 Predicted error on some common observables; from the phase shift solution

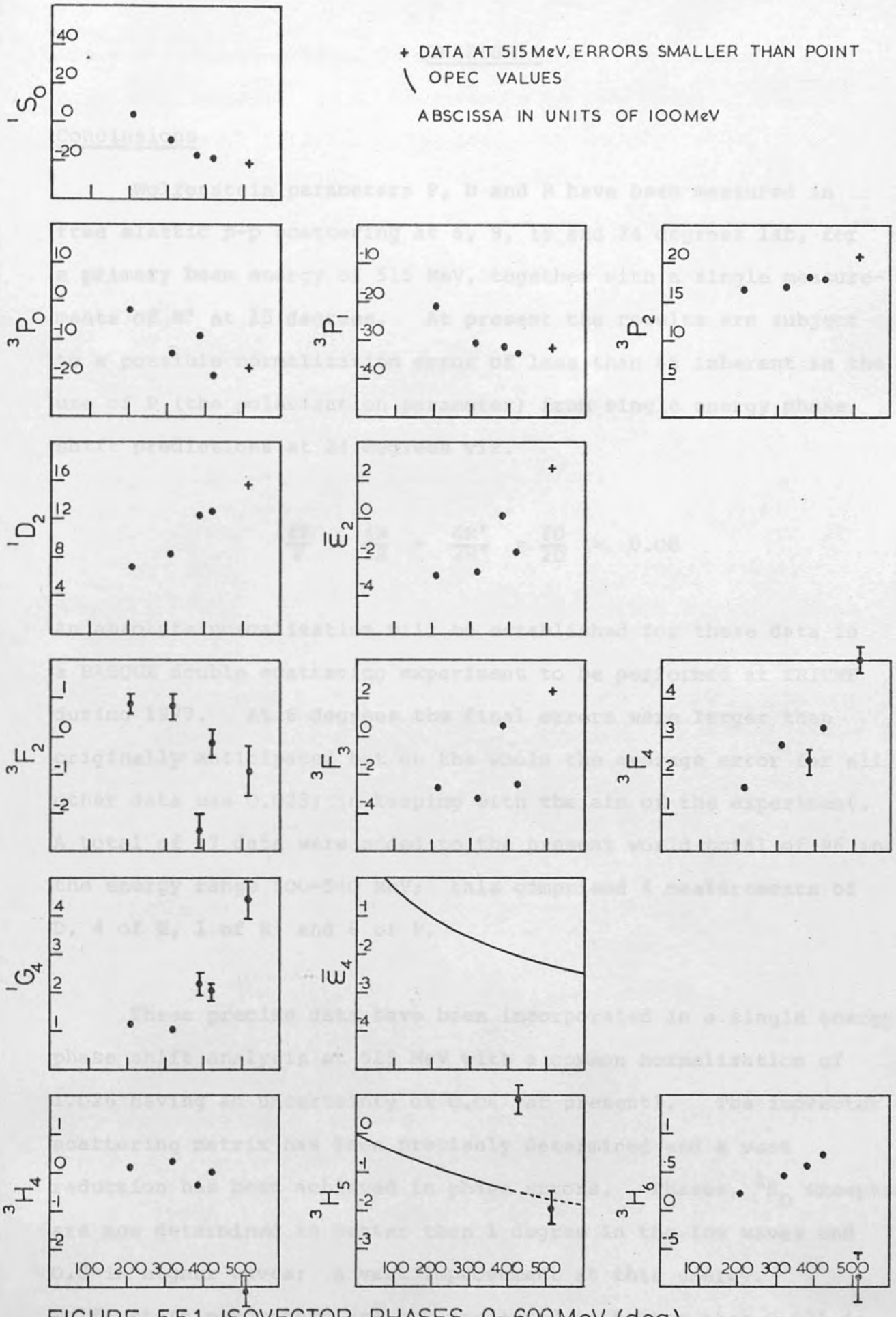

FIGURE 5·5·1 ISOVECTOR PHASES 0-600 MeV (deg)

CHAPTER 6

Conclusions

Wolfenstein parameters P, D and R have been measured in free elastic p-p scattering at 6, 9, 15 and 24 degrees lab, for a primary beam energy of 515 MeV, together with a single measurements of R' at 15 degrees. At present the results are subject to a possible normalization error of less than 6% inherent in the use of P (the polarization parameter) from single energy phase shift predictions at 24 degrees viz.

$$\frac{\delta P}{P} = \frac{\delta R}{2R} = \frac{\delta R'}{2R'} \simeq \frac{\delta D}{2D} \simeq 0.06$$

An absolute normalization will be established for these data in a BASQUE double scattering experiment to be performed at TRIUMF during 1977. At 6 degrees the final errors were larger than originally anticipated but on the whole the average error for all other data was 0.023; in keeping with the aim of the experiment. A total of 17 data were added to the present world total of 96 in the energy range 500-540 MeV; this comprised 4 measurements of D, 4 of R, 1 of R' and 8 of P.

These precise data have been incorporated in a single energy phase shift analysis at 515 MeV with a common normalization of 1.026 having an uncertainty of 0.06 (at present). The isovector scattering matrix has been precisely determined and a vast reduction has been achieved in phase errors. Phases, $^1S_0$ excepted, are now determined to better than 1 degree in the low waves and 0.5 in higher waves; a vast improvement at this energy. Wolfenstein parameters are now predicted to better than 0.025 in

the forward region below 70 degrees CM. A' is, however, still a suitable observable for measurement to this level of accuracy at all angles.

APPENDIX A

Geometry of the straight track veto system

Straight tracks through the polarimeter provided no information about the polarization of the incident beam. It was required therefore that these events be vetoed quickly (order of 10^{-7}s) as they constituted typically 95-98% of all tracks. The proton telescope ensured that incident tracks lay within a cone of approximately 10 milliradians. Any counter positioned to intercept the beam downstream of the carbon analyser became a straight track veto. The following discussion relates to the simple calculation of the veto position once the minimum scatter angle and polarimeter position are known. Table A.1 lists the actual veto Z co-ordinates used during the Wolfenstein parameter experiments as a function of beam energy and proton angle of scatter in the target.

Chapter 5 showed that the analysing power of carbon, below 4 degrees, was small compared with the peak values (although the number of events was large) and the polarimeter was less able to determine the azimuthal scattering angle Ø (Appendix C). In order to usufully record data with polar scattering angle $\theta \geq 4$ degrees, the angle θ_s (figure A.1) must not be greater than this. Events which multiply scatter in the carbon must be vetoed. The root mean square angle $(\theta^c_{RMS})^{(A.1)}$ for Coulomb scattering of proton by 60mm of carbon at 240 MeV is 13 milliradians. A figure of twice this angle was chosen for good veto efficiency, hence $\theta_m \geq 2\theta^c_{RMS}$. From figure A.1 we see that

$$g/f \geq \theta_m \quad \ldots\ (A.1)$$

$$(c+g)/f \leq \theta_s \quad \ldots\ (A.2)$$

Distance C was calculable as SOAA', SOB and the carbon analyser had known positions. The angular acceptance of the proton telescope (θ_t) is given by

$$\theta_t = (a+b)/d \qquad \ldots\ldots (A.3)$$

hence

$$c = b + \theta_t\,(e+f) \qquad \ldots\ldots (A.4)$$

leaving c, g and f to be determined from the solutions of the inequalities A.1-A.4.

Straight tracks which scattered after the polarimeter and missed the veto counter were rejected by the PDP-11 computer software and off-line analysis.

Energy (MeV) \ Lab scattering angle (DEG)	6°	9°	15°	24°
515	3.723	3.608	3.483	3.063
427	3.113	2.320*	2.908	2.583
382	2.803	2.300*	2.603	2.323†
327	2.393	2.300*	2.323†	2.323†

*(incorrectly set) †(as close to the carbon as was physically possible)

TABLE A.1 Z co-ordinates of the straight track veto counter (metres) for the Wolfenstein experiments (as a function of EPB energy and lab. scattering angle).

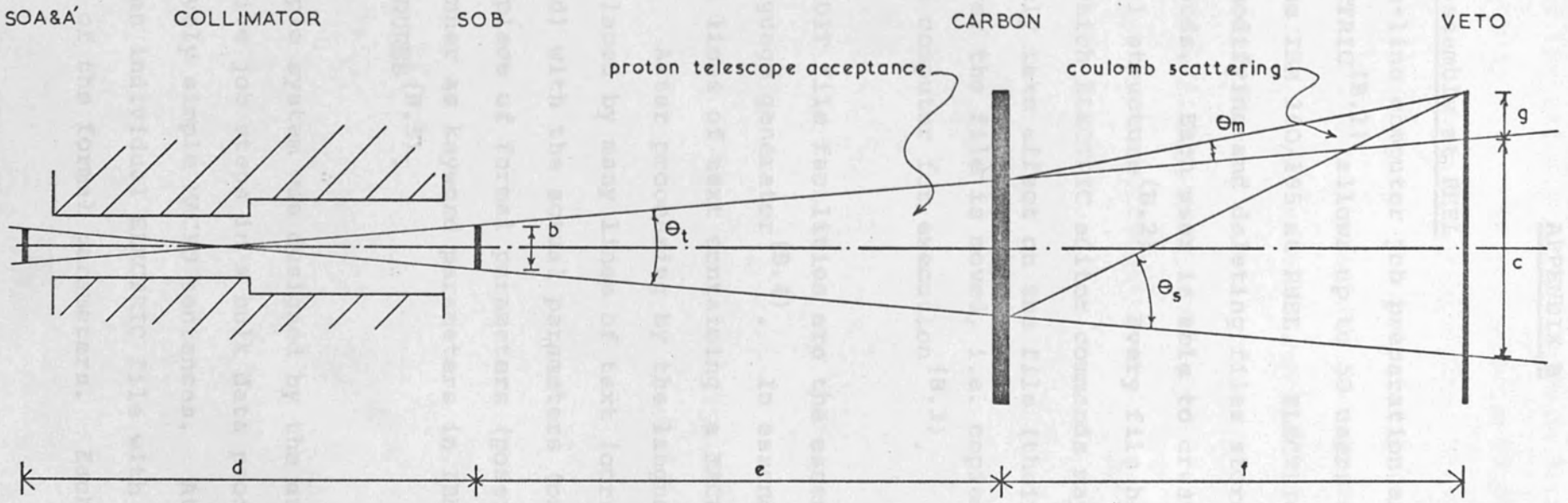

FIGURE A-1 GEOMETRY OF THE STRAIGHT TRACK VETO

APPENDIX B

Large job assembly at RHEL

An on-line computer job preparation and submission program called ELECTRIC[B.1] allows up to 50 users to interact with stored files on the IBM 360/195 at RHEL. ELECTRIC provides methods for creating, modifying and deleting files stored under individual user passwords. Each user is able to create files within a tree hierarchical structure[B.2]. Every file has an associated EDIT file into which ELECTRIC editor commands may be placed. These commands only take effect on the file (their action may be suppressed) whenever the file is moved, i.e. copied, printed or "sent" to the main computer for execution[B.3].

The EDIT file facilities are the essential ingredients of a MACRO language generator[B.4]. In essence a MACRO language consists of lines of text containing a MACRO name and possibly parameters. After processing by the language generator each line is replaced by many lines of text (corresponding to the MACRO called) with the actual parameters (on the line of text) taking the place of formal parameters (possible default values) in the same manner as keyword parameters in IBM Job Control Language (JCL) PROCEDURES[B.5].

A simple system was designed by the author to generate JCL for repetitive job steps in a bulk data processing computer job from relatively simple MACRO sentences. At RHEL each MACRO resides in an individual ELECTRIC file with the EDIT part storing the details of the formal parameters. Each job step usually

consisted of identical JCL (and perhaps data) with a few parameters modified, e.g. file number on a tape, and was therefore ideally suited to being generated from MACRO calls. This system was implemented using the ELECTRIC facilities rather than IBM PROCEDURES as the former provided more powerful facilities for designing MACROs. Using this simple system it was possible to process a single energy's data in one large computer job, hence improving the efficiency of our computer usage and reducing the manual overheads for the computer staff.

APPENDIX C

Geometrical resolution of the polarimeter

Program MONTE was designed and written by the author to investigate aspects of the polarimeter's "geometrical resolving power" by Monte Carlo methods. An intensive study was undertaken early in 1975 with the ultimate aim of deducing which algorithm was best suited to extracting asymmetries from a Θ-$\emptyset$ matrix (produced by REDUCE 2). The conclusions drawn below present a logical argument for the adoption of "the method of moments" (Appendix F) for this task.

Historically the first method used by the BASQUE group to extract asymmetries was by fitting the function $N(1+\varepsilon\cos(\emptyset+\beta))$ to each Θ bin using a non linear χ^2 algorithm (which varied N, ε and β). It was subsequently found that the χ^2 value for the sum of two "identical" runs was larger than that for the individual runs. This indicated the presence of non statistical "bumps" in the $\emptyset$ distribution possibly caused by "co-ordinate quantization effects" inherent in the use of MWPC arrays on the polarimeter. MONTE was therefore commissioned to test the track reconstruction algorithms used by REDUCE 1 and deduce methods for extracting unbiased asymmetries.

Actual MWPC positions and deviations (corrections to MWPC lateral positions) were used in the program, but no allowance was made for multiple scattering. Each "Monte Carlo event" consisted of the following sequence:

1) randomly generate true incident and final tracks; each

uniformly distributed in polar and azimuthal angle (several runs employed Gaussian distributions for the polar angle).

2. Calculate true scattering angles Θ_{TRUE} and $\emptyset_{TRUE}$ from the tracks (1).

3. Convert true tracks to observed MWPC wire numbers (i.e. those that would have been activated by the track).

4. Deduce co-ordinates for the activated wires (possibly adding the randomising factor between $\pm$ 2 to each co-ordinate).

5. Use REDUCE 1 track reconstruction routines to determine the observed tracks and observed scattering angles Θ, $\emptyset$.

6. Form histograms from "true" and "observed" slopes, angles, differences of slopes, etc.

Reconstructed angles Θ and $\emptyset$ were binned in a matrix 66 x 3600, with a lower limit of 2 degrees being placed on Θ (due to errors $\sim$ 5 degrees in $\emptyset$ below this angle). A fine binning for $\emptyset$ allowed many smaller matrices to be formed (3600 has many factors); the following algorithms were compared using the data so binned:

a) Non linear χ^2 fitting of the function $N(1+\varepsilon\cos(\emptyset+\beta))$; where N, ε, β were parameters to be determined.

b) Method of moments to $N(1+\sum_n a_n\cos(n\emptyset)+b_n\sin(n\emptyset))$; where N, a_i, b_i were parameters to be determined.

c) ε=(left-right)/(left+right) where "left" was defined as the sum of all events for $-\pi/2 \leq \phi \leq \pi/2$ and "right" was the remainder.

The method of moments was finally chosen for the analysis after polarimeter data revealed that coefficients higher than the first in expression (b), were non zero. The algorithm allowed each a_i, b_i to be extracted independently whereas χ^2 fitting procedures can only be effectively used to test a hypothesis that data were taken from a known population and method (c) was biased by the presence of odd "cos" terms in the expression (b). Having decided upon an algorithm for extracting asymmetries the matrix dimensions could have been reduced, giving bin widths closer to the resolution of these angles by the polarimeter. Historically this did not happen until the p-p analysis, under the maxim "if it works - leave it alone".

Tracks in any one plane (XZ or YZ) were fitted before and after the carbon analyser to straight lines viz.

$$Z = ax + b \qquad \ldots\ (C.1)$$

where

$$a = (x_1 - x_3)/L \qquad \ldots\ (C.2)$$

x_1, x_2, x_3 were co-ordinates of wires in the three MWPC's of a triplet; L was the distance between the first and last MWPC of the three. It followed that the variance ($\delta^2 a$) of "a" was given by:

$$\delta^2 a = 2\delta^2 x/L^2 \qquad \ldots\ (C.3)$$

for equal variance ($\delta^2 x$) on the x_i. This latter variance was calculated using a simple "top hat" distribution of $\pm$ 2mm about each wire[3.12, 3.13] to be

$$\delta^2 x = 4/3 mm^2$$

Values obtained for $\delta^2 a$ by MONTE were in excellent agreement with the theoretical values of(C.3) (distances L being 358mm and 287mm in front and back respectively).

Resolution in Θ was found to be independent of Θ and $\emptyset$ and given by the incident and final slope resolutions summed in quadrature ($\delta^2\Theta$ = 3.5 milliradians). Error in $\emptyset$ varied inversely as sin(Θ) but was independent of $\emptyset$. Figures C.1 and C.2 illustrate these findings whilst figure C.3 shows how the error in $\emptyset$ varies with $\emptyset$ when no corrections are made for known MWPC misalignments. Figure C.4 shows a typical historgram of the minimum distance between observed incident and final tracks (when the true tracks intersected at Z=0), figure C.5 shows the "Moire Fringes" effect brought about by quantization of measured angles. Each fringe corresponds to the image of an MWPC wire in Θ-$\emptyset$ co-ordinates, i.e.

a) at $\emptyset$=0, 180 degrees vertical wires were represented by

$$\cos(\Theta)\tan(\emptyset) = \text{constant} \quad \ldots \text{(C.4)}$$

b) at $\emptyset$=90, 270 degrees horizontal wires were represented by

$$\sin(\Theta)\tan(\emptyset) = \text{constant} \quad \ldots \text{(C.5)}$$

Diffuse fringes were seen at 45, 135, 225 and 315 degrees corresponding to "virtual wires" formed by drawing a diagonal line through points where vertical and horizontal wires crossed.

Simulations were only performed for small angle of incidence tracks (corresponding to experimental conditions). Fringes generated by MONTE were compared with those from actual data and found to be in good agreement, both in intensity and location; these led to definite non statistical lumps in the ϕ distribution that were sensitive to the accuracy with which chamber deviations were corrected for. Deviations were extracted from raw data by fitting straight tracks to unscattered proton paths through the polarimeter (this method was itself checked by MONTE to 1% confidence level). Randomizing wire co-ordinates reduced our sensitivity by smoothing the data in a θ-ϕ matrix, without increasing the resolution in θ or ϕ by more than a factor 2: which was still within the 0.5 degrees for θ x 350/360 degree in ϕ bin size chosen for the pp experiments.

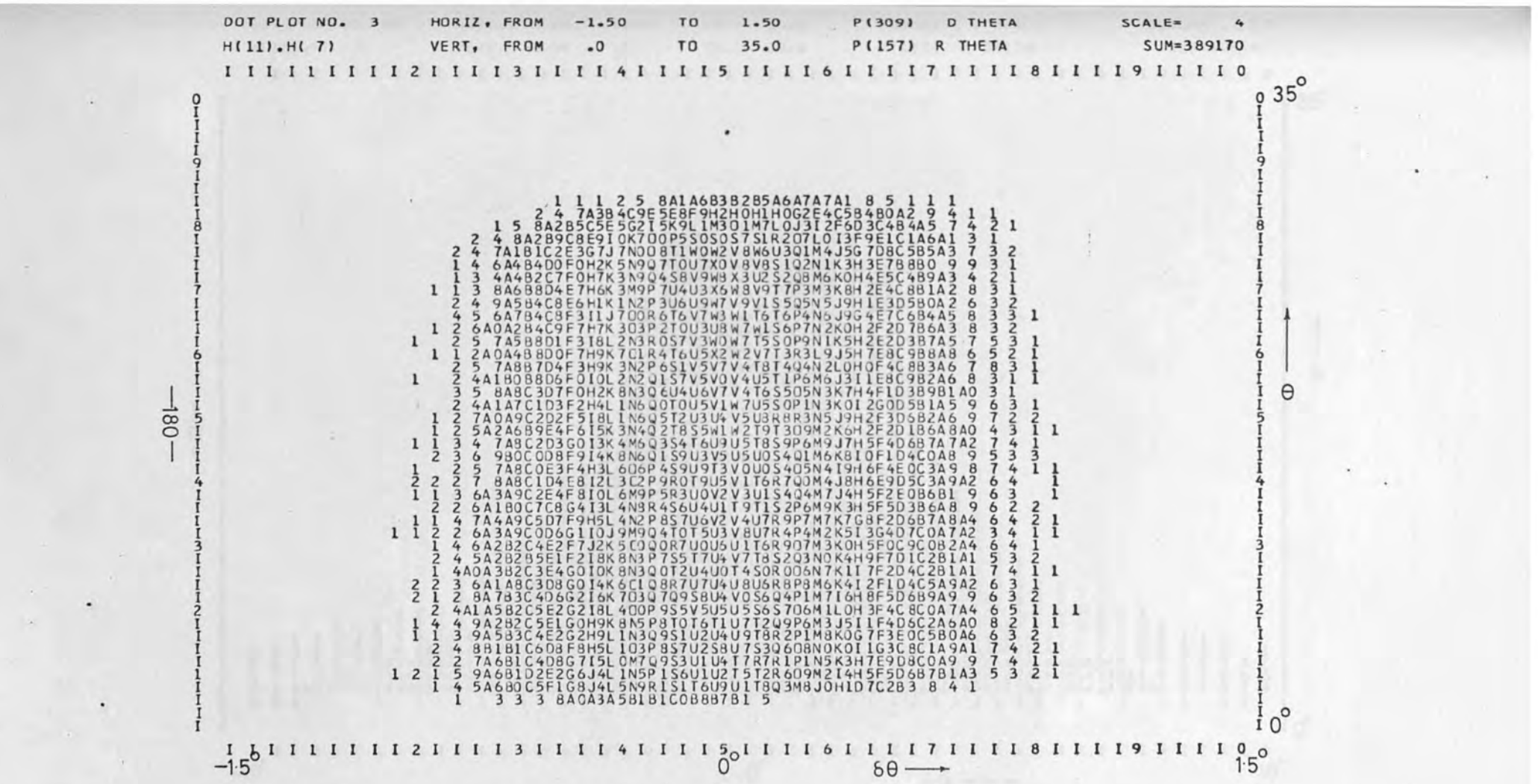

FIGURE C·1 POLARIMETER RESOLUTION IN θ AS A FUNCTION OF θ ($\delta^2\theta = 0{\cdot}28$)

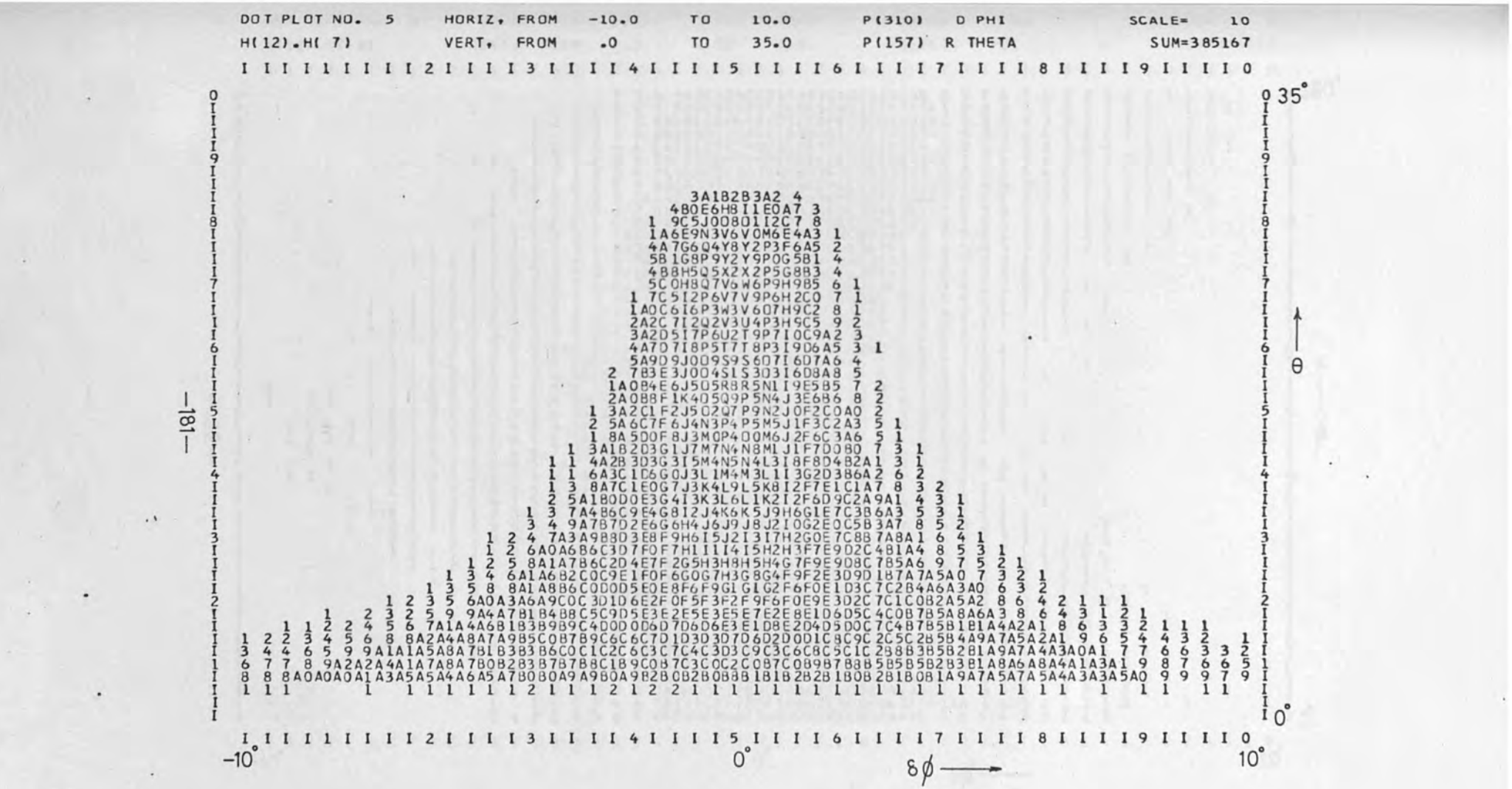

FIGURE C-2 POLARIMETER RESOLUTION IN ϕ AS A FUNCTION OF θ

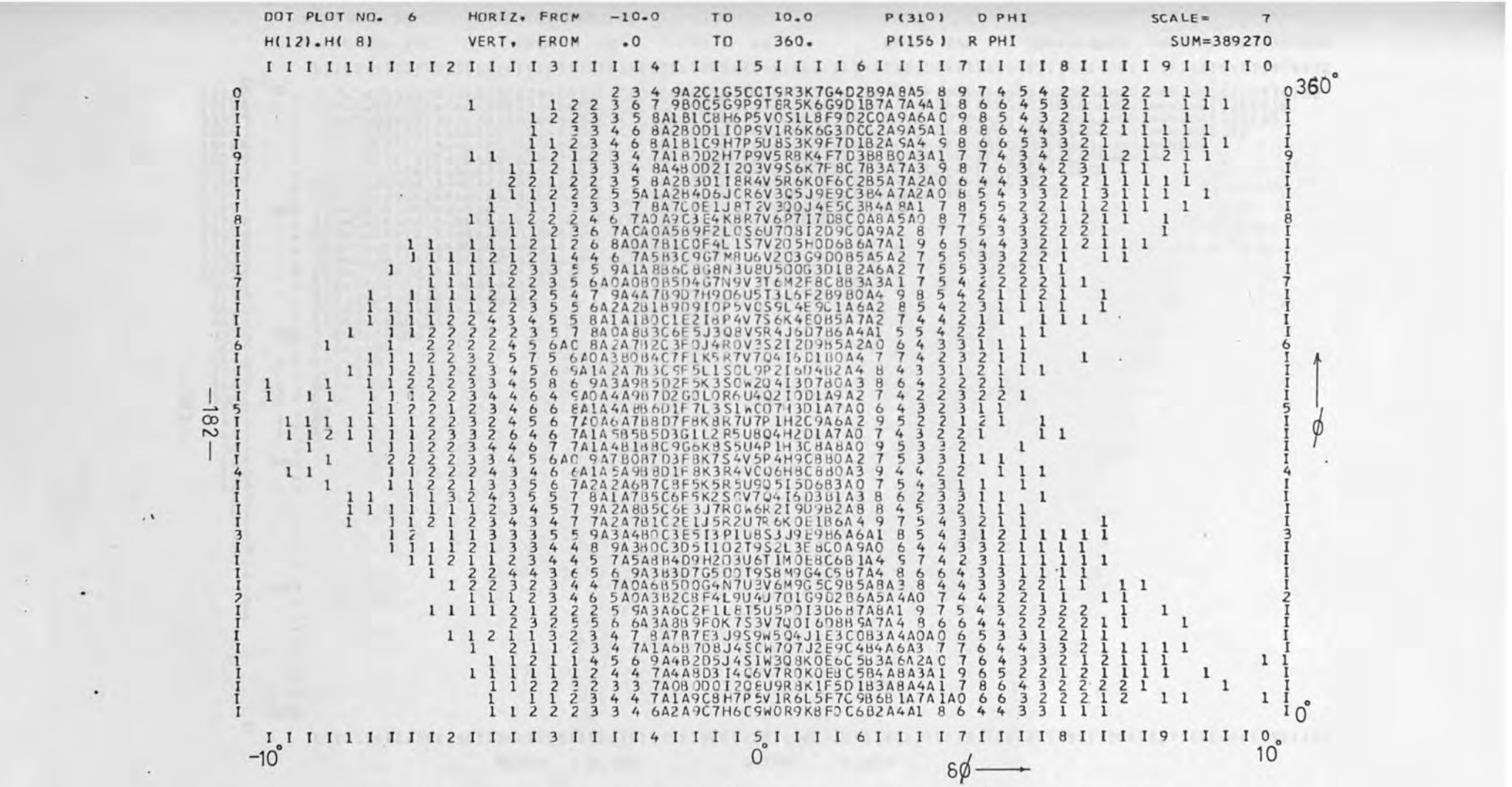

FIGURE C·3 POLARIMETER RESOLUTION IN ϕ AS A FUNCTION OF ϕ, WHEN NO CORRECTION FOR MWPC DEVIATIONS HAS BEEN MADE

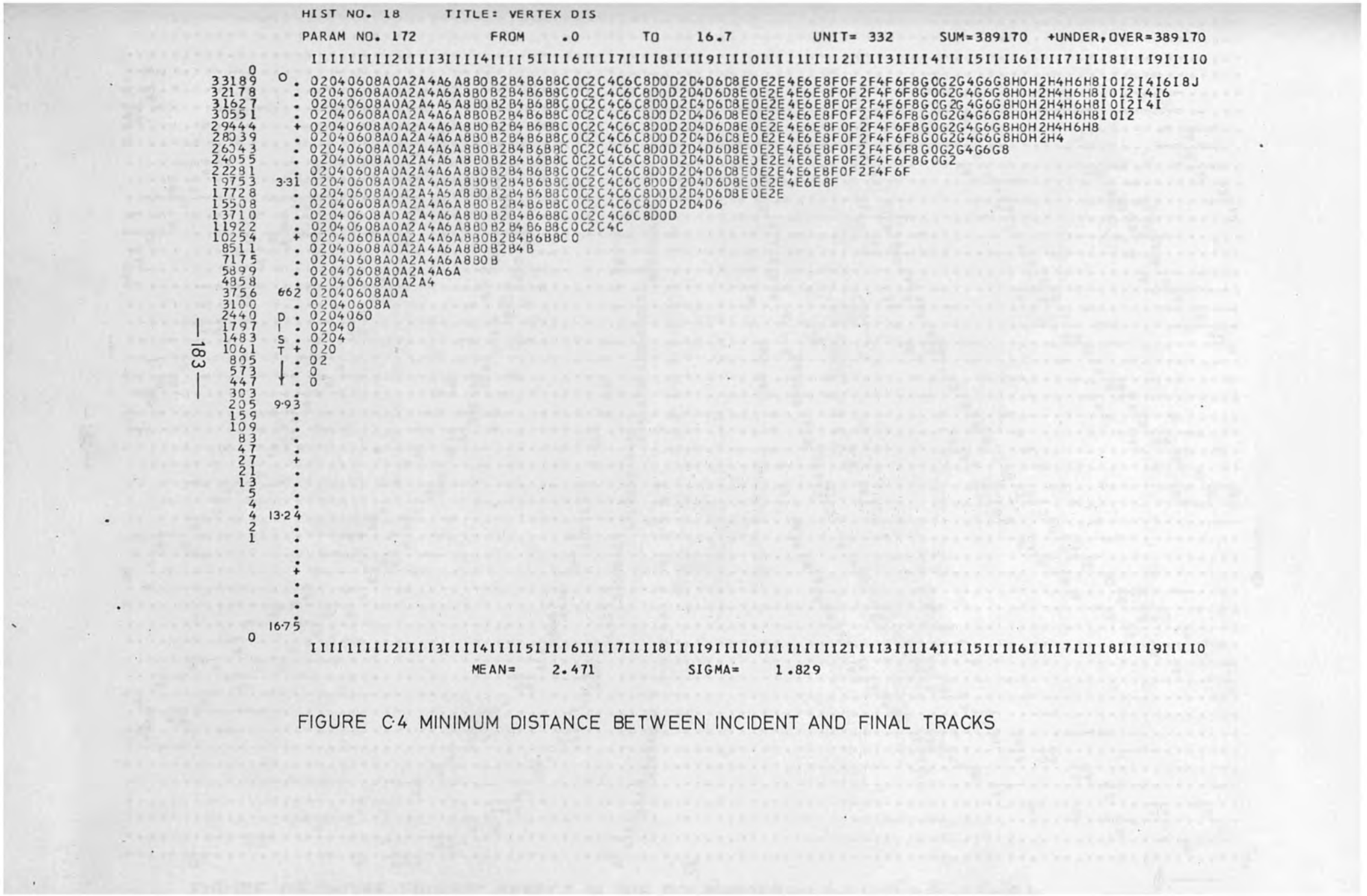

FIGURE C-4 MINIMUM DISTANCE BETWEEN INCIDENT AND FINAL TRACKS

FIGURE C·5 "MOIRE FRINGE" EFFECT IN THE POLARIMETER (at $\phi = 0$) ($0{\cdot}1^{\circ}$ in $\phi \times 0{\cdot}5^{\circ} \sin\Theta$)

APPENDIX D

Collected acronyms

This short appendix brings together the standard acronyms used throughout this thesis.

Acronym	Derivation
ADC	Analogue to Digital Converter
BASQUE	Bedford College, AERE Harwell, Surrey University, Queen Mary College, Universities of British Columbia and Victoria Experiment
CCU	Chamber Control Unit
CM	Centre of Mass
EPB	Extracted Proton Beam
FWHM	Full Width at Half Maximum
MLS	Miniature Logic System
MWPC	Multi Wire Proportional Chamber
NN	Nucleon-Nucleon
OPEC	One Pion Exchange Contribution
P-P	Proton-Proton
RF	Radio Frequency
RHEL	Rutherford High Energy Laboratory
TDC	Time to Digital Converter
TOF	Time-of-Flight
TRIUMF	TRI University Meson Facility
UBC	University of British Columbia
UCLA	University of California, Los Angeles

APPENDIX E

Relativistic 2-body kinematics

Consider scattering of a proton by a stationary hydrogen atom in the lab

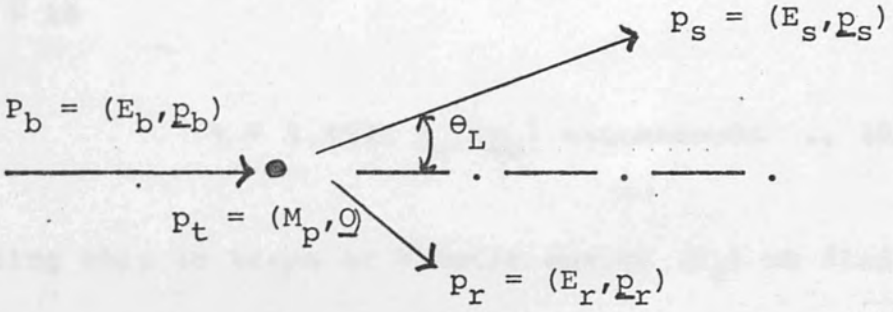

The invariant length of any proton 4-momentum vector ($p'=(E',\underline{p}')$) is given by

$$(p')^2 = E'^2 - |\underline{p}'|^2 = M_p^2 \qquad \ldots\ (E.1)$$

where M_p is the proton rest mass. Energy-momentum conservation for the scatter implies:

$$p_r = p_b + p_t - p_s$$

squaring each side and using (E.1) we find

$$M_p^2 = 3M_p^2 + 2E_b M_p - 2E_b E_s + 2\underline{p}_b \cdot \underline{p}_s - 2E_s M_p$$

solving for the dependence on θ_L

$$\cos(\theta_L) = \frac{E_b E_s + E_s M_p - E_b M_p - M_p^2}{\sqrt{E_b^2 - M_p^2}\ \sqrt{E_s^2 - M_p^2}}$$

or in terms of kinetic energies ($T = E - M_p$)

$$\cos(\theta_L) = \sqrt{\frac{T_s(T_b + 2M_p)}{T_b(T_s + 2M_p)}} \qquad \ldots\ (E.2)$$

The time-of-flight (τ) of the scattered proton over a path length L is

$$\tau = 3.333L\ E_s/|\underline{p}_s| \text{ nanoseconds} \quad \ldots\ (E.3)$$

Expressing this in terms of kinetic energy (T_s) we find

$$\log(\tau) = \log(3.333L) + \log(T_s+M_p) - \tfrac{1}{2}\log(T_s) - \tfrac{1}{2}\log(T_s+2M_p)$$

differentiating and re-arranging

$$\frac{d\tau}{\tau} = -\frac{M_p^2}{T_s(T_s+M_p)(T_s+2M_p)}\, dT_s \qquad \ldots\ (E.4)$$

or

$$d\tau \simeq -\frac{\tau}{\varepsilon(\varepsilon+1)(\varepsilon+2)}\, d\varepsilon \qquad \ldots\ (E.5)$$

if $\varepsilon = T_s/M_p$.

APPENDIX F

Asymmetry algorithm

Consider protons scattering in the carbon analyser with polar angle Θ and azimuthal angle ϕ. Within a given Θ bin the distribution of events in ϕ was expanded in a "Fourier series". If $f(\phi_i)$ represented the number of events in the ϕ_i bin then

$$f(\phi_i) \equiv f_i = N\left[1+ \sum_{n=1} \{a_n\cos(n\phi_i)+b_n\sin(n\phi_i)\}\right] \quad \ldots. \text{ (F.1)}$$

where the centre of the ϕ_k bin (k=1, ..., 50) was given by

$$\phi_k = 2\pi(k - 0.5)/50 \text{ radians} \quad \ldots. \text{ (F.2)}$$

Corresponding to the identity (for continuous f):

$$a_n = \overline{2\cos(n\phi)} = \frac{\int_0^{2\pi} 2\cos(n\phi) f(\phi) d\phi}{\int_0^{2\pi} f(\phi) d\phi} \quad \ldots. \text{ (F.3)}$$

the approximation

$$a_n = \overline{2\cos(n\phi_i)} = \sum_i 2\cos(n\phi_i) f_i / \sum_i f_i \quad \ldots. \text{ (F.4)}$$

was used. The point f_i was normally distributed with variance $(\delta^2 f_i)$ of f_i. To a good approximation a change (Δa_n) in a_n was related to changes (Δf_i) in f_i by

$$\Delta a_n = \sum_i \frac{\partial a_n}{\partial f_i} \Delta f_i \quad \ldots. \text{ (F.5)}$$

squaring and averaging we find that the error squared ($\delta^2 a_n$) in a_n was related to the uncertainties in f_i by

$$\delta^2 a_n = \sum_i \left(\frac{\partial a_n}{\partial f_i}\right)^2 \delta^2 f_i = \sum_i \left(\frac{\partial a_n}{\partial f_i}\right)^2 f_i \quad \ldots\ldots (F.6)$$

as the f_i were approximately independent points. Differentiating (F.4) with respect to f_i

$$\frac{\partial a_n}{\partial f_i} = \frac{2\cos(n\phi_i) - a_n}{N} \quad \ldots\ldots (F.7)$$

where $$N = \sum_i f_i \quad \ldots\ldots (F.8)$$

Then (F.6) becomes

$$\delta^2 a_n = \frac{1}{N} \sum_i \frac{(2\cos(n\phi_i) - a_n)^2 f_i}{N} = \frac{\overline{(2\cos(n\phi_i) - a_n)^2}}{N} \quad \ldots\ldots (F.9)$$

A similar result holds for b_n if "cos" is replaced by "sin".

APPENDIX G

Simplistic empty target subtraction

The following nomenclature is used throughout this thesis:

q_B = probability of a background scatter being accepted through the analyses.

I_F = beam intensity during a target full experiment.

I_E = beam intensity during an empty target experiment.

ε_F = asymmetry (amplitude) "seen" in the polarimeter during target full experiment.

ε_E = true asymmetry (amplitude) of background "seen" in the polarimeter during the empty target experiment.

ε_H = true asymmetry (amplitude) of hydrogen.

N_F = total number of events accepted during target full experiment.

N_E' = number of background events accepted during the target full experiment.

N_E = total number of background events accepted during the empty target experiment.

N_H = number of events from hydrogen accepted during the target full experiment.

Consider target full and empty experiments carried out at the same EPB energy, then

$$N_E' = q_B I_F \qquad N_E = q_B I_E \qquad \ldots\ (G.1)$$

$$N_F = N_E' + N_H \qquad \ldots\ (G.2)$$

During the target full experiment the polarimeter "saw" the sum of distributions in ϕ from the liquid hydrogen and target flask viz.

$$N_H(1 + \varepsilon_H \cos(\phi)) + N_E'(1 + \varepsilon_E \cos(\phi)) \quad \ldots\ (G.3)$$

say, in the form

$$N_F(1 + \varepsilon_F \cos(\phi)) \quad \ldots\ (G.4)$$

equating these it follows that

$$N_F = N_E' + N_H \quad \ldots\ (G.5)$$

and

$$\varepsilon_F = (N_H\varepsilon_H + N_E'\varepsilon_E)/N_F \quad \ldots\ (G.6)$$

Using (G.1) and (G.2) we find that (G.6) becomes

$$N_F\varepsilon_F = (N_F - \frac{I_F}{I_E} N_E)\varepsilon_H + \frac{I_F}{I_E} N_E\varepsilon_E \quad \ldots\ (G.7)$$

solving for ε_H, the asymmetry due to hydrogen.

$$\varepsilon_H = \frac{\varepsilon_F - \frac{I_F}{I_E}\frac{N_E}{N_F}\varepsilon_E}{\left[1 - \frac{I_F}{I_E}\frac{N_E}{N_F}\right]} \quad \ldots\ (G.8)$$

Finally we note that this analysis could have been carried through for each θ_j bin (j=1, ..., 16) to give

$$\varepsilon_H(\Theta_j) = \frac{\varepsilon_F(\Theta_j) - \frac{I_F}{I_E}\frac{N_E(\Theta_j)}{N_F(\Theta_j)}\,\varepsilon_E(\Theta_j)}{\left[1 - \frac{I_F}{I_E}\frac{N_E(\Theta_j)}{N_F(\Theta_j)}\right]} \qquad \ldots\ (G.9)$$

REFERENCES

I.1 MacGREGOR, M H. Phys.Rev. 182, 1714 (1969).

I.2 SIGNELL, P. Phys.Rev.Lett. 27, 1393 (1971).

I.3 BRYAN, R. Research Institute for Theoretical Physics, University of Helsinki, Preprint in Theoretical Physics 11-75 (1975).

1.1 CHADWICK, J. Nature, 129, 312 (1932).

1.2 HEISENBERG, W. Zeit.F.Phys, 77, 1 (1932).

1.3 WIGNER, E. Zeit.F.Phys. 83, 253 (1933).

1.4 DUNNING, J.R. Phys.Rev. 47, 970 (1935).

1.5 YAKAWA, H. Proc.Phys-Math.Soc. Japan, 20, 319, 720 (1938).

1.6 KELLOGG, J M B. Phys.Rev. 55, 318 (1939).

1.7 WIGNER, E. Proc.Nat.Acad.Sci. U.S. 27, 281 (1941).

1.8 JENSEN, J H D. Phys.Rev. 75, 1766 (1949).

1.9 WIGNER, E. Phys.Rev. 51, 106 (1937).

1.10 ADAIR, R K. Phys.Rev. 87, 1041 (1952).

1.11 KROLL, N M. Phys.Rev. 88, 1177 (1952).

1.12 MacGREGOR, M H. Ann.Rev.Nucl.Sci. 11, 95 (1961).

1.13 WILSON, R. "The Nucleon N ucleon Interaction", Wiley (1963).

1.14 BREIT, G. Ann.Rev.Nucl.Sci. 2, 365 (1953).

1.15 BRINK, D M. "Nuclear Forces", Pergammon Press (1965).

1.16 STAPP, H P. Ann.Rev.Nucl.Sci. 10, 291 (1960).

1.17 MORAVCSIK, M J. "The Two Nucleon Interaction" Oxford Press (1963).

1.18 McKEE, J S C. Meeting on Polarization Physics, Ebermannstadt (1973).

1.19 EDGINGTON, J A. Symposium on Intermediate Energy Physics, Zuos (1973).

1.20 BROWN, G E. "The Nucleon-Nucleon Interaction", Nordita (1971-72).

1.21 SINHA, B. Physics Reports 20C, 1 (1975).

1.22 ERKELENZ, K. Physics Reports 13C, 5 (1974).

1.23 WORTMAN, W R. "Mathematics in Science and Engineering" 71, 333 (1970).

1.24 Proceedings of the Fifth International Conference on High Energy Physics and Nuclear Structure, Uppsala (1973).

1.25 BUGG, D V. Nucl.Phys. B5, 29 (1968).

1.26 TAYLOR, J R. "Scattering Theory", Wiley (1972).

1.27 Proceedings of the Fourth International Symposium on Polarization Phenomena in Nuclear Reactions, Zurich (1975).

1.28 de BOER, W. Nucl.Inst.Meth. 136, 331 (1976).

1.29 MacGREGOR et al. Phys.Rev. 169, 1128 (1968).

1.30 MacGREGOR et al. Phys.Rev. 169, 1149 (1968).

1.31 MacGREGOR et al. Phys.Rev. 173, 1272 (1968).

1.32 ARNDT, R A. Phys.Rev. C9, 555 (1974).

1.33 GOTTFRIED, K. "Quantum Mechanics", Benjanin (1966).

1.34 BINSTOCK, J. Phys.Lett. 48B, 77 (1974).

1.35 SAUER, P U. Phys.Rev.Lett. 32, 626 (1974).

1.36 HAMILTON, J. "Theory of Elementary Particles", Oxford Press (1959).

1.37 HANNA, R.C. 2nd International Symposium on Polarisation Phenomena of Nucleons, Karlsruhe (1965).

1.38 WOLFENSTEIN, L. Phys.Rev. 85, 947 (1952).

2.1 BASQUE, TRIUMF Research Proposal 40 (1974).

2.2 BUGG, D V. "What np Elastic Scattering Data Are Needed" TRI-75-5 (1975).

2.3 BASQUE, TRIUMF Research Proposal 74 (1975).

2.4 ARNDT, R A. Nucl.Phys. B50, 285 (1972).

2.5 BUGG, D V., ORAM, C J. "What pp Parameters Need Measuring from 200-500 MeV?" TRI-75-4 (1975)

2.6 MacGREGOR, M H. "pp and np Data Listing 0-750 MeV" UCRL-50426.

2.7 BYSTRICKY, J. "Elastic Nucleon Nucleon Scattering Data 370-3000 MeV" CEA-N-154-7(E).

2.8 CHENG, D. Phys.Rev. 163, 1470 (1967).

2.9 ALBROW, M G. Nucl.Phys. B23, 445 (1970).

2.10 COZZIKA, G. Phys.Rev. 164, 1672 (1967).

2.11 SURKO, P H. Ph.D. Thesis. UCRL-19451 (1970).

2.12 LEUNG, KWOK-CHU. Ph.D. Thesis. UCRL-19705 (1970).

2.13 ABE, K. Phys.Rev. D12, (1975).

2.14 HAGEDORN, R. "Relativistic Kinematics", Benjamin (1963).

3.1 RICHARDSON, J R. IEEE Trans.Nuc.Sci. 22, 3 (1975).

3.2 BEVERIDGE, J. TRIUMF Report TRI-PP-75-5 (1975).

3.3 POIRER, R L. TRIUMF Report TRI-PP-75-3 (1975).

3.4 AULD, E G. TRIUMF Report TRI-PP-75-6 (1975).

3.5 BROWN, K L. "Transport 360", SLAC Report 91, (1970).

3.6 GALLAGHER DAGGIT, G. "Report on the BASQUE Superconducting Solenoid" RL 75-008.

3.7 HODGES, T A. TRIUMF Internal Report, TRI-I-73-2 (1973).

3.8 BARGHANN. Phys.Rev.Lett. 2, 435 (1959).

3.9 CESATI, A. Progr. Nucl.Phys. 10, 119 (1969).

3.10 CLARK, RICHARDSON and WRIGHT. Nuc.Inst.Meth. 18-19 (1962).

3.11 CHARPAK, G. Ann.Rev.Nuc.Sci. 20, 195 (1970).

3.12 CHARPAK, G. Nucl.Inst.Meth. 62, 262 (1968).

3.13 BOUCLIER, R. Nucl.Inst.Meth. 88, 149 (1970).

3.14 CHARPAK, G. Nucl.Inst.Meth. 99, 279 (1972).

3.15 WATERS, WHITE and BARTLETT. "BASQUE MWPC Readout System" RHEL-HEP Electronics Group Report (1974).

3.16 GALLAGHER DAGGIT, G. Rutherford Lab. Report RLN 74-104 (1974).

3.17 KIRSTEN, F A. Ann.Rev.Nucl.Sci. 25, 509 (1975).

3.18 "CAMAC Tutorial Issue" IEEE. Trans.Nucl.Sci. 18, 1 (1971).

3.19 MILBORROW, R S. Rutherford Lab. Report RHEL/M141.

5.1 ARNDT, R A. Phys.Rev. 141, 873 (1966).

5.2 "Methods of Experimental Physics" 5, Part B, Academic Press (1963).

5.3 AEBISCHER, D. Nucl.Inst.Meth. 124, 49 (1975).

5.4 BUGG, D V. Private Communication.

5.5 "Nuclear Forces" Supp. Prog. of Theo. Physics, Vol.38 (1967) and 42 (1968).

5.6 MARTIN, B R. "Statistics for Physicists" Academic Press (1971).

5.7 KEEPING, E S. "Intro. to Statistical Inference" Van Nostrand (1962).

A.1 HIGHLAND, V L. Nucl.Inst.Meth. 129, 497 (1975).

B.1 "Electric Users Manual" Rutherford Report RHEL 72-003 (1972).

B.2 HALL, P V. "Computational Structures" MacDonald/ Elsevier.

B.3 "CIGAR Manual" Rutherford Report 2nd Edition (1972).

B.4 CAMPBELL-KELLY, M. "An Introduction to Macros" MacDonald/Elsevier.

B.5 "FORTRAN G & H Programmers Guide" IBM Systems Ref.LIB.